SPATIAL CONTRAST SENSITIVITY AND EXTERNAL NOISE; APPLICATIONS TO OPTICAL AND NEURAL MODULATION TRANSFER FUNCTIONS

Juvi Katri Mustonen

Doctor of Philosophy

The University of Aston in Birmingham

August 1995

The University of Aston in Birmingham

SPATIAL CONTRAST SENSITIVITY AND EXTERNAL NOISE; APPLICATIONS TO OPTICAL AND NEURAL MODULATION TRANSFER FUNCTIONS

Juvi Katri Mustonen

Doctor of Philosophy
1995

THESIS SUMMARY

The thesis will show how to equalise the effect of quantal noise across spatial frequencies by keeping the retinal flux (If^{-2}) constant. In addition, quantal noise is used to study the effect of grating area and spatial frequency on contrast sensitivity resulting in the extension of the new contrast detection model describing the human contrast detection system as a simple image processor. According to the model the human contrast detection system comprises low-pass filtering due to ocular optics, addition of light dependent noise at the event of quantal absorption, high-pass filtering due to the neural visual pathways, addition of internal neural noise, after which detection takes place by a local matched filter, whose sampling efficiency decreases as grating area is increased.

Furthermore, this work will demonstrate how to extract both the optical and neural modulation transfer functions of the human eye. The neural transfer function is found to be proportional to spatial frequency up to the local cut-off frequency at eccentricities of 0 - 37 deg across the visual field. The optical transfer function of the human eye is proposed to be more affected by the Stiles-Crawford -effect than generally assumed in the literature. Similarly, this work questions the prevailing ideas about the factors limiting peripheral vision by showing that peripheral optical acts as a low-pass filter in normal viewing conditions, and therefore the effect of peripheral optics is worse than generally assumed.

Keywords:

Quantal noise
Luminous flux
Internal noise
Optical modulation transfer function
Neural modulation transfer function

To my Ukko and Mamma

ACKNOWLEDGEMENTS

I am now privileged to thank my enthusiastic supervisor, Dr Jyrki Rovamo for his valuable help and support during this work. I also wish to express my sincere gratitude to Dr Risto Näsänen for his help, my colleagues Heljä Kukkonen, Olavi Luntinen, Kaisa Tiippana and Outi Ukkonen for their patient participation in the experiments, and Dr Lea Hyvärinen for her support.
The invaluable encouragement and support from my Family and my Friends was never in doubt, I gratefully wish to thank you all.

I wish to thank the Head of Department, Mr Derek Barnes, and the whole personnel of the Department of Vision Sciences at the University of Aston in Birmingham. The Security personnel of the University deserves a special acknowledgement.

This work was financially supported by Finnish Ministry of Education, the Association of Finnish Ophthalmic Opticians, the Association of Optometry in Finland, the Information Centre of Optics Business in Finland, Finnish National Agency for Health and Welfare, the Academy of Finland, and the Suomalainen Konkordia-liitto, which are all gratefully acknowledged.

Juvi Mustonen
August 1995

LIST OF CONTENTS

LIST OF FIGURES

LIST OF EQUATIONS

$$g_q(x,y) = \text{int}\,[g(x,y)+d(x,y)] \tag{2.1}$$

$$E = \sum\sum c^2(x,y)p^2 \tag{2.2}$$

$$c_{r.m.s.} = \sqrt{(E/A)} \tag{2.3}$$

$$N_s = c_n^2 p_h p_v \tag{2.4}$$

$$S^{-2} = k_1 + k_2/\, I \tag{3.1}$$

$$S^{-2} = S_{max}^{-2} + k_2/\, I \tag{3.2}$$

$$S = S_{max}\,[1 + I_c/\, I]^{-0.5} \tag{3.3}$$

$$S = S_{max}\,[1 + I_0F^2/I]^{-0.5} = S_{max}\,[1 + I_0/(I/F^2)]^{-0.5} \tag{3.4}$$

$$E'_{human} = O_{MTF}^2(f)\; P_{MTF}^2(f)\; c^2\; A \tag{3.5}$$

$$E'_{ideal} = d'^2\; N, \tag{3.6}$$

$$N = P_{MTF}^2(f)\; N_q + N_i \tag{3.7}$$

$$\eta = d'^2[P_{MTF}^2(f)\; N_q + N_i] \,/\, [O_{MTF}^2(f) P_{MTF}^2(f) c^2 A] \tag{3.8}$$

$$S^2 = O_{MTF}^2(f)\; P_{MTF}^2(f)\; A\,\eta/\,\{d'^2\,[P_{MTF}^2(f)\; N_q + N_i]\} \tag{3.9}$$

$$\eta = \eta_{max}\,(1 + A/A_c)^{-1}, \tag{3.10}$$

$$S^2 = O_{MTF}^2(f)\; P_{MTF}^2(f)\; A\eta_{max}(1 + A/A_c)^{-1} d'^{-2}\,[P_{MTF}^2(f)\; N_q + N_i]^{-1} \tag{3.11}$$

$$S^2 = \eta_{max} d'^{-2}\; O_{MTF}^2(f)\; P_{MTF}^2(f) A_c\,[1+A_c/A]^{-1}[P_{MTF}^2(f) N_q + N_i]^{-1} \tag{3.12}$$

$$S^2 = S_{max}^2\,[1+A_c/A]^{-1}\;[P_{MTF}^2(f) N_q/N_i + 1]^{-1} \tag{3.13}$$

$$S_{max}^2 = K_o^2\; O_{MTF}^2(f)\; P_{MTF}^2(f)\; A_c, \tag{3.14}$$

$$P_{MTF}^2(f)\; N_{qc} = N_i. \tag{3.15}$$

$$N_q = K/\, I, \tag{3.16}$$

$$N_{qc} = K\,/\, I_c\,, \tag{3.17}$$

$$S^2 = S_{max}^2(1+A_c/A)^{-1}(1+N_q/N_{qc})^{-1} = S_{max}^2(1+A_c/A)^{-1}(1+I_c/I)^{-1}. \tag{3.18}$$

$$A_c = A_0\,(1 + f^2\,/\, f_0^2)^{-1}, \tag{3.19}$$

$$S = S'_{max}\,(1+A_c\,/\,A)^{-0.5} \tag{3.20}$$

$$S_0\; O_{MTF}(f) = S_0\; \exp\,[-(f\,/\, f_c)^n] \tag{3.21}$$

$$I = K N_q^{-1}, \tag{4.1}$$

$$P_{MTF}^2(f)\; N_{qc} = N_i, \tag{4.2}$$

$$P_{MTF}^2(f) = (N_i\,/\,K)\; I_c, \tag{4.3}$$

$$N_q^{-1} = k' I, \tag{5.1}$$

$$O_{MTF}^2(f)\, N_{sc} = k'' N_{qc}, \tag{5.2}$$

$$k\, O_{MTF}(f) = (I_c N_{sc})^{-0.5}, \tag{5.3}$$

$$O_{MTF}(f) = \exp [-(f/f_c)^n] \tag{5.4}$$

$$K = K_0\, O_{MTF}(f) \tag{5.5}$$

$$\ln K = \ln K_0 - (f/f_c)^n, \tag{5.6}$$

$$S = S_{max} (1 + N_s / N_{sc})^{-0.5}, \tag{5.7}$$

$$S = S_{max} (1+Z_c/Z)^{-0.5} \tag{5.8}$$

$$N_{qc} = O_{MTF}^2(f)\, N_{sc}, \tag{5.9}$$

$$K''\, O_{MTF}(f) = (N_{sc} \times I_c)^{-0.5} \tag{5.10}$$

$$K\, O_{MTF}(f) = (N_{sc} \times f^2)^{-0.5} \tag{5.11}$$

$$\ln K = \ln K_0 - (f/f_c)^n \tag{5.12}$$

1. INTRODUCTION

The functioning of our visual system as a whole can be studied by measuring human visual performance by means of contrast sensitivity measurements. Contrast sensitivity refers to the inverse of the threshold contrast, which is required for the detection of a stimulus at a certain probability level. Already the early stages of vision seem to compute contrast, as the responses of retinal, geniculate, and primary cortex neurones are dependent on contrast (Shapley & Enroth-Cugell, 1984; Shapley, 1991). The responsiveness of the visual system to contrast is primarily the result of an automatic gain control which produces light adaptation and regulates the contrast sensitivity of a receptive field centre so that contrast is computed locally (Shapley & Enroth-Cugell, 1984). The automatic gain control therefore acts as the main link between visual adaptation determined by the ganglion cells and retinal adaptation, which refers to the adaptation state of photoreceptors (Barlow & Levick, 1969). The most important purpose of light adaptation is to maximise visual contrast sensitivity and to keep it constant as the background luminance varies (Shapley & Enroth-Cugell, 1984; Shapley, 1991). Using systemic theoretical approach this thesis will concentrate on modelling of spatial properties of the early stages of the visual system on the basis of contrast sensitivity, which - as a function of spatial frequency - describes the ability of the human visual system to detect the surrounding environment.

The normal photopic contrast sensitivity curve for stationary spatial gratings shows a band-pass shape attenuation of neural and optical origin. The visual system is thus most sensitive to medium spatial frequencies (Campbell & Robson, 1968; Kelly, 1977). However, with decreasing luminance the peak is shifted towards lower spatial frequencies, making the attenuation of low spatial frequencies less prominent (Patel, 1966; Daitch & Green, 1969). On the

other hand, with smaller gratings the peak is shifted towards higher spatial frequencies (Cohen, 1978; Rovamo, Luntinen & Näsänen, 1993).

In the following I will first concentrate on the dependence of contrast sensitivity on retinal illuminance (I) at different spatial frequencies (f). In general, grating detection obeys Weber's law at high luminance levels, as contrast sensitivity is then independent of luminance. At low luminance levels contrast sensitivity increases with luminance following then DeVries-Rose law (DeVries, 1943; Rose, 1948). According to the results of Van Nes and Bouman (1967) the critical retinal illuminance (I_c) denoting the transition luminance between the above mentioned laws is proportional to spatial frequency squared. Section 3.2. confirms the Van Nes-Bouman law and extends it to low spatial frequencies. Furthermore, I will show that the effect of retinal illuminance (I) and quantal noise can be equalised across spatial frequencies (f) by keeping the retinal flux (If^{-2}) constant. In Chapter 4 I will also show that the Van Nes-Bouman law is valid across spatial frequencies.

In Section 3.3. I will describe a study concerning the interaction of retinal illuminance and spatial integration. Spatial integration describes the ability of the visual system to sum information over space, and is dependent on the number of cycles in the stimulus grating (Hoekstra, Van der Goot, Van den Brink & Bilsen, 1974; Howell & Hess, 1978). At small grating areas contrast sensitivity increases with grating area obeying Piper's law (Piper, 1903) but gradually saturates and reaches an asymptote at large grating areas. The critical area (A_c) indicates the transition point from Piper's law to situation when the increase in grating size does not increase contrast sensitivity. Section 3.3. will show that spatial integration is similar at all luminance levels, as the critical area (A_c) was independent of retinal illuminance. Likewise, the effect of retinal illuminance on contrast sensitivity is similar at all grating areas, because I_c was independent of grating area. Chapter 3 also extends the

contrast detection model of spatial vision (Rovamo et al. 1993) to low light levels by including the effect of quantal noise into the model. The human spatial contrast detection will thus be modelled as a simple image processor comprising low-pass filtering of the eye optics, addition of light-dependent noise at the event of quantal absorption, high-pass filtering due to the neural visual pathways, addition of internal neural noise, and detection by a local matched filter, whose efficiency decreases with grating area.

However, the area over which the visual system is able to collect information is limited both in deg^2 (Rovamo et al., 1993), and to a certain number of elements (Hoekstra et al., 1974; Virsu & Rovamo, 1979; Verghese & Pelli, 1992). Hence, at low spatial frequencies the critical number of details (grating bars) would require a larger area than the neural system can sum over, thus contrast sensitivity at low spatial frequencies is reduced by the neural system (Nachamias, 1968; Davila & Geisler, 1991). Chapter 4 will study the neural modulation transfer function of the visual pathways (P_{MTF}) by using quantal noise. The masking power, i.e. the spectral density of quantal noise (N_q) is not affected by ocular optics (Graham & Hood, 1992), but is only filtered by the neural transfer function of the visual pathways (Rovamo et al., 1993). As critical retinal illuminance is proportional to spatial frequency squared (Van Nes and Bouman, 1967) and the spectral density of quantal noise is inversely proportional to I_c (Pelli, 1990), I will show that according to the extended contrast detection model P_{MTF} (f) is proportional to spatial frequency (f).

The detection of fine detail, i.e. high spatial frequencies, is limited by the optical system of the eye (Campbell & Green, 1965; Campbell & Gubisch, 1966). The studies where the effect of eye optics is bypassed by producing interference gratings on the retina indicate that the optical defects do not completely account for the perceived loss at high spatial frequencies (DeValois & DeValois, 1990). Another limiting factor is the spatial sampling of

photoreceptors, which by setting the upper limit for the spatial frequencies transmitted also contributes to the high frequency fall-off. Studies incorporating an ideal discriminator which takes into account the effect of spatial integration, the transfer through the ocular media, and spatial distribution of photoreceptors show that the high spatial frequency attenuation can be explained by pre-neural factors alone (Banks, Geisler & Bennett, 1987).

A substantial part of my thesis is dedicated to the measurement of the optical modulation transfer function of the human eye. In Section 5.2 I will introduce two independent psychophysical methods to estimate the attenuation of contrast sensitivity caused by the eye's optics. The results obtained in the fovea agree partly with previously published estimates of the O_{MTF}s (e.g. Campbell & Green, 1965; Campbell & Gubisch, 1966; Van Meeteren, 1974; Deeley, Drasdo & Charman, 1991; Artal & Navarro, 1994). Section 5.3 extends the study to different pupil sizes, and estimates the diffraction limited O_{MTF} of a circular aperture eye considering also the effect of retinal light scatter (Ohzu & Enoch, 1972).

Finally, Section 5.4. studies the peripheral optics. As visual information is transmitted by discrete neurones, the visual system samples the retinal image at spatially discrete locations. This makes the system susceptible to sampling artefacts, or aliasing (Anderson & Hess, 1990). In the fovea this is prevented to a great degree by the quality of eye optics, which roughly matches the sampling capabilities of the foveal retina (Williams, 1985). In the periphery, however, the optical quality has traditionally been considered to be too good to accomplish the task. Logically the most efficient way to avoid aliasing would, however, be to prevent potentially aliased spatial frequencies from reaching the sampling site. Therefore, it would be useful to match also the quality of peripheral optics to the sampling properties of the peripheral retina.

In Chapter 5.4 I have applied the techniques introduced in Chapter 5.2. to measure uncorrected peripheral O_{MTF}s, and show that the quality of peripheral optics might well be suitable in preventing aliasing, as Galvin and Williams (1992) have also suggested.

2. GENERAL METHODS

This chapter explains the general methods of the work and applies to all experiments described in the thesis. In the experiments contrast sensitivity was measured for simple cosine gratings of different spatial frequencies, grating areas, and retinal illuminances.

2.1. Apparatus

The same apparatus was used in every experiment of this work. It consisted of a PC 486 -computer driven by a VGA graphics board, and of a 16 inch RGB monitor. The monitor (with a fast phosphor B22) could show 1280 x 800 pixels, but the graphics board was used in a mode that utilised 640 x 480 pixels. The pixel size was then 0.42 x 0.42 mm^2, and the frame rate was 60 Hz.

The monitor was used in a white mode with an average photopic luminance at 50 cd/m^2, which corresponded to an average scotopic luminance of 130 cd/m^2. The CIE 1931 chromacity co-ordinates (x,y) of the monitor were (0.30, 0.31). The luminance was measured first with a Minolta Luminance Meter ILS-110, and later validated with a Bentham PMC 3B spectroradiometer. The exact spectral composition of the monitor in white mode was measured with the Spectroradiometer, and will be illustrated in the Appendix 1.

The VGA board was capable of showing $2^8 = 256$ colours at a time, but as every colour channel, red, green or blue, was able to produce $2^6 = 64$ intensity levels, the total colour palette was $2^{(3x6)} = 262144$. To increase the number of grey levels needed especially at low contrasts, the digital to analog converters (DACs) of the three colour channels were combined using the method described in Pelli and Zhang (1991): Only the four most significant bits of the

red and green colour guns were used in order to avoid inaccuracies in voltages corresponding to the less significant bits which could cause distortion in the contrast response. The bits of the green colour gun were attenuated (1/13) in comparison to the red colour gun. All suitably attenuated (1/182) six bits of the blue colour gun were used.

The two additional bits were obtained by using a periodic dither signal of very small contrast before intensity quantization (Näsänen, Kukkonen & Rovamo, 1993). The size of the period was 2x2 pixels and the amplitude of the dither signal was one quantization interval. The lowest spatial frequency of the dither on the screen was 12 c/cm, which is three times higher than the highest spatial frequency (4 c/deg) in the stimuli used. If the size and the contrast of the dither signal is kept sufficiently small, as was the case in all experiments, the dither is completely invisible guaranteeing that there were no masking effects (Näsänen, 1989). The dither signal was d(0,0)=0, d(0,1)=0.75, d(1,0)=0.5, d(1,1)=0.25. It produced a fourfold increase in the number of grey levels. The dithering algorithm is

$$g_q(x,y) = \text{int}\,[g(x,y)+d(x,y)], \qquad (2.1)$$

where int [.] denotes rounding to the nearest integer, $g_q(x,y)$ is the quantized signal with dither, g(x,y) is the continuous signal, and d(x,y) is the dither signal.

A colour index value corresponds to a certain combination of the three colour channels. The index values are stored in the look-up table (LUT) which provides the information to the VGA board. The relationship between the measured luminance and the corresponding index values was described as $L(I)=0.005298\ I^{2.409}$, where L is the luminance in cd/m^2, and I is the index value. To linearize the non-linear luminance response of the display, gamma-

correction was performed by using the inverse function of the non-linear luminance response when computing the images.

The luminance response described by the function $L(I)=0.005298\ I^{2.409}$ has been determined by using 64 index values. However, with the summation device (Pelli & Zhang, 1991) the total number of bits is 14. In order to calculate the total number of luminance steps the luminance response function is transformed to $L(I_e) = 0.005298(I_e/256)^{2.409}$, where I_e is the extended index value. After calculating the index values for the maximum and minimum luminances at a certain contrast, their difference + 1 gives the number of grey levels produced by the summation device. The 2 x 2 pixel dither signal added three intensity levels to each step, thus quadrupling the number of grey levels. In this manner the number of grey levels was large enough to produce sinusoidal waveform with sufficiently small quantization errors at all Michelson contrasts used. The monochrome signal of $2^{10} = 1024$ was thus drawn from a palette of $2^{16} = 65536$. The number of grey levels depended on the grating contrast. At high contrasts the number of grey levels was thus 1024, which decreased at lower contrast levels so that the monitor was able to produce about 50 grey levels even at a Michelson contrast of 0.00125.

Contrast energies of sinusoidal gratings were calculated by integrating the contrast waveform pixel by pixel. For this purpose the local contrast for each pixel was determined first, then these measures were squared and multiplied by the pixel area. Their sum indicates the contrast energy:

$$E = \sum\sum c^2(x,y)p^2 \qquad (2.2)$$

where $c(x,y) = [L(x,y)-L_0]/L_0$ is the local contrast, $L(x,y)$ is luminance, p^2 is pixel area in solid degrees, and L_0 is luminance averaged across the pixels. Thus,

contrast energy takes into account both the effect of luminance distribution and stimulus area.

The r.m.s. contrast of the grating was then calculated as

$$c_{r.m.s.} = \sqrt{(E/A)}, \tag{2.3}$$

where A is stimulus area. Thus $c_{r.m.s.}$ is equal to the standard deviation of contrast waveform or luminance distribution normalised by average luminance. For simple cosine gratings, which are mainly used in this work, r.m.s.-contrast is approximately equal to Michelson contrast divided by $\sqrt{2}$. Michelson contrast is calculated as $(L_{max}-L_{min})/(L_{max}+L_{min})$, where L_{max} and L_{min} are the maximum and minimum luminances of the simple cosine grating. The reason for using root-mean-square contrast instead of Michelson contrast is the complexity of luminance distribution when noise is examined. As explained above, r.m.s. contrast is first determined locally at each image pixel which then determine the stimulus contrast. Michelson contrast is much less precise with complex luminance distributions as it is defined only by using the extreme luminance levels. Therefore, unless otherwise stated, contrast (or contrast sensitivity) in this work refers to a r.m.s. measure.

Calibration of the spatial frequency response of the monitor

The contrast check of the monitor was done for six spatial frequencies of 0.25 - 4.0 c/deg at contrast levels of 0.1 and 0.5. The sinusoidal gratings were tested in three orientations; vertical, horizontal and 45° oblique. The minimum luminance was searched for by changing the phase of the grating in small steps. The maximum luminances for each grating were obtained by changing the phase of the grating from 0° to 180°. The contrast measured turned out to be independent of spatial frequency and orientation up to 2 c/cm.

The calibration check was performed by Minolta Luminance Meter LS-110 with a close-up lens (No.110) having a spot diameter of 0.4 mm.

2.2. Stimuli

Throughout this work, the stimuli were vertical cosine gratings in either a circular or a square field of different sizes. They had sharply truncated edges, which made the calculation of stimulus area straightforward and well-defined. Black cardboard in front of the screen masked the equiluminous surround to either a circular, 20 cm in diameter, or a square field of 20 x 20 cm^2.

External added spatial white noise was used in some of the experiments of this work. Gratings embedded in one or two-dimensional spatial noise and pure noise stimuli were produced by adding to each noise pixel consisting of one or several image pixels within the stimulus area a random number drawn independently from a Gaussian distribution with zero mean and truncation at ±2.5 units of standard deviation. Spatial noise is white, when its spectral density is constant at all spatial frequencies. The spectral density of noise was varied by changing the standard deviation of the Gaussian distribution. The luminances of neighbouring noise pixels were uncorrelated. Thus, noise was white up to a cut-off frequency, which is defined as the inverse of two noise pixel sidelengths (Pelli, 1990).

The spectral density of added spatial noise was calculated (Rovamo & Kukkonen, 1995) as

$$N_S = c_n^2 \, p_h \, p_v, \qquad (2.4)$$

where the r.m.s. contrast of noise (c_n) is the standard deviation of the contrast waveform of noise (random luminance increment or decrement divided by the average screen luminance), p_h is the noise pixel width, and p_v is the noise pixel height, which in the case of one-dimensional noise is equal to the grating height. Hence, one-dimensional spatial noise has larger pixel area and it thus reduces contrast sensitivity more than is possible by means of two-dimensional spatial noise with the same r.m.s. contrast (Rovamo & Kukkonen, 1995).

The stimuli were created and experiments were run by means of a software developed by Dr. Risto Näsänen. A two-alternative forced-choice method was used throughout the work. The stimulus was rapidly switched on and off by changing the colour look-up table during the vertical retrace period of the monitor, which made the exposure duration well-defined. Each trial consisted of two 500 msec exposures, separated by 600 msec. Both exposures with abrupt on- and off-sets contained the grating stimulus and were accompanied by similar sound signals. However, only one exposure contained a stimulus with non-zero contrast; in the other the contrast was always zero. Between the two exposures and during the inter-trial intervals the observer saw only the homogeneous field. A new trial began 250 msec after the observer's response. The observer indicated which exposure contained the grating by pressing one of the two keys on a computer keyboard. A wrong choice was followed by another sound signal to provide feedback to the observer.

When gratings with noise were used there were 5 different grating+noise stimuli for each grating contrast level. One of them was chosen randomly for each exposure. The comparison stimulus was chosen randomly from a set of 21 different noise stimuli. The same comparison set was used at all contrast levels.

Contrast sensitivity is the inverse of contrast at threshold. Thresholds were determined by a two-alternative forced-choice algorithm with a staircase routine described by Wetherill and Levitt (1965). The staircase routine followed the up-and-down transformed routine, which is a modification of a simple up-and-down rule yielding the probability level of guessing, i.e. 50% of correct answers. In the up-and-down transformed routine the number of correct answers required to produce a decrease in stimulus contrast is increased, but the number of wrong answers causing the stimulus contrast to increase, is kept constant at one. This results to a correct answer at the probability level of p where $p^n = 0.50$, and n is the number of correct answers required. Hence, the probability level depends on the number of correct answers required. In the experiments of this thesis four correct answers were required to decrease the stimulus contrast, thus producing the probability level of 0.84. The step size was always 0.1 log units.

In order to let the subject learn the stimulus to be detected, the first contrast shown in the beginning of a trial was always above threshold. Therefore the algorithm consisted of two parts: A subthreshold level was established at the contrast level of the second wrong answer. The threshold was determined as an arithmetic mean of the following eight reversal points. Altogether, there were ten turning points of the direction of contrast change - the subthreshold level, eight reversals in the actual threshold determination phase, and the last one to mark the end of the trial, which always took place after four correct answers. All data points are geometric means (Chapter 3) or medians (Chapters 4 and 5) of 3 threshold estimates.

The experiments were performed in a dark room. The subject's head was stabilised using a chin rest. The only light source was the display, except in the experiments of Chapters 3 and 4.4, where a self-luminous fixation point was used. The luminance of the red LED was adjusted according to the

screen luminance. Otherwise a small black dot served as a fixation point in the centre of the stimulus field.

Viewing was always monocular. However, monocular fixation to the small back dot does not guarantee an accurate accommodative response. The resulting blur might reduce contrast sensitivity at high spatial frequencies. Therefore, a control experiment was performed using 0.5% Cyclopentolate hydrochloride that both dilated pupil and paralysed accommodation. Even with optimal refraction, contrast sensitivity at 16 c/deg was no better than in the principal experiments. On this basis I conclude that the possible inaccuracies of accommodation did not affect my results.

2.3. Filters

In order to reduce the luminance of the screen, neutral density filters were placed in front of the screen. Neutral density filters are neutral to the colour of the light passing through them, i.e. the transmission is independent of wavelength. The optical density - which is the log10 of the reciprocal of the transmitted fraction - of the filters (No. 210, Lee Filters Ltd, U.K.) was 0.6, thus reducing the luminance to 25%. When several filters were superimposed, the screen luminance was reduced by several logarithmic units.

The neutrality of the filters, i.e. independence of their transmittance of light wavelength was checked by Bentham PMC3 Spectroradiometer. Furthermore, each filter was checked by Minolta Luminance Meter II Incident.

2.4. Drugs

As mentioned earlier, viewing was always monocular. The pupil of the dominant eye of each subject was dilated to 8 mm. After a drop of benoxinate

(oxybuprocaine) hydrochloride USP 0.4% to increase drug absorption, two drops of phenylephrine (metaoxedrine) hydrochloride BP 10% were used for dilation. Benoxinate is a local anaesthetics with short duration of action. It modifies the trans-membrane ionic flow and inhibits the reflex tearing, thus enabling faster absorption of the second drug. Phenylephrine is a sympathomimetic mydriatic with duration of action for several hours. It's α_1 agonist activity on smooth muscle causes pupil dilation. In general, sympathomimetic substances have little effect on accommodation.

In a control experiment performed to test whether uncontrolled accommodation had any effect on our results, a cycloplegic cyclopentolate hydrochloride BP 0.5% was used. Cyclopentolate is a muscarinic blocking drug acting at the sphincter pupillae muscle. As the sphincter is more powerful muscle than the dilator, the relaxation causes mydriasis and paralysis of accommodation, with an average duration of 45 minutes. All drugs were obtained from single-dose *Minims* disposable units (Smith & Nephew Pharmaceuticals Ltd, Romford, U.K.).

The resulting pupil size was subjectively measured by each subject with an entoptic pupillometry. The gauge was a firm plastic slip, that had a series of pairs of adjacent holes separated by a distance equal to the pupil size. Whilst holding the slip close to one's eye and looking through the holes, the pair of circles that appeared to touch each other indicated the pupil size. Thus it was possible to measure the entrance pupil at the luminance level preferred with satisfying accuracy without any infrared equipment.

3. THE EFFECTS OF RETINAL ILLUMINANCE, SPATIAL FREQUENCY AND GRATING AREA ON CONTRAST SENSITIVITY

3.1. Introduction

3.1.1. DeVRIES-ROSE LAW AND WEBER'S LAW

Light adaptation is ideal when contrast sensitivity follows Weber's law, i.e. contrast sensitivity (S) is independent of retinal illuminance (I). This can be expressed as S (I) = k. For most targets Weber's law holds throughout the photopic range of luminance backgrounds. However, when luminance is decreased below a critical level, contrast sensitivity begins to decrease as a function of light level. The decrease in contrast sensitivity with diminishing light can be expressed as $S = K\sqrt{L}$. This is called as the square-root law of luminance (L) or DeVries-Rose law (DeVries, 1942; Rose, 1948).

The basis for the square-root law is the Poisson distribution of light quanta (DeVries, 1942; Rose, 1948). Another explanation (Lillywhite, 1981) for the square-root behaviour could be light-dependent multiplicative intrinsic noise.

As the visual system is always limited by statistical fluctuations (Rose, 1948; Barlow, 1964), the detection must be limited by another source of noise at high luminance levels. The release of neural transmitters in response to neurone depolarisation creates internal neural noise, which seems to be the limiting factor when contrast sensitivity obeys Weber's law (Nagaraja, 1964; Barlow, 1964,1977; Pelli, 1990).

At some luminance level the effects of internal noise responsible for Weber's law and quantal noise responsible for DeVries-Rose law on contrast sensitivity

are equal. At intermediate light levels the performance thence falls between DeVries-Rose and Weber's laws (Kelly, 1972; Koenderink et al., 1978; Savage & Banks, 1992), as then both N_q and N_i affect contrast sensitivity.

The transition illuminance level, where contrast sensitivity changes its behaviour from the one law to the other, is called the critical retinal illuminance (I_c). The critical illuminance (I_c) is dependent on the spatial and temporal properties of the stimulus, and thus varies with spatial frequency (Van Nes & Bouman, 1967), retinal location (Koenderink, Bouman, Bueno de Mesquita & Slappendel, 1978), and possibly with grating area (Hoekstra, Van der Goot, Van den Brink & Bilsen, 1974 versus Savage & Banks, 1992).

When retinal illuminance decreases, high spatial frequencies enter the DeVries-Rose region but low spatial frequencies are still governed by Weber's law. This was first shown by Van Nes and Bouman (1967), who studied sinusoidal gratings covering the area of 4.5 x 8.25 deg^2 at spatial frequencies of 0.5 - 48 c/deg for luminance levels of 0.009 - 900 td. Their results implied that the critical illuminance (I_c) is proportional to the square of the spatial frequency.

In peripheral viewing the effect of retinal illuminance on contrast sensitivity as a function of spatial frequency has been studied by Koenderink et al. (1978), who found that the transition from DeVries-Rose to Weber's law occurs at lower luminance levels with increasing eccentricity. Thus, at the same retinal illuminance contrast sensitivity at a spatial frequency is governed by Weber's law in the periphery, but in the fovea it obeys DeVries-Rose law. Koenderink et al. (1978) even proposed a location-dependent scaling factor for retinal illuminance, as they found that foveal results obtained at 10 td illuminance were indistinguishable from results obtained at the eccentricity of 50 deg at 0.1 - 0.01 td illuminance.

3.1.2. SPATIAL INTEGRATION

The visual system is capable of integrating information over space. This improvement in visual performance with increasing stimulus size is termed as spatial integration. However, in grating detection it is not the angular size of the stimulus that is the primary determinant factor. Instead, the number of cycles was concluded to be significant (Van Nes, 1968; Kulikowski, 1969; Hoekstra et al., 1974) and the sole determinant for modulation thresholds at 1 - 7 c/deg (Hoekstra et al., 1974). Hoekstra et al. also discovered that above a critical number of cycles, contrast sensitivity is independent of spatial frequency. The effect of the length of the grating bars was studied by Howell and Hess (1978), who found out that the critical length of the bars also depends on spatial frequency so that the critical size A_C in deg^2 is inversely related to the spatial frequency. Thus, if the square-shaped gratings have a constant number of cycles which is equivalent to or more than A_C/f^2, the increase in the number of cycles no more affects contrast thresholds (Hoekstra et al., 1974; Howell & Hess, 1978), i.e. spatial integration is saturated.

At small grating sizes contrast sensitivity increases according to the square-root law, now called Piper's law (1903) of spatial integration, before the increase saturates and contrast sensitivity becomes independent of grating size. The critical grating area (A_C) indicates the saturation of spatial integration. The critical area is inversely proportional to spatial frequency squared (Howell & Hess, 1978; Rovamo et al., 1993) at and above 0.5 c/deg, in agreement with the scale invariance principle (Näsänen, Kukkonen & Rovamo, 1993). At very low spatial frequencies the lateral inhibition or other neural interaction causes contrast sensitivity to decrease despite the sufficient number of grating bars (Robson & Graham, 1981; Virsu & Rovamo, 1979). In fact, the increase in A_C compensates the attenuating effect of lateral inhibition.

However, at low spatial frequencies the critical area seems to be constant in solid degrees of the visual field (Rovamo et al., 1993b), although Savage & Banks (1992) obtained results at scotopic light levels where the number of grating cycles where contrast sensitivity first fell under one seemed to increase with spatial frequency. However, below 0.5 c/deg the equivalent number of cycles corresponds to a constant size in degrees of the visual angle, thus agreeing with Rovamo et al. (1993).

The scale invariance means that magnifying or minifying the target grating does not effect its detectability. A change in the viewing distance would either magnify or minify the original grating. McCann et al. (1974), Savoy and McCann (1975), Virsu and Rovamo (1979), and Rovamo, Franssila and Näsänen (1992) have all shown that the spatial integration is not affected by viewing distance, as long as the optical blur is negligible. Based on the principle of scale invariance Virsu and Rovamo developed the concept of the number of square cycles. The number of square cycles (Af^2) is defined as the product of grating area (A) and spatial frequency (f) squared. In consequence, gratings of different spatial frequencies but with a constant number of square cycles are magnified or minified versions of each other. If the grating size is expressed as the number of square cycles (Af^2) the spatial integration obeys a single saturating function at all spatial frequencies in bright light (Virsu and Rovamo, 1979).

The effect of retinal illumination on spatial integration was studied by Savage and Banks (1992) at the eccentricity of 20 deg in the nasal visual field by ideal-observer analysis. They concluded that spatial integration does not vary markedly with retinal illuminance over the low range of luminances of 0.6 - 0.05 scot. td. However, in the foveal results of Hoekstra et al. (1974) the critical number of cycles increased with luminance.

In the following experiments I will first study the relationship between retinal illuminance and spatial frequency and whether the Van Nes-Bouman law holds also at low spatial frequencies. It would also be predicted that if a constant number of square cycles was used, the contrast sensitivity functions would have the same shape and maximum sensitivity at all spatial frequencies (0.125 - 4 c/deg), where the attenuating effect of the modulation transfer function of eye optics is still small (Deeley, Drasdo & Charman, 1991). Furthermore, the results of Van Nes and Bouman (1967) indicated that the critical retinal illuminance (I_c) is directly proportional to spatial frequency squared. Therefore, it should be possible to superimpose the contrast sensitivity functions by expressing the luminance in terms of retinal flux, calculated as If^{-2}.

Secondly, based on the finding of Virsu and Rovamo (1979) that a constant number of square cycles (Af^2) equalises the effect of spatial integration across spatial frequencies, and on the finding of my first experiment, that the effect of quantal noise can be equalised across spatial frequencies by keeping the retinal flux (If^{-2})constant, the interaction between spatial integration and retinal illuminance is extensively studied. It will be shown that the dependence of contrast sensitivity on retinal illuminance is similar for all grating areas and that the increase of contrast sensitivity with spatial integration is similar at different light levels.

As a consequence the contrast detection model developed within our research group is extended to take into account the effect of quantal noise, so that contrast sensitivity at all grating areas and retinal illuminances can be predicted by $S = S_{max} (1+A_c/A)^{-0.5}(1+I_c/I)^{-0.5}$.

3.2. Modelling of human contrast sensitivity as a function of retinal illuminance and spatial frequency

With increasing light level contrast sensitivity first increases in direct proportion to the square root of retinal illuminance, thus obeying the DeVries-Rose law. Then, at higher light levels the increase saturates and contrast sensitivity becomes independent of luminance according to the Weber's law (Van Nes & Bouman, 1967). To comply with this I now assume that the inverse of contrast sensitivity (S) squared is linearly related to the inverse of retinal illuminance (I):

$$S^{-2} = k_1 + k_2/ I \qquad (3.1)$$

where S is contrast sensitivity, I is retinal illuminance, and k_1 and k_2 are parameters of the model. Equation (3.1) means that contrast sensitivity stays constant equal to $S_{max} = 1/\sqrt{k_1}$ in bright light, but increases in proportion to $\sqrt{I}$ in dim light. Equation (3.1) can thus be transformed to

$$S^{-2} = S_{max}^{-2} + k_2/ I \qquad (3.2)$$

The transition between the increasing and constant parts of equation (3.1) is denoted by critical retinal illuminance (I_c). At the crossing point of the constant ($S^{-2} = S_{max}^{-2}$) and increasing ($S^{-2} = k_2/ I$) parts of equation (3.1) $S_{max}^{-2} = k_2/ I$. It therefore gives the critical retinal illuminance as $I_c = k_2 S_{max}^2$, which means that $k_2 = I_c S_{max}^{-2}$. Equation (3.2) then becomes

$$S = S_{max} [1 + I_c/ I]^{-0.5} \qquad (3.3)$$

When $I = I_c$, contrast sensitivity is 71% of the maximum contrast sensitivity.

From the work of Van Nes & Bouman (1967) it is known that the critical retinal illuminance marking the transition between DeVries-Rose and Weber's laws is directly proportional to spatial frequency squared (Van Nes et al. 1967). Hence, $I_c = I_0F^2$, where I_0 is the value of I_c at 1 c/deg and F = f / (c/deg). Equation (3.3) can now be transformed to

$$S = S_{max} [1 + I_0F^2/I]^{-0.5} = S_{max} [1 + I_0/(I/F^2)]^{-0.5} \quad (3.4)$$

3.2.1. METHODS

3.2.1.1. Apparatus and stimuli

The apparatus, stimuli, and procedures are described in General Methods. Therefore only the special features of the stimuli and procedures are described here.

The stimuli were circular vertical cosine gratings of diameters 0.5, 1, 2, 4, 8, and 16 cm. The spatial frequency on the monitor was varied between 0.125 and 4 c/cm but the viewing distance was always constant at 57.3 cm.

3.2.1.2 Subjects

In this work I used five experienced subjects, including myself. Four subjects were females and one was male, all my colleagues from our laboratory, varying in age between 24 and 33 years. Viewing was monocular, using the dominant eye, with optimal refractive correction. H.K. was a hyperope (os. +0.50 D), and the rest of us were myopes: O.L.(od. -1.25 D), J.M.(od. -0.75 D), K.T.(od. -6.25 D), and O.U.(od. -1.25 D). The respective monocular Snellen acuities at 5 m were 1.25, 1.6, 1.6, 1.6, and 1.3.

3.2.2. RESULTS

I measured contrast sensitivity as a function of retinal illuminance. The span of retinal illuminances tested covered a range of 6 logarithmic units from 2510 td to 0.00248 td. Spatial frequency (f) varied from 0.125 to 4 c/deg, grating area (A) from 0.785 to 201 deg^2, and the number of square cycles (Af^2) from 3.14 to 201 square cycles. Hence, the largest number of square cycles was 201, which is at or just above the saturation limit of spatial integration (Howell & Hess, 1978; Virsu & Rovamo, 1979; Rovamo et al., 1993).

In my experiments spatial frequency and the diameter of the circular grating area varied in inverse proportion to each other but the number of cycles remained constant. Accordingly, when spatial frequency increased, grating area decreased so that the number of square cycles (Af^2) remained constant. When the number of square cycles is kept constant, it is as if spatial frequency were increased by increasing viewing distance, and all gratings are thus magnified or minified versions of each other.

Figures 3.1 - 3.2 show the experimental results. Contrast sensitivity at each number of square cycles (Af^2) was measured for two observers, the other being always myself. Irrespective of grating area or spatial frequency, contrast sensitivity in Figs. 3.1 - 3.2 first increased as a function of retinal illuminance with approximately a slope of 0.5 thus obeying DeVries-Rose law. The increase then saturated and contrast sensitivity became independent of retinal illuminance according to Weber's law. However, with two subjects (O.U. and KT) the slope of increase was less than 0.5 at retinal illuminances below 1-3 td, possibly because of rod intrusion.

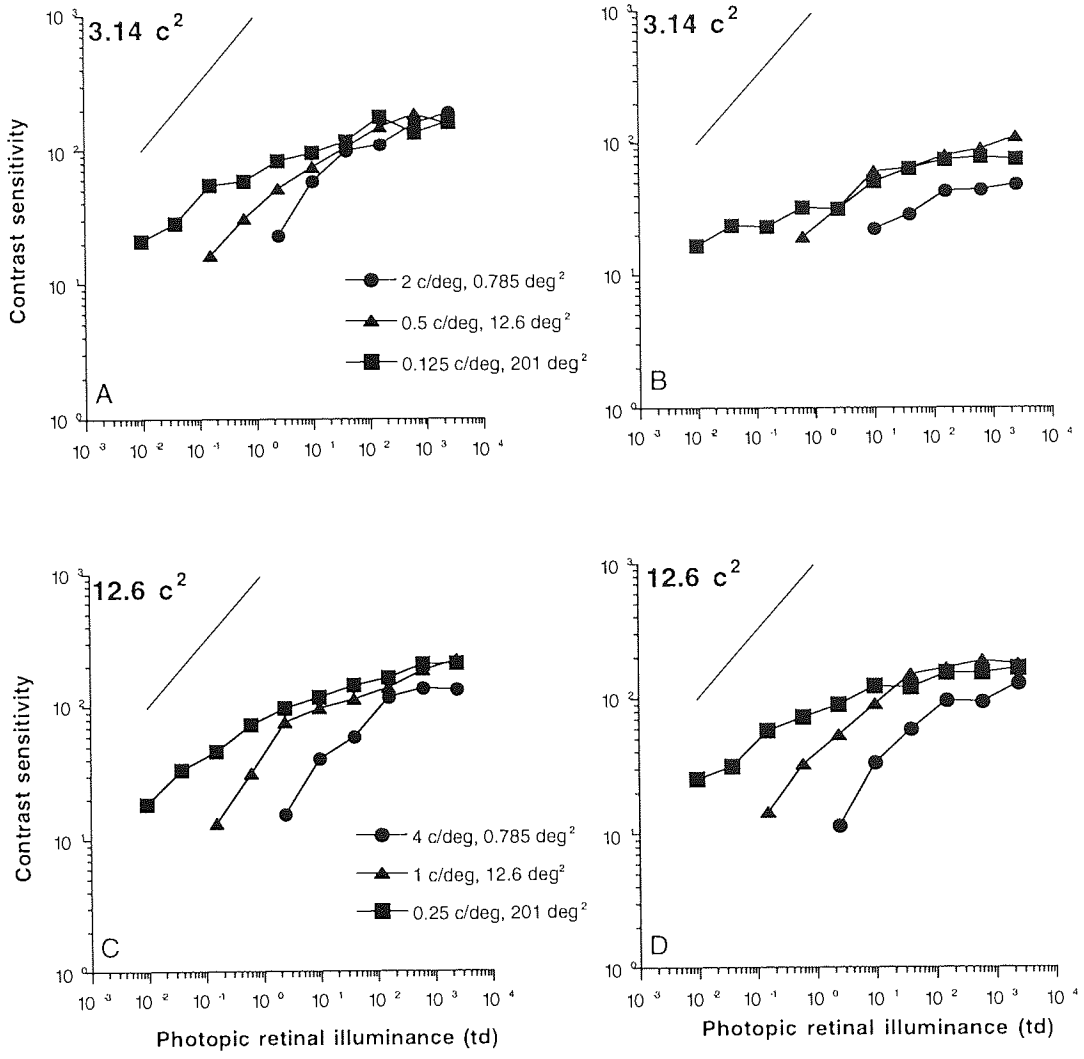

Fig. 3.1. *Monocular contrast sensitivity as a function of retinal illuminance for gratings with constant number of square cycles. A reference line indicates the slope of 0.5. Subjects JM (A, C), OU (B), HK (D).*

At high retinal illuminances contrast sensitivity for each number of square cycles was quite independent of spatial frequency, in agreement with Virsu and Rovamo (1979). However, although the number of square cycles was the same for all spatial frequencies in each frame contrast sensitivity decreased with increasing spatial frequency at lower levels of retinal illuminance.

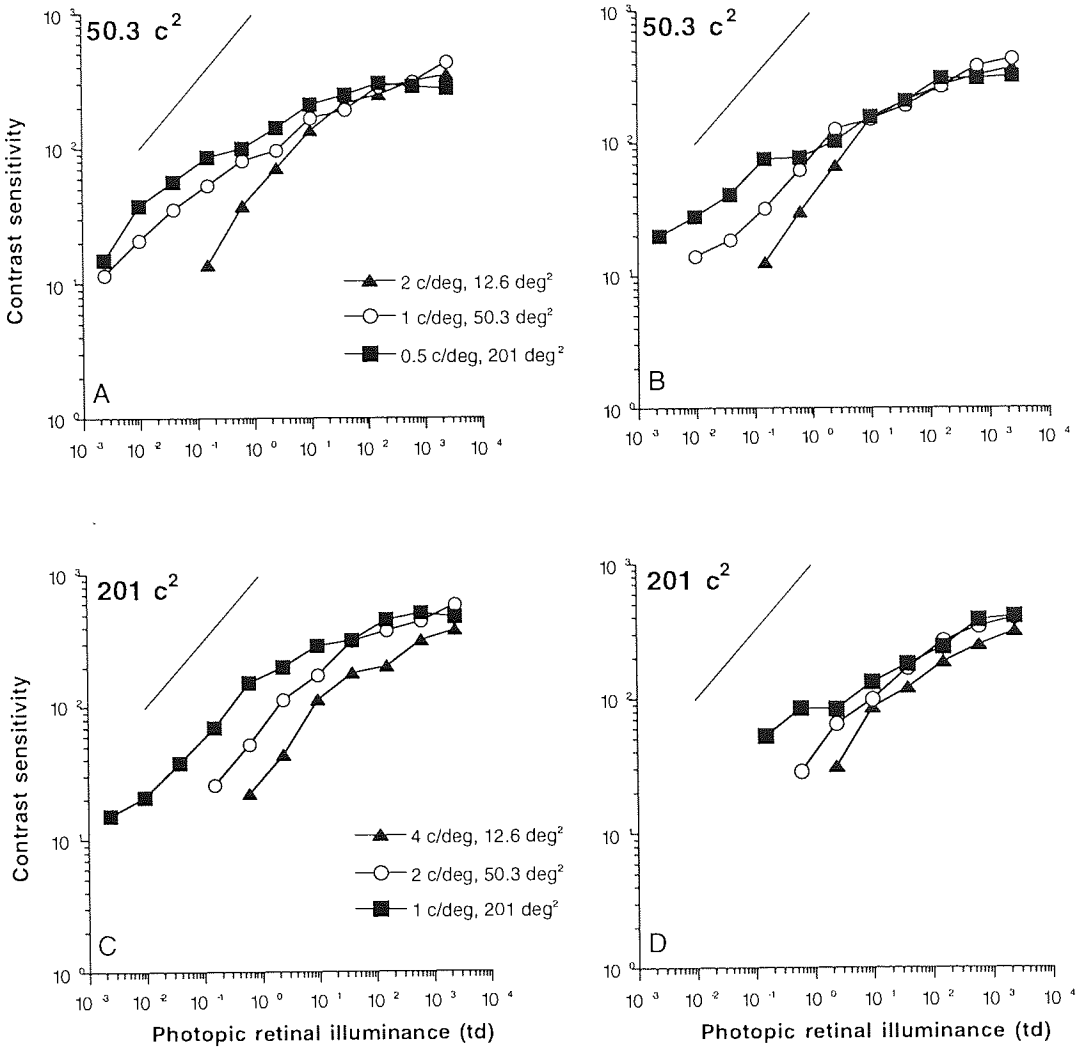

Fig. 3.2. *Monocular contrast sensitivity as a function of retinal illuminance for gratings with constant number of square cycles. A reference line indicates the slope of 0.5. Subjects JM (A, C), OL (B), KT (D).*

For each number of square cycles contrast sensitivity functions in Figs. 3.1 and 3.2 tend to have the same maximum sensitivity and shape, but the curves seem to be shifted along the horizontal axis towards lower retinal illuminances with decreasing spatial frequency. Based on the proportionality of I_c to spatial frequency squared (Van Nes & Bouman, 1967), the data of Figs 3.1 and 3.2

has been replotted as a function of retinal flux (If^{-2}) in Figs. 3.3 and 3.4, respectively.

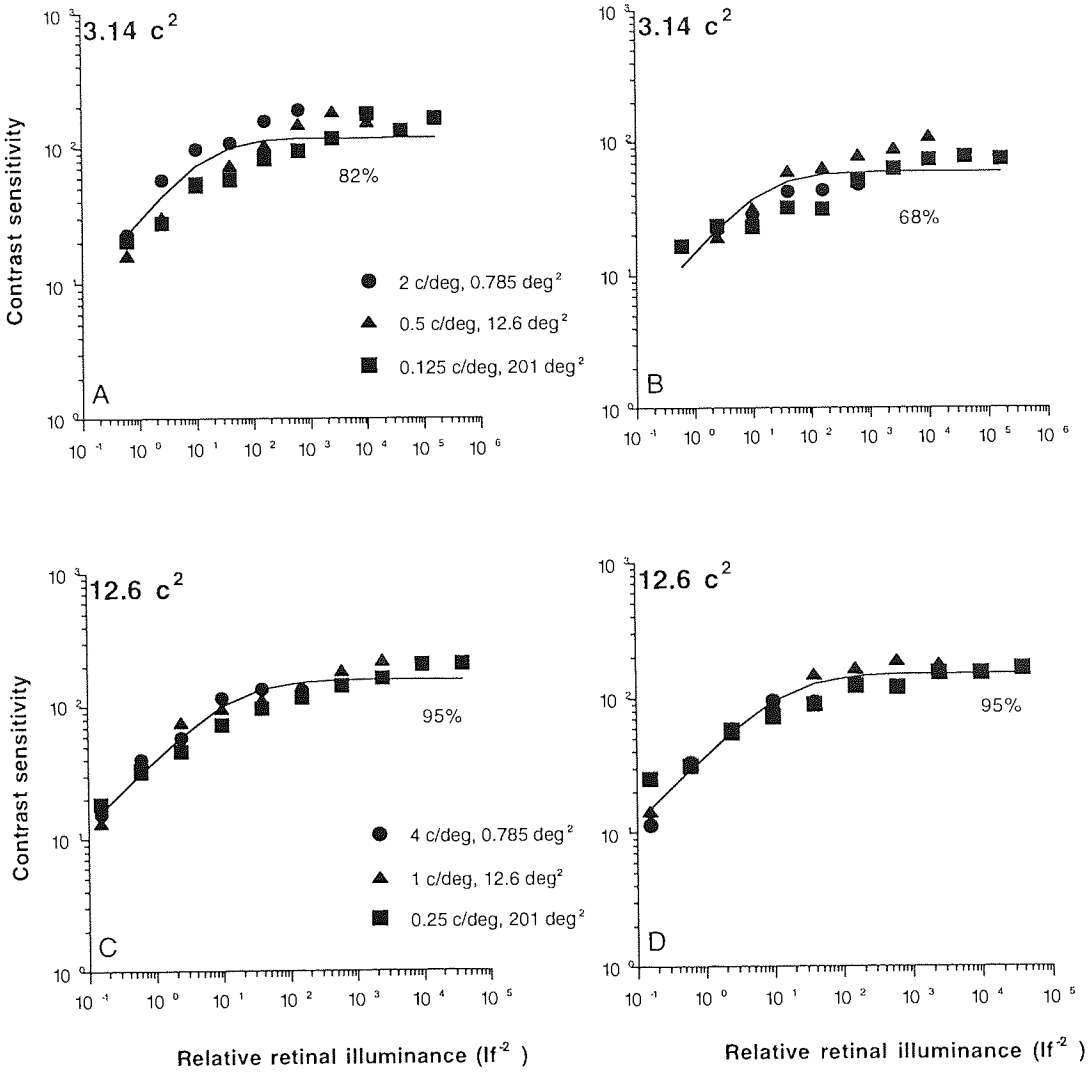

Fig. 3.3. *Data of Fig. 3.1 plotted as a function of retinal flux. A reference line indicates the slope of 0.5.*

The contrast sensitivity functions of Figs. 3.1 and 3.2 now collapsed together at all levels of retinal flux. Thus, contrast sensitivity for gratings with constant number of square cycles was independent of spatial frequency (f ≤4 c/deg) at all levels of retinal flux (If^{-2}). Scrutiny of Figs. 3.3 and 3.4 reveals that the

transition from DeVries-Rose to Weber's law now takes place at the same level of retinal flux (If^{-2}) for all grating areas studied.

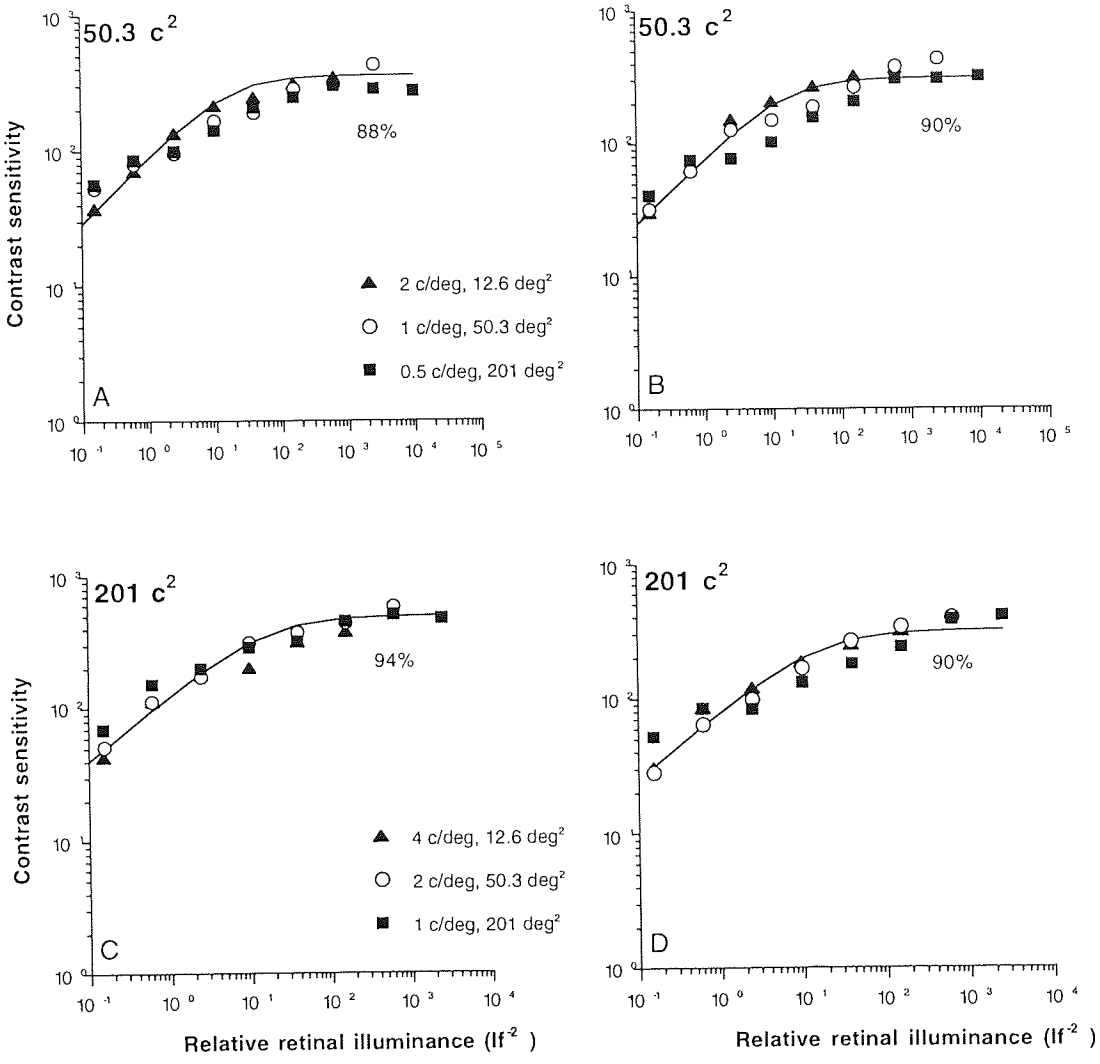

Fig. 3.4. *Data of Fig. 3.2 plotted as a function of retinal flux. A reference line indicates the slope of 0.5.*

To obtain the smooth least squares curves equation (3.4) was fitted to the data of Figs. 3.3 and 3.4 under the condition that S_{max} increases with the number of square cycles. In practice, contrast sensitivity values of Figs. 3.3 and 3.4 measured at each level of retinal flux were first averaged across all numbers of square cycles studied. Equation (3.4) was then fitted to the geometrical

mean in order to find an estimate for I_0, which was found to be 21 phot. td deg. Thereafter, contrast sensitivity values measured for each number of square cycles and each subject were first divided by $(1+ 21\ F^2/I)^{-0.5}$ after which they were geometrically averaged to obtain estimates of S_{max} for each subject and number of square cycles of 3.14 - 201. The explained variance was calculated according to Appendix 2. On the average it was 88%, with a range of 68-95%.

3.2.3. DISCUSSION

The experiments showed that contrast sensitivity with gratings of various areas (A) and spatial frequencies (f ≤4 c/deg) first obeyed DeVries-Rose law by increasing as a function of retinal illuminance (I) with a slope of 0.5. Then the increase saturated and contrast sensitivity became independent of retinal illuminance obeying Weber's law. The result is in agreement with Van Nes and Bouman (1967) who studied a partially overlapping range of spatial frequencies (0.5 and 4 - 48 c/deg) at a single grating area (37 deg^2). Contrast sensitivity functions for gratings with constant number of square cycles (Af^2) had a similar shape and maximum sensitivity but were shifted along the horizontal axis towards lower retinal illuminances with decreasing spatial frequency. When the same data was plotted as a function of retinal flux (If^{-2}), contrast sensitivity functions became similar for all spatial frequencies and fell on a common curve.

The experiments also showed that the transition from DeVries-Rose to Weber's law took place at the same level of retinal flux (If^{-2}) for all grating areas. The dependence of contrast sensitivity (S) on retinal illuminance (I) can then be described by $S = S_{max}\ (1+ I_0F^2/I)^{-0.5}$, where S_{max}, the maximum contrast sensitivity obtainable in bright light, is allowed to increase with the number of square cycles, F is f / (c/deg), and the value of I_0 indicates the

retinal illuminance that marks the transition between DeVries-Rose and Weber's laws at 1 c/deg.

The result that at high levels of retinal illuminance contrast sensitivity was independent of spatial frequency for gratings with constant number of square cycles (Af^2) at 0.125 - 4 c/deg is in agreement with Virsu and Rovamo (1979), who found a similar invariance at 1 - 4 c/deg. Pointer and Hess (1989) have shown that within 0.4 - 3.2 c/deg contrast sensitivity for Gaussian weighted gratings with a constant relative area is the same, but at 0.2 c/deg sensitivity is lower. However, my stimuli had sharply truncated edges and an abrupt on-off exposure implying that the independence of contrast sensitivity at 0.125 - 0.25 c/deg in my experiments was caused by sharply truncated edges.

The main finding of this experiment was that irrespective of grating area the transition from DeVries-Rose to Weber's law took place at the same level of retinal flux (If^{-2}) for all spatial frequencies. An explanation for this could be that the detection of each spatial frequency is mediated by mechanisms with circular receptive fields whose diameter decreases in proportion to increasing spatial frequency (see Graham, 1989). Then the luminous flux (light quanta per time unit) collected by the receptive fields decreases in proportion to increasing spatial frequency squared. Thus, the luminous flux collected in dim light would be greater for lower spatial frequencies, which could still be governed by Weber's law, whereas higher spatial frequencies with smaller receptive fields would have already entered the DeVries-Rose region. However, the above finding could equally well be explained by assuming that the effect of quantal or light dependent noise increases in proportion to spatial frequency squared. Thus, in dim light the detection of lower spatial frequencies could still be limited by internal neural noise so that Weber's law is valid whereas the detection of higher spatial frequencies would already be limited by quantal or light dependent noise so that DeVries-Rose law is valid.

An alternative but functionally equivalent explanation would be to assume that the spectral density of internal neural noise decreased in proportion to increasing spatial frequency squared.

Contrast sensitivity of an ideal observer that is solely limited by stimulus noise decreases in direct proportion to spatial frequency (f) for circular gratings of constant average luminance and number of cycles (Banks, Geisler & Bennett, 1987). Consequently, my finding that the dependence of contrast sensitivity (S) on retinal illuminance (I) can be described by $S = S_{max}\,(Af^2)\,(1+ I_oF^2/I)^{-0.5}$ indicates that also human performance in the DeVries-Rose region is dependent on spatial frequency similarly to an ideal observer limited by quantal fluctuations or light dependent noise.

Virsu and Rovamo (1979) have suggested that the number of neurones stimulated by a grating is determined by the number of square cycles not by grating area per se. Constant number of square cycles and constant retinal flux across spatial frequencies is thus analogous to MF-scaling (Rovamo & Virsu, 1979; Rovamo & Raninen, 1984), which was designed to keep the number of neurones stimulated and the amount of luminous flux collected constant (Shapley & Enroth-Cugell, 1984). MF-scaling was needed to make critical flicker frequency and cortical acuity independent of visual field location at all retinal illuminance levels (Rovamo & Raninen, 1984, 1990).

In conclusion, my experiments showed that contrast sensitivity functions for gratings of constant number of square cycles (Af^2) became independent of spatial frequency ($f \leq 4$ c/deg) and fell on a common curve when plotted as a function of retinal flux (If^{-2}).

3.3 CONTRAST SENSITIVITY AS A FUNCTION OF RETINAL ILLUMINANCE AND GRATING AREA

I have now shown that when the number of square cycles (Af^2) is constant, contrast sensitivity increases as a single saturating function of retinal flux at all spatial frequencies. Retinal flux (If^{-2}), calculated by dividing retinal illuminance (I) by spatial frequency (f) squared, is expressed in td deg^2. Division by spatial frequency squared normalises retinal illuminance and the effect of quantal noise in the sense that transition between DeVries-Rose and Weber's laws takes place at the same retinal flux irrespective of spatial frequency.

Next I will show that spatial integration is similar at different illuminance levels, in accordance with Savage and Banks (1992), although Hoekstra et al. (1974) found that spatial integration becomes less extensive at low light levels.

3.3.1. MODELLING THE CONTRAST SENSITIVITY IN QUANTAL NOISE

In this Section the contrast detection model of human visual system (Rovamo et al., 1993) is extended to low light levels by taking into account the effect of light-dependent quantal noise.

Before being interpreted by the human brain visual stimuli are filtered by the ocular optics and neural visual pathways. This complex neurobiological process can be modelled as a simple image processor shown in Fig. 3.5. The visual signal is first low-pass filtered by the optical modulation transfer function (O_{MTF}) of the eye. The light-dependent noise (N_q) is then added at the event of quantal absorption that takes place in the outer segments of photoreceptors. Addition of light-dependent noise (N_q) takes place after O_{MTF} because individual light quanta are not affected by the point spread function of the ocular optics. Thereafter comes neural high-pass filtering (P_{MTF}) reflecting the

lateral inhibition of visual pathways and addition of internal neural noise (N_i) before signal interpretation (e.g. detection, discrimination, recognition, restoration).

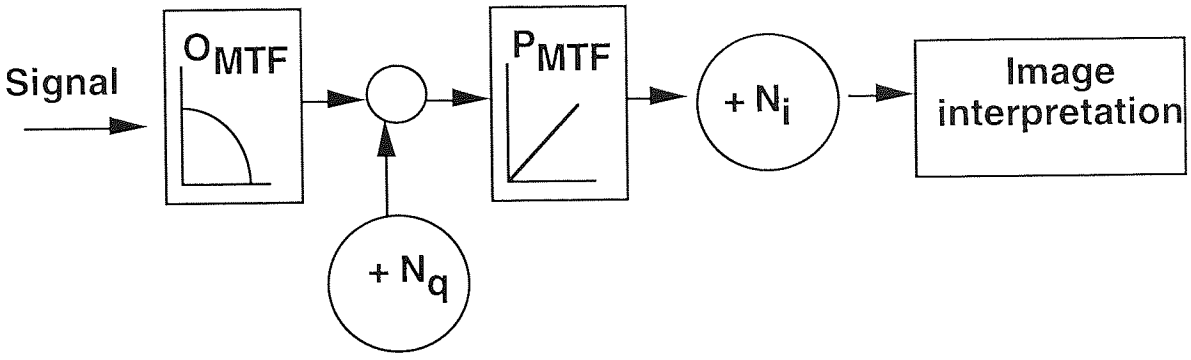

Fig. 3.5. *Human visual system as a simple image processor. First the visual signal is low-pass filtered by ocular optics, after which light-dependent quantal noise is added to the image at the event of quantal absorption. Neural visual pathways high-pass filter the signal, and finally internal neural noise is added before signal interpretation in the brain.*

Contrast sensitivity as a function of grating area and luminance

After the low-pass filtering of the optical modulation transfer function (O_{MTF}) of the eye and the high-pass filtering of the neural modulation transfer function (P_{MTF}) of visual pathways, the grating contrast energies at threshold are

$$E'_{human} = O_{MTF}^2(f)\, P_{MTF}^2(f)\, c^2\, A \qquad (3.5)$$

for the human detection filter and

$$E'_{ideal} = d'^2\, N, \qquad (3.6)$$

for the ideal detection filter. Here ideal detector refers to a global matched filter, which in white noise offers the best possible signal-to-noise ratio for a signal known exactly (Tanner & Birdsall, 1958). In equation (3.5) f is spatial frequency, A is grating area, c is the experimentally measured contrast of a

cosine grating at threshold, and c^2A is the corresponding contrast energy. In equation (3.6) d' is the detectability index (Tanner & Birdsall, 1958) and N is the spectral density of the total noise in the visual system. The detectability index refers to the signal-to-noise ratio at a detection filter. As the threshold estimation algorithm used in my study yields the probability level of 0.84 of correct responses in a two-alternative forced-choice task, the value of d' from Elliot's (1964) forced-choice tables is 1.4.

I now assume that image quality is very good so that image noise is negligible. Therefore, the total noise in the visual system is

$$N = P_{MTF}^2(f)\, N_q + N_i \qquad (3.7)$$

where N_q refers to the effective light-dependent quantal noise within the human eye and N_i to internal neural noise. As quantal noise (N_q), which is created at the event of quantal absorption according to the Poisson distribution of light, is unaffected by the O_{MTF} of ocular optics, it is only filtered by the neural modulation transfer function P_{MTF} of the visual pathways before N_i is added.

The efficiency (Tanner & Birdsall, 1958) of the human detection filter is $\eta = E'_{ideal} / E'_{human}$. By combining equations (3.5) - (3.7) we get

$$\eta = d'^2[P_{MTF}^2(f)\, N_q + N_i] / [O_{MTF}^2(f) P_{MTF}^2(f) c^2 A] \qquad (3.8)$$

Replacing contrast threshold (c) by contrast sensitivity (S), which is the inverse of c, we can write equation (3.8) as

$$S^2 = O_{MTF}^2(f)\, P_{MTF}^2(f)\, A\, \eta / \{d'^2\, [P_{MTF}^2(f)\, N_q + N_i]\} \qquad (3.9)$$

According to the contrast detection model of human spatial vision (Rovamo et al., 1993), visual signals are detected in the brain by a local matched filter whose efficiency for cosine gratings is

$$\eta = \eta_{max} (1 + A/A_c)^{-1}, \tag{3.10}$$

where η_{max} is maximum efficiency, A is grating area, and A_c is critical area marking the saturation of spatial integration and cessation of Piper's law. The saturation takes place in the range around $A = A_c$, where $\eta = \eta_{max}/2$. Equation (3.10) means that efficiency of small grating areas is equal to maximum efficiency (η_{max}), but efficiency of large gratings is equal to $(\eta_{max}A_c)/A$ thus decreasing in proportion to increasing area.

By combining equations (3.9) and (3.10) we get

$$S^2 = O_{MTF}^2(f)\, P_{MTF}^2(f)\, A\eta_{max}(1 + A/A_c)^{-1} d'^{-2} [P_{MTF}^2(f)\, N_q + N_i]^{-1} \tag{3.11}$$

By taking A into the parentheses and A_c out of the parentheses we get

$$S^2 = \eta_{max} d'^{-2}\, O_{MTF}^2(f)\, P_{MTF}^2(f) A_c\, [1 + A_c/A]^{-1} [P_{MTF}^2(f) N_q + N_i]^{-1}. \tag{3.12}$$

Further, by taking N_i out of the parentheses we get

$$S^2 = S_{max}^2\, [1 + A_c/A]^{-1}\, [P_{MTF}^2(f) N_q/N_i + 1]^{-1} \tag{3.13}$$

and

$$S_{max}^2 = K_0^2\, O_{MTF}^2(f)\, P_{MTF}^2(f)\, A_c, \tag{3.14}$$

where $K_0^2 = \eta_{max}(d'^2 N_i)^{-1}$ is a constant independent of spatial frequency. S_{max} refers to the maximum contrast sensitivity obtainable by spatial integration in bright light at the exposure duration used. In equation (3.14) variables A_c,

O_{MTF}, and P_{MTF} all depend on spatial frequency but parameters η_{max}, d', and N_i are constant. Thus, at all spatial frequencies S_{max} is proportional to the product of $\sqrt{A_c}$,O_{MTF}, and P_{MTF}.

Internal neural and critical quantal noises

Let the critical spectral density (N_{qc}) of the effective quantal noise transferred through the ocular optics and neural visual pathways be equal to N_i. As mentioned earlier, N_{qc} is not affected by O_{MTF} because light quanta cannot be blurred by the point spread function of eye optics. Thus,

$$P_{MTF}^2(f)\, N_{qc} = N_i. \qquad (3.15)$$

Equation (3.15) means that the critical spectral density of effective quantal noise (N_{qc}) transferred into the brain is equal to the spectral density of internal neural noise (N_i). The equation also means that if it was possible to backproject the internal neural noise into the outer segments of retinal receptors, it would be equivalent to critical quantal noise.

Retinal illuminance and quantal noise

Let retinal illuminance (I) correspond to n quanta on the average. Because light quanta obey Poisson distribution, one standard deviation from the mean is equal to $\sqrt{n}$. By definition, r.m.s. contrast of noise is equal to standard deviation divided by the mean i.e. $c = \sqrt{n}/n = 1/\sqrt{n} = 1/\sqrt{I}$. Quantal noise is white because the number of quanta falling onto neighbouring retinal locations at any time are uncorrelated. Therefore, by definition (Legge, Kersten & Burgess, 1987) the spectral density of quantal noise (N_q) is proportional to its r.m.s. contrast squared, which is equal to I^{-1}. Thus,

$$N_q = K/ I, \qquad (3.16)$$

If detection always takes place at a constant signal-to-noise ratio $d' = c_{r.m.s}/c_n$, and as $c_n \sim kI^{-0.5}$, also $c_{r.m.s}$ must be $\sim I^{-0.5}$, and hence contrast sensitivity $S \sim I^{0.5}$ thus obeying DeVries-Rose law, when detection is limited by quantal noise.

Critical retinal illuminance

According to equation (3.16) we also get

$$N_{qc} = K / I_c , \qquad (3.17)$$

where I_c is the critical retinal illuminance marking the transition between DeVries-Rose and Weber's laws. By substituting equations (3.15) - (3.17) into equation (3.13) we get

$$S^2 = S_{max}^2(1+A_c/A)^{-1}(1+N_q/N_{qc})^{-1} = S_{max}^2(1+A_c/A)^{-1}(1+I_c/I)^{-1}. \qquad (3.18)$$

Equation (3.18) means that at constant retinal illuminance $S = S'_{max}(1+A_c/A)^{-0.5}$, where $S'_{max} = S_{max}(1+I_c/I)^{-0.5}$. Thus contrast sensitivity for large gratings is constant equal to the maximum contrast sensitivity S'_{max}. However, for small gratings contrast sensitivity increases in proportion to the square root of area (A), obeying Piper's law (1903).

When grating area is constant equation (3.18) means that $S = S''_{max}(1+I_c/I)^{-0.5}$, where $S''_{max} = S_{max}(1+A_c/A)^{-0.5}$. Thus contrast sensitivity in bright light obeys Weber's law being constant equal to the maximum contrast sensitivity S''_{max}, because contrast sensitivity is independent of retinal illuminance. However, in

dim light contrast sensitivity obeys DeVries-Rose law increasing in proportion to the square root of retinal illuminance.

The dependence of A_c on spatial frequency

According to the contrast detection model of human vision (Rovamo et al., 1993b) the critical area of spatial integration is defined as

$$A_c = A_0 (1 + f^2 / f_0^2)^{-1}, \qquad (3.19)$$

where A_0 is the maximum area of spatial integration, f is spatial frequency, and f_0 is the critical spatial frequency. This means that A_c is a constant equal to A_0 at very low spatial frequencies but equal to $(A_0 f_0^2) f^{-2}$ at very high spatial frequencies, i.e. A_c decreases in inverse proportion to spatial frequency squared. The critical number of square cycles is defined $Z_c = A_c f^2 = Z_0(1 + f_0^2/f^2)^{-1}$, where $Z_0 = A_0 f_0^2$. This means that for $f << f_0$ the critical number of square cycles $Z_c = A_0 f^2$ thus increasing in proportion to spatial frequency squared whereas Z_c is constant equal to Z_0 when $f >> f_0$.

3.3.2. METHODS

3.3.2.1. Apparatus, Stimuli and Procedures

The apparatus, stimuli, and procedures are described in Chapter 2, General Methods. Therefore again only the special features are described here. The stimuli consisted of vertical cosine gratings within sharp-edged circular apertures of 0.5, 1, 2, 4, 8, and 16 cm in diameter. The equiluminous surround was limited to a circular aperture of 20 cm in diameter by black cardboard. Spatial frequency on the screen varied within 0.125 - 4 c/cm, and the viewing distance within 28.6 - 458 cm. Additional amount of light needed in the

experiment of Fig 3.7 was produced by two defocused slide projectors placed on both sides of the observer and obliquely directed towards the screen.

3.3.2.2. Subjects

Six experienced subjects, aged 24-33 years, served as observers. Each subject used his/her dominant eye. H.K. was an uncorrected hyperope (0.50 DS), and O.L., J.M., P.M., K.T., and O.U. were corrected myopes (1- 6 DS). None had astigmatism greater than 0.25 D. Their accommodation had a range of at least 6 D. Hence, they were emmetropes at the viewing distances used in my experiments. With optimal refraction their binocular Snellen acuities at 5 m were within 1.3-1.7.

The least square curves

Contrast sensitivity as a function of retinal illuminance was modelled already in Section 3.2 by equation

$$S = S_{max} (1+I_c / I)^{-0.5} \qquad (3.3)$$

which was now fitted to the contrast sensitivity data of Figs 3.6 and 3.7.A by the method of least squares (see Appendix 3).

Contrast sensitivity as a function of grating area was modelled by fitting equation

$$S = S'_{max} (1+A_c / A)^{-0.5} \qquad (3.20)$$

to the data of Figs 3.7.B and 3.8. with the method of least squares.

Optical attenuation as a function of spatial frequency was modelled as a low-pass filter according to Johnson (1972). Hence, equation

$$S_0 O_{MTF}(f) = S_0 \exp [-(f / f_c)^n] \qquad (3.21)$$

was fitted to the data of Fig. 3.9.B at 0.5 - 32 c/deg with the method of least squares. In equation (3.21) f_c refers to the spatial frequency at which O_{MTF} has decreased to 1/e and S_0 is the value of S_{max} at spatial frequencies where O_{MTF} is still equal to unity, and on the basis of equation (3.19) $P_{MTF}\sqrt{A_c}$ is already constant equal to $f_0\sqrt{A_0}$, because $f > f_0$ and $P_{MTF}(f) = F$ (Rovamo & al., 1993). Hence, according to equation (3.14) $S_0 = K_0 f_0 \sqrt{A_0}$.

3.3.3. RESULTS

In the experiments of Figs 3.6 and 3.7.A. I measured contrast sensitivity as a function of retinal illuminance for vertical cosine gratings at spatial frequencies of 0.125 - 32 c/deg. Retinal illuminance varied across 8 logarithmic units from 1.50×10^{-4} to 2.50×10^{4} phot. td, whereas retinal flux (If^{-2}) varied from 2.39×10^{-3} phot. td deg^2 at 2 c/deg to 1.61×10^{5} phot. td deg^2 at 0.125 c/deg. Test grating areas covered a range from 0.00649 deg^2 to 804 deg^2 as shown in Appendix 7. The number of square cycles (Af^2) varied from 0.785 to 3220.

Figs 3.6 and 3.7.A. show that contrast sensitivity increased with retinal illuminance at all spatial frequencies and grating areas. The slope of increase was 0.5 at low levels of retinal illuminance, obeying DeVries-Rose law (DeVries, 1943; Rose, 1948). At high levels of retinal illuminance the increase saturated and contrast sensitivity became independent of luminance level, obeying Weber's law. The data also shows that at low spatial frequencies contrast sensitivity fell between DeVries-Rose and Weber's laws at intermediate light levels, in agreement with Kelly (1972), Koenderink et al.

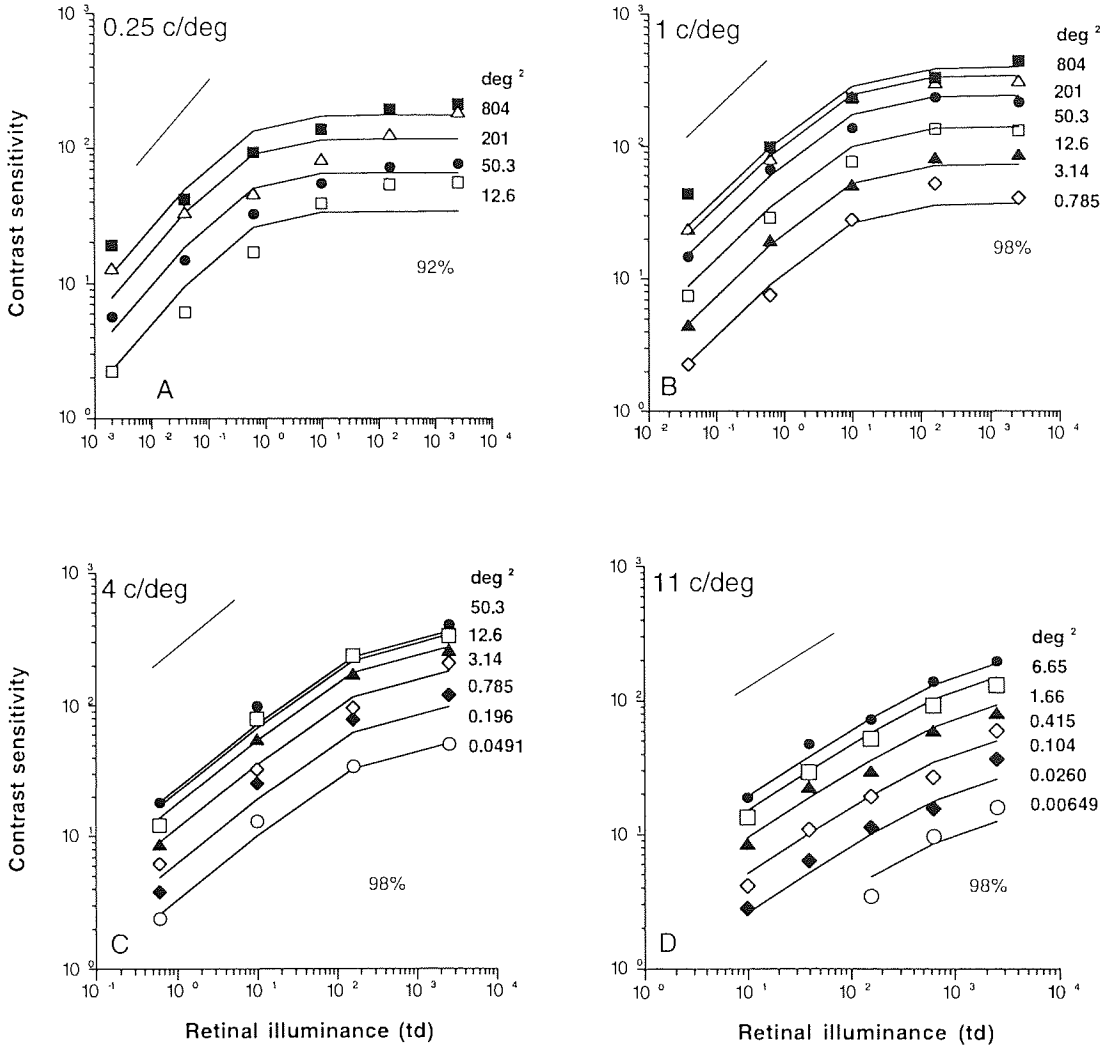

Fig. 3.6. *Contrast sensitivity as a function of retinal illuminance at spatial frequencies of 0.25, 1, 4, and 11 c/deg. Grating area is indicated by the smooth curves.*

(1978), and Savage and Banks (1992). The critical retinal illuminance marking the transition between DeVries-Rose and Weber's laws increased with spatial frequency, in accordance to Van Nes and Bouman (1967) and my previous study in Section 3.2. However, critical illuminance (I_c) was independent of grating area (A), because the contrast sensitivity functions measured for each spatial frequency in Fig. 3.6 were parallel at all grating areas.

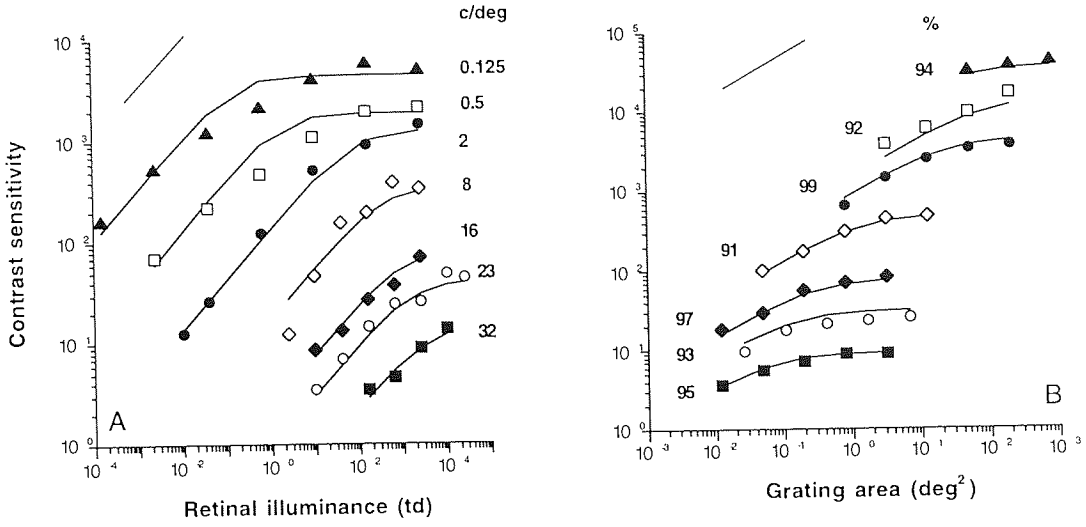

Fig. 3.7. *Contrast sensitivity as a function of A) retinal illuminance and B) grating area for various spatial frequencies. At 0.125 - 16 c/deg curves and datapoints have been shifted upwards for more clear presentation by factors 48, 8, 4, 3, and 2 in (A), and by 360, 36, 12, 4, and 2 in (B).*

In the experiments of Fig. 3.7.B. I measured contrast sensitivity as a function of grating area for vertical cosine gratings at spatial frequencies 0.125, 0.5, 2, 8, 16, 23, and 32 c/deg. Grating area varied from 0.0123 deg^2 at 32 c/deg to 804 deg^2 at 0.125 c/deg. The number of square cycles (Af^2) varied again from 0.785 to 3220. Retinal illuminance was 2510 phot. td. In Fig. 3.8 the contrast sensitivity data of Fig. 3.6 have been replotted as a function of grating area. In Figs 3.7.B and 3.8 retinal flux (If^{-2}) varied from 3.83×10^{-2} phot. td deg^2 at 0.25, 1, and 4 c/deg to 1.61×10^5 phot. td deg^2 at 0.125 c/deg.

As Figs 3.7.B and 3.8 show, contrast sensitivity increased with grating area at all spatial frequencies and retinal illuminance levels. The slope of increase was about 0.5 at small grating areas, obeying Piper's (1903) law. The increase then saturated at large grating areas and contrast sensitivity became independent of area. Scrutiny of the data revealed that the critical grating area marking the cessation of Piper's law and saturation of spatial integration

decreased with spatial frequency, in agreement with Virsu and Rovamo (1979) and Rovamo et al. (1993b). However, critical area (A_c) was independent of retinal illuminance (I), because the contrast sensitivity functions measured for each spatial frequency in Fig. 3.8 were parallel at all levels of retinal illuminance.

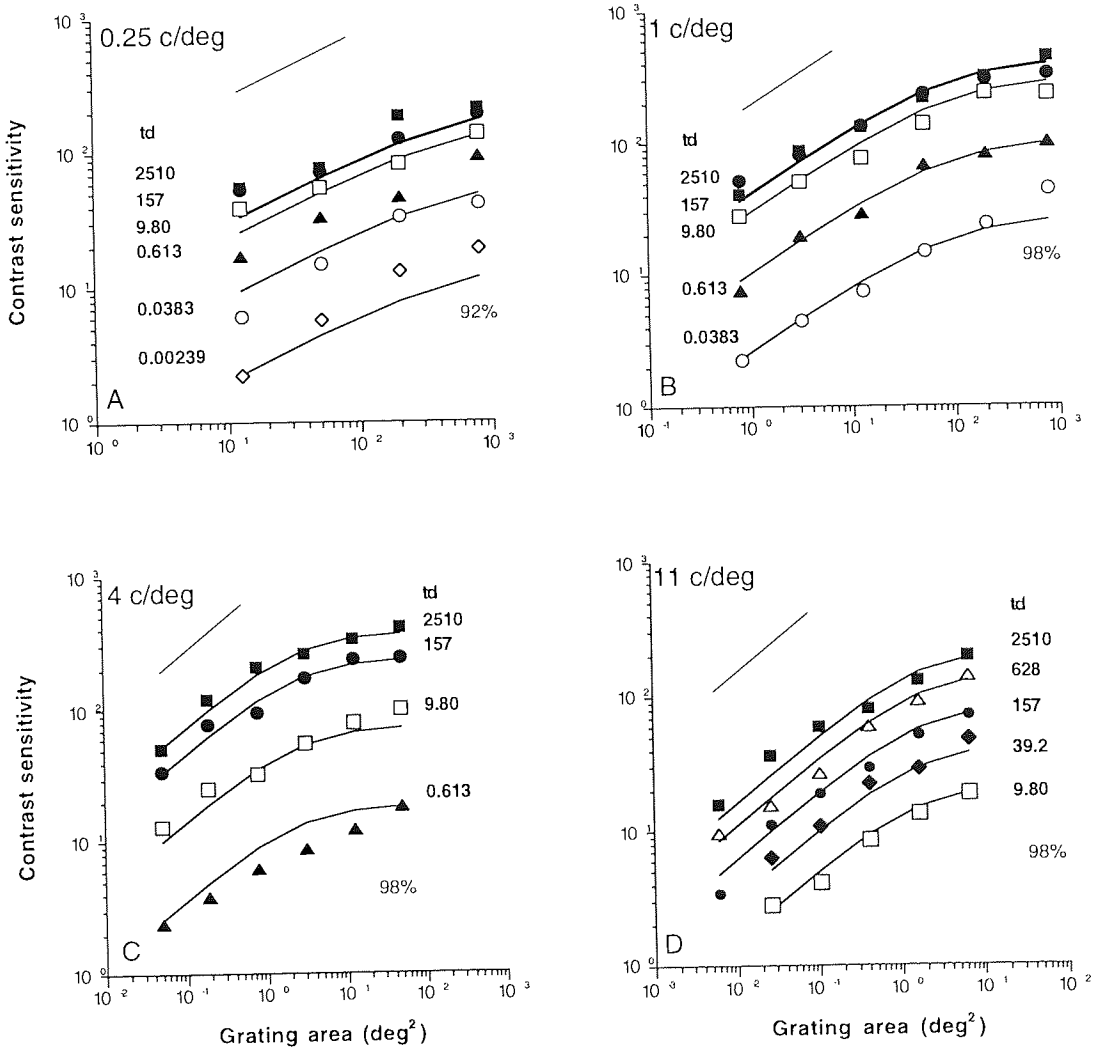

Fig. 3.8. *The data of Fig 3.6 replotted as a function of grating area*

Equation (3.18) was fitted to the data of Figs 3.6 - 3.8 in the following way: The contrast sensitivity functions of Fig. 3.6 for each spatial frequency were averaged in the vertical direction across grating areas and equation (3.3) was fitted to this geometrical average in order to find the values of I_c for 0.25, 1, 4,

and 11 c/deg. Similarly, equation (3.3) was fitted to the contrast sensitivity functions of Fig. 3.7.A in order to find the values of I_c for 0.125, 0.5, 2, 8, 16, 22, and 32 c/deg. The contrast sensitivity functions of Fig. 3.8 for each spatial frequency were also averaged in the vertical direction across retinal illuminances and equation (3.20) was fitted to this geometrical average in order to find the values of A_c for 0.25, 1, 4, and 11 c/deg. And similarly, equation (3.20) was fitted to the contrast sensitivity functions of Fig. 3.7.B. in order to find the values of A_c for 0.125, 0.5, 2, 8, 16, 22, and 32 c/deg. Thereafter on the basis of equation (3.18) the contrast sensitivity values measured for each spatial frequency at various grating areas and levels of retinal illuminance were first divided by the corresponding values of the expression $[(1+A_c/A)(1+I_c/I)]^{-0.5}$ and finally geometrically averaged in order to get the estimates of S_{max} for 1-32 c/deg.

The smooth curves in Figs. 3.6 - 3.8 were calculated by equation (3.18) fitted to the data of each spatial frequency separately. The explained variance was on average 95%, with a range of 91 - 99 % for 0.125 - 32 c/deg.

In Fig. 3.9.A critical retinal illuminance (I_c) marking the transition between DeVries-Rose and Weber's laws was plotted as a function of spatial frequency in double logarithmic co-ordinates. As explained above, the estimates of I_c were obtained when equation (3.18) was fitted to the data of Figs 3.6 - 3.7.A. Fig. 3.9.A shows that log I_c increased linearly with log f of 0.125 to 32 c/deg with a slope of 2, which means that I_c increased in direct proportion to spatial frequency squared, in agreement with my previous study (Section 3.2) and Van Nes et al. (1967). This means that the critical retinal flux, calculated by dividing critical retinal illuminance (I) by spatial frequency (f) squared, was constant within 0.125-32 c/deg. The straight line in Fig. 3.9.A was calculated by equation $I_c = I_0F^2$ fitted to the data. The explained variance was 97%. The

value of I_0 = 7.9 phot. td. deg^2 in the least squares equation refers to the critical retinal flux that is valid for all spatial frequencies.

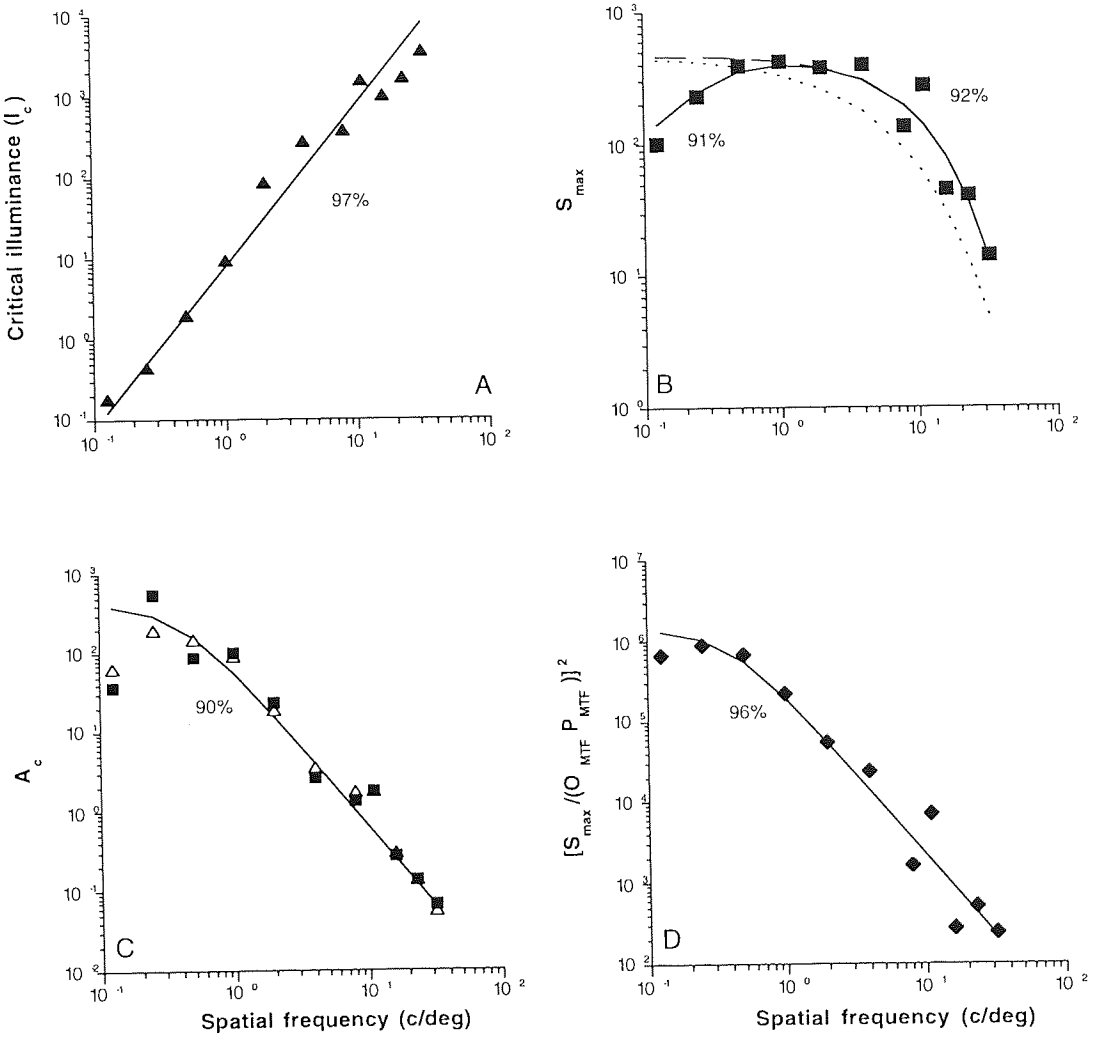

Fig. 3.9. *A) Critical illuminance as a function of spatial frequency. B) Maximum contrast sensitivity and an estimate by the model (dashed + solid curve), O_{MTF} (solid curve), and the O_{MTF} of Deeley et al.,(1991) (dotted curve) as a function of spatial frequency. C) Critical area as a function of spatial frequency. Open symbols from Rovamo et al. (1993). D) The estimates of $[S_{max}/(O_{MTF}\,P_{MTF})]^2$ as a function of spatial frequency.*

In Fig. 3.9.B the maximum contrast sensitivity (S_{max}) was plotted as a function of spatial frequency in double logarithmic co-ordinates. The estimates of S_{max} were obtained when equation (3.18) was fitted to the data of Figs. 3.6 - 3.8. It is

seen in Fig. 3.9.B that S_{max} first increased with spatial frequency at 0.125 - 0.5 c/deg, was constant at 0.5-4 c/deg and then decreased with increasing spatial frequency at 4-32 c/deg.

The slope of increase was about 1 in Fig. 3.9.B, which is in agreement with the extended model of contrast detection in human vision: According to equation (3.14) S_{max} is proportional to the product of O_{MTF}, P_{MTF} and $\sqrt{A_c}$. Hence, S_{max} increases in proportion to spatial frequency at low spatial frequencies, because O_{MTF} is approximately equal to unity (Deeley et al., 1991), P_{MTF} is proportional to spatial frequency and A_c is constant at low frequencies (Rovamo et al., 1993b). The increase of S_{max} at f = 0.125 - 0.5 c/deg was therefore due to the neural modulation transfer function, $P_{MTF}(f) = F$ (lateral inhibition), revealed by the breakdown of scale invariance (A_c is constant) at low spatial frequencies.

The decrease of S_{max} at medium and high spatial frequencies is on the basis of equation (3.14) solely due to contrast attenuation resulting from the O_{MTF} of the human eye, because P_{MTF} is directly proportional but $\sqrt{A_c}$ is inversely proportional to spatial frequency at medium and high spatial frequencies (Rovamo et al., 1993b). Optical attenuation as a function of spatial frequency was modelled by a low-pass filter (Johnson, 1972). Its parameters f_c and n were estimated by fitting equation (3.21) to the S_{max} data at 0.5 - 32 c/deg of Fig. 3.9.B. The value of f_c indicating the spatial frequency where maximum contrast sensitivity has decreased to 1/e was found to be 9.10 c/deg, and the value of n, indicating how steeply the O_{MTF} decreases above f_c, was found to be 1.0, S_0 was found to be 470. The least squares equation obtained is thus $S_0\, O_{MTF}(f) = 470 \exp [-(f/9.10)^{1.0}]$. The dashed curve was calculated by equation (3.21) fitted to the data of Fig. 3.9.B at 0.5 - 32 c/deg. The explained variance at 0.5 - 32 c/deg was 92%.

In Fig. 3.9.C. the critical area (A_c) marking the cessation of Piper's law and saturation of spatial integration was plotted as a function of spatial frequency in double logarithmic co-ordinates. My estimates of A_c were obtained when equation (3.20) was fitted to the data of Figs 3.7.B. - 3.8. Fig. 3.9.C. also shows the estimates of A_c for simple cosine gratings from Rovamo et al. (1993b). At 0.125 - 0.5 c/deg A_c tended to be constant independent of spatial frequency but then decreased linearly with increasing spatial frequency at 1 - 32 c/deg with a slope of -2 on log-log co-ordinates, which means that A_c decreased in inverse proportion to spatial frequency squared. Hence, the critical number of square cycles, calculated by multiplying critical grating area (A) by spatial frequency (f) squared, was constant at 1 - 32 c/deg. The deviation of A_c from the straight line at spatial frequencies of 0.125 - 0.5 c/deg means that scale invariance (e.g. Näsänen et al., 1993) broke down at low spatial frequencies.

For Fig. 3.9.D S_{max} was first divided by O_{MTF} and P_{MTF} and then squared, because according to equation (3.14) this new measure is proportional to A_c. Then $S_{max}^2/(O_{MTF}\ P_{MTF})^2$ was plotted as a function of spatial frequency in double logarithmic co-ordinates. As Fig. 3.9.D shows, the new measure behaved like A_c tending to be constant at low spatial frequencies but decreased linearly with increasing spatial frequency of 0.5 to 32 c/deg. The slope of decrease was again -2.

In order to obtain an estimate for critical spatial frequency f_0, equation (3.19) was fitted to my data in Figs 3.9.C. and 3.9.D. averaged geometrically at each spatial frequency. Critical spatial frequency was found to be $f_0 = 0.39$ c/deg. Thereafter, on the basis of equation (3.19), the values of A_c at each spatial frequency (my datapoints in Fig. 3.9.C) were first divided by the corresponding values of expression $(1 + f^2 / 0.39^2)^{-1}$ and then geometrically averaged in order to get an estimate for A_0, which was found to be 420. The smooth curve in Fig. 3.9.C. was then calculated by equation $A_c = 420\ (1 + f^2 / 0.39^2)^{-1}$. The

explained variance was 90%. The equation means that critical area of spatial integration was constant 420 deg^2 at low spatial frequencies but decreased in inverse proportion to spatial frequency squared above 0.39 c/deg. The critical number of square cycles ($A_c f^2$) increased in proportion to spatial frequency squared below 0.39 c/deg but was constant equal to $Z_0 = 64.3\ c^2$ at higher spatial frequencies.

The smooth (dashed+solid) curve in Fig. 3.9.B was calculated by using the combination of equations (3.14), (3.19), (3.21) and the fact that $P_{MTF}(f) = F$. $K_0 = 56.8$ was obtained from of the relationship $S_0 = K_0 f_0 \sqrt{A_0}$. The explained variance was 91%. On the basis of equation (3.14) the smooth curve in Fig. 3.9.D. was calculated by multiplying the value of equation (3.19) at each spatial frequency by $K_0^2 = 3430$. The explained variance was 96%.

Using the combination of equations (3.14), (3.18), (3.19), (3.21) and the finding that $I_c = 7.9F^2$ I calculated the values of contrast sensitivity at all spatial frequencies, grating areas and retinal illuminances studied and found that the calculated values explained 92% of the total variance of the contrast sensitivity data in Figs 3.6 - 3.8.

In order to compare the predictions of the extended model of contrast detection in human vision with the experimental data of Van Nes & Bouman (1967) I calculated contrast sensitivity values at various spatial frequencies (5-48 c/deg) and levels of retinal illuminance (0.009 - 900 td) for a grating area of 37 deg^2 using equations (3.14), (3.18), (3.19), (3.21) together with the finding that $I_c = 7.9F^2$ and plotted the values as a function of spatial frequency in Fig. 3.10.A.

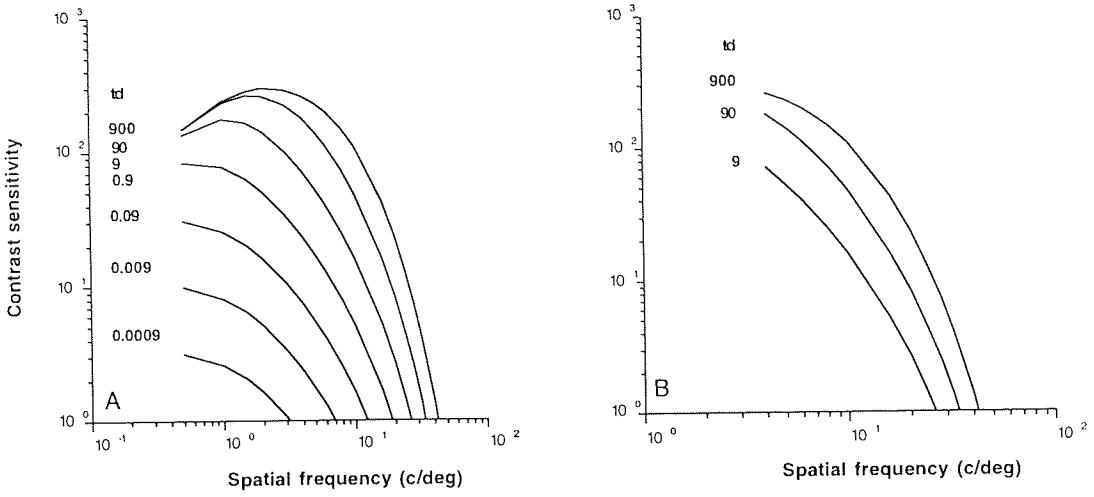

Fig. 3.10 *A) Monocular contrast sensitivity functions predicted by the model for various illuminance levels at grating area of 37 deg^2. B) The curves at 9 - 900 td replotted from (A) within spatial frequencies 5 - 40 c/deg.*

With decreasing retinal illuminance the shape of the spatial contrast sensitivity function changed from band-pass to low-pass. The decrease of contrast sensitivity with retinal illuminance was greater at high than low spatial frequencies. The contrast sensitivity functions for 9-900 phot td converged at low spatial frequencies. All these predictions agree with the experimental data of Van Nes and Bouman (1967).

In addition, the calculated spatial contrast sensitivity functions at 9, 90, and 900 phot. td which are partially redrawn in Fig. 3.10.B. can be compared with the experimental data of Banks, Geisler and Bennett (1987). They measured contrast sensitivity for 5-40 c/deg at 11, 110 and 1,100 phot. td with gratings having a constant number of square cycles at all spatial frequencies. The comparison is valid because at 5-40 c/deg the grating area of 37 deg^2 used in my calculations is greater than the saturation limit A_c of spatial integration that is constant in square cycles. At 9 - 900 phot. td the spatial contrast sensitivity functions for 5-40 c/deg were parallel in Fig. 3.10.B, in agreement with Banks

et al. (1987). The sensitivities I obtained were, however, higher because Banks et al. (1987) used gratings damped in space by half-cosine.

3.3.4. DISCUSSION

The main finding of my experiments was that the increase of contrast sensitivity with retinal illuminance was similar at all grating areas and the increase of contrast sensitivity with grating area was similar at all light levels. In fact, the dependence of contrast sensitivity on grating area and retinal illuminance for cosine gratings was described by equation (3.18) at spatial frequencies of 0.125-32 c/deg. The explained variance was on average 92%, with a range of 91 - 99 %. The equation means that contrast sensitivity increased in proportion to the square root of area at small grating areas, as predicted by Piper's law, and in proportion to the square root of retinal illuminance in dim light, as predicted by DeVries-Rose law, but was independent of area at large grating areas and of retinal illuminance in bright light, obeying Weber's law.

The experimental data showed that $I_c = I_0 F^2$, where I_0 = 7.9 phot. td deg^2 and F = f /(c/deg). The explained variance was 97%. The finding means that critical retinal illuminance increased in proportion to spatial frequency squared at 0.125-32 c/deg, in agreement with Van Nes et al. (1967) and the study introduced in Section 3.2. The value of I_0, calculated by dividing critical retinal illuminance (I_c) by spatial frequency squared, indicates the critical retinal flux valid for all spatial frequencies. My present result thus agrees with my previous finding that the transition between DeVries-Rose and Weber's laws takes place at the same retinal flux irrespective of spatial frequency. The estimate of I_0 is in accordance with Section 3.2, where I_0 = 21 phot. td deg^2 for spatial frequencies 0.125 - 4 c/deg.

Analysis of the experimental data showed that $A_c = 420\ [1+(f/0.39^2)]^{-1}$ with an explained variance equal to 92%. The equation means that critical grating area was constant $A_0 = 420$ deg^2 at low spatial frequencies but decreased in inverse proportion to spatial frequency squared above $f_0 = 0.39$ c/deg. The critical number of square cycles was found to be $Z_c = 64.3\ [1 + (0.39/ f)^2]^{-1}$, which means that it increased in proportion to spatial frequency squared below 0.39 c/deg but was constant $Z_0 = 64.3$ c^2 at higher spatial frequencies. The above findings at medium and high spatial frequencies agree with the results of Virsu and Rovamo (1979) obtained in bright light. The estimates are also in agreement with Rovamo et al. (1993) who measured spatial integration only in bright light and found $A_0 = 269$ deg^2, $f_0 = 0.650$ c/deg, and $Z_0 = 114$ c^2.

According to Savage & Banks (1992) the equivalent number of cycles marking the point at which the best-fitting curve for contrast sensitivity vs. number of cycles first fell below 1 seems to increase with spatial frequency at 0.12-2.0 c/deg in scotopic vision. However, comparison with Fig. 3B of Rovamo et al. (1993) would suggest that in Fig. 4 of Savage & Banks (1992) the equivalent number of cycles is in fact constant above 0.5 c/deg but corresponds to a constant size in degrees of the visual field at lower spatial frequencies, in agreement with Rovamo et al. (1993). According to Banks et al. (1992) the equivalent number of cycles increases by a factor of two from 0.5 to 6.5 c/deg and remains constant thereafter. This is also in agreement with Fig. 3B of Rovamo et al. (1993b).

Analysis of the experimental data also showed that at medium and high spatial frequencies the maximum contrast sensitivity $S_{max} = 470\ O_{MTF}(f)$, where $O_{MTF}(f) = \exp\ [-(f/9.1)^{1.0}]$. The explained variance was 92%. The equation means that $O_{MTF}(f)$ was independent of spatial frequency at low spatial frequencies but decreased with a slope of 1.0 above 9.1 c/deg.

According to equation (3.14) S_{max} is directly proportional to the product of O_{MTF}, P_{MTF}, and $\sqrt{A_c}$. Analysis of the experimental data revealed that the proportionality constant $K_0 = 56.8$. Rovamo et al. (1993b) found K_0=96.3 in bright light. In fact, their $K_0 = 68.1$, but it was multiplied by $\sqrt{2}$ for comparison, because their S_{max} was expressed in terms of Michelson contrast. At medium spatial frequencies S_{max} was constant $S_0 = 470$. In bright light Rovamo et al. (1993b) found $S_0 = 1030$ when expressed in terms of r.m.s. contrast. In their experiments viewing was binocular whereas in my experiments it was monocular, which (see e.g. Anderson & Movshon, 1989) evidently explains most of the 2 -fold difference between the estimates of K_0 and S_0. The combination of equations (3.14), (3.19), and (3.21) together with the fact that $P_{MTF}(f)$ is proportional to f was found to explain 91% of the total variance of the values of S_{max} at 0.125-32 c/deg.

The combination of equations (3.14), (3.18), (3.19), (3.21) and the finding that $l_c = 7.9\ F^2$ was found to explain 92% of the total variance of the contrast sensitivity data in Figs. 3.6 - 3.8. In double logarithmic co-ordinates the inter-subject correlation coefficient squared between the contrast sensitivities from the principal subject and four control subjects measured at various grating areas, spatial frequencies, and levels of retinal illuminance was found to be 91%. The percentage indicates the accuracy by which the experimental data of one subject can be predicted by another suggesting that pure error not explainable by any model fitted to the experimental data of more than one subject is of the order of 9%. Thus, the extended contrast detection model of human vision described the experimental data at all spatial frequencies, grating areas and retinal illuminances studied quite accurately.

The contrast detection model extended in this Section to account for the effect of quantal noise was the basis for all the equations used to fit and analyse the

data. The extended model described the human visual system in a detection task as a simple image processor comprising (i) low-pass filtering due to ocular optics, (ii) addition of light dependent noise at the event of quantal absorption in the outer segments of photoreceptors, (iii) neural high-pass filtering, (iv) addition of internal neural noise, and (v) signal detection by a local matched filter whose efficiency decreased with increasing grating area. Its limited aperture is in agreement with the fact that the size of human sampling aperture, i.e. the area from where visual information is collected, seems to have an upper limit (Burgess, 1990) that is signal dependent.

The finding that the dependence of contrast sensitivity on retinal illuminance was described by equation (3.3) for each grating area and spatial frequency means that the square of contrast threshold increased as a linear function of the spectral density of quantal noise. Thus, my result is in agreement with Nagaraja (1964) who found that Weber fraction ($\Delta I/I$) squared increases as a linear function of the square of the r.m.s. contrast of quantal noise. My finding also means that the contrast energy threshold ($E = S_{RMS}^{-2}A$) increased as a linear function of the spectral density of quantal noise. This is in agreement with Burgess, Wagner, Jennings and Barlow (1981) who found that contrast energy threshold increases as a linear function of the spectral density of external spatial noise.

The result that the dependence of contrast sensitivity on grating area and retinal illuminance was described by equation (3.18) means that contrast sensitivity for gratings with constant retinal flux (If^{-2}) and constant number of square cycles (Af^2) is directly proportional to $O_{MTF}(f)$ at medium and high spatial frequencies. In addition, according to equation (3.18) contrast sensitivity remains directly proportional to O_{MTF} at medium and high spatial frequencies, if instead, grating area is so large that contrast sensitivity is independent of area and/or retinal illuminance is so high that human vision is

not limited by quantal noise and Weber's law is thus valid at all spatial frequencies. The extended model of contrast detection in human vision is thus in complete agreement with Banks et al. (1987) who deduced that the decrease of contrast sensitivity with increasing spatial frequency for gratings with a constant number of square cycles is solely due to the optical modulation transfer function of the human eye at medium and high spatial frequencies if human vision is not limited by quantal noise.

The above result also means that when visual performance is limited by quantal noise, contrast sensitivity for gratings with a constant number of square cycles and constant retinal illuminance is directly proportional to O_{MTF} divided by spatial frequency at 1-32 c/deg. This is again in complete agreement with Banks et al. (1987) who showed that for gratings with constant average luminance and number of square cycles the decrease of contrast sensitivity with increasing spatial frequency is only due to preneural factors i.e. ocular optics and quantal noise at medium and high spatial frequencies so that the contribution of quantal noise to the decrease of contrast sensitivity as a function of spatial frequency has a slope of -1 in double logarithmic co-ordinates.

The result that the transition from DeVries-Rose to Weber's law took place at the same retinal flux for all spatial frequencies can be explained by assuming that the effect of quantal or light dependent noise is proportional to spatial frequency squared as I have shown in Section 3.2. This suggestion is in agreement with the extended contrast detection model of human vision, because its lateral inhibition due to $P_{MTF}(f) = F$ produces the required attenuation of quantal noise with decreasing spatial frequency. In my model there are no receptive fields and the spectral density of internal neural noise is constant at all spatial frequencies. Therefore, the model validates my earlier possible explanation for $I_c = I_0F^2$ (in Section 3.2.4.) that the spectral density of

internal neural noise decreases in proportion to spatial frequency squared. On the other hand it disagrees with the possible explanation that the detection of each spatial frequency is mediated by mechanisms with circular receptive fields whose diameter decreases in inverse proportion to spatial frequency, in which case the luminous flux collected by the receptive fields decreases and consequently quantal noise increases in proportion to spatial frequency squared (Graham, 1989).

The dependence of critical retinal illuminance (I_c) on spatial frequency (Van Nes et al., 1967) indicates that transition from DeVries-Rose to Weber's law cannot be totally explained by light adaptation of retinal photoreceptors. According to my model of human vision the transition only means that the dominance of light dependent quantal noise is replaced by constant internal neural noise, in agreement with Nagaraja (1964), Watson, Barlow and Robson (1983), and Pelli (1990).

In conclusion, the increase of contrast sensitivity with retinal illuminance was similar at all grating areas and the increase of contrast sensitivity with grating area was similar at all light levels. The dependence of contrast sensitivity on retinal illuminance and grating area was successfully described by the contrast detection model of human vision (Rovamo et al., 1993) extended in this study to take into account the quantal noise of dim light.

4. THE NEURAL MODULATION TRANSFER FUNCTION ACROSS THE VISUAL FIELD

In this chapter I will show that the critical retinal illuminance (I_c) marking the transition between DeVries-Rose and Weber's laws is independent of retinal location. In the context of the contrast detection model introduced in the previous chapter, this means that neural modulation transfer function of the visual pathways (P_{MTF}) is proportional to spatial frequency up to the local cut-off frequency across the nasal visual field.

4.1. Introduction

In this work the neural modulation transfer function of the visual pathways is defined to reflect the attenuating effect of lateral inhibition on contrast sensitivity. In the contrast sensitivity function the effect becomes visible at low spatial frequencies, when spatial integration reaches the limit over which the system is able to sum in deg^2 of the visual field (Rovamo et al., 1993).

As already explained in the preceding chapter, human contrast sensitivity obeys Weber's law in bright light but DeVries-Rose law (DeVries, 1943; Rose, 1948) in dim light. Performance at intermediate light levels falls between DeVries-Rose and Weber's laws (Kelly, 1972; Koenderink, Bouman, Bueno de Mesquita & Slappendel, 1978; Savage & Banks, 1992). The two laws mean that at higher levels of retinal illuminance contrast sensitivity is independent of light level but at lower levels of retinal illuminance contrast sensitivity for gratings is directly proportional to the square root of the average luminance (Van Nes & Bouman,1967) as shown also in Section 3.2.

Transition from Weber's to DeVries-Rose law depends on spatial frequency so that the lower the spatial frequency the lower the retinal illuminance where the transition occurs (Van Nes & Bouman, 1967). In fact, as was shown in the previous Section 3.2, the transition luminance is directly proportional to spatial frequency squared (Van Nes et al., 1967).

On the basis of the experiments Koenderink et al. (1978) performed with a 1 c/deg moving grating, foveal contrast sensitivity decreases when retinal illuminance decreases from 10 to 0.1 phot. td whereas peripheral contrast sensitivity remains independent of retinal illuminances within 0.1-10 phot. td. This suggests that for the same spatial frequency and range of retinal illuminance the periphery is in the Weber region whereas the fovea is in the DeVries-Rose region. There are at least two possible reasons for peripheral contrast sensitivity remaining independent of retinal illuminance even at such low luminances as within 0.1-10 phot. td. Either the rods have taken over from the cones, or critical retinal illuminances are lower in the peripheral than foveal vision. The latter could be explained either by the decrease of the proportionality constant between I_c and spatial frequency squared with increasing eccentricity or by the otherwise different dependency of I_c on spatial frequency in foveal and peripheral vision. Koenderink et al. (1978) explained their finding by the fact that the receptive fields of ganglion cells are larger in the peripheral than foveal vision and therefore collect more light quanta and are consequently more light adapted at the same level of retinal illuminance (Enroth-Cugell & Shapley, 1973).

The purpose of this chapter was thus to study systematically the effect of retinal illuminance on contrast sensitivity across the visual field by using stationary cosine gratings of various spatial frequencies. The second aim was to find out the relationship between I_c and spatial frequency at different retinal locations, because according to the extended contrast detection model of

spatial vision introduced in the previous chapter, the modulation transfer function (P_{MTF}) of the neural visual pathways is proportional to the square-root of I_C.

4.1.1. MODELLING THE RELATIONSHIP OF P_{MTF} AND I_C

Visual stimuli are filtered by the ocular optics and neural visual pathways before being interpreted by the human brain. In the previous chapter this sequence was modelled as a simple image processor comprising (i) low-pass filtering due to the optical modulation transfer function of the eye, (ii) addition of light-dependent noise at the event of quantal absorption, (iii) high-pass filtering due to the modulation transfer function of the neural visual pathways, (iv) addition of internal neural noise, and (v) detection by a local matched filter whose efficiency decreases with increasing grating area.

On the basis of equation (3.16) the relationship between retinal illuminance (I) and the spectral density of quantal noise (N_q) is

$$I = KN_q^{-1}, \tag{4.1}$$

where K is constant. In Chapter 3 the dependence of contrast sensitivity on retinal illuminance was modelled as

$$S = S_{max}\,(1+I_C/I)^{-0.5}, \tag{3.3}$$

where S is contrast sensitivity, S_{max} is the maximum contrast sensitivity obtainable in bright light for the stimulus used, I is photopic retinal illuminance, and I_C is the critical retinal illuminance marking the transition between DeVries-Rose (De Vries, 1943; Rose, 1948) and Weber's laws. The equation means, that at high luminance levels $S = S_{max}$ (i.e., independent of luminance level) as Weber's law predicts. At luminance levels below I_C, contrast

sensitivity obeys De Vries-Rose law decreasing in proportion to the square root of decreasing retinal illuminance. Equation (3.3) applies to all grating areas, because the effect of spatial integration can be taken into account by allowing S_{max} to grow with area.

According to equation (3.3) contrast sensitivity becomes reduced to $S_{max}/\sqrt{2}$ when illuminance is reduced to I_c. By definition contrast energy threshold is proportional to S^{-2}. Hence, at $I = I_c$ the contrast energy threshold is twice its minimum value obtainable in bright light. The doubling of contrast energy threshold due to quantal noise at $I = I_c$ means that the effect of critical spectral density of quantal noise (N_{qc}) corresponding to I_c is equivalent to the effect of additive internal neural noise (N_i).

In fact, N_{qc} transferred through the ocular optics and neural visual pathways is equal to N_i. However, the spectral density of quantal noise corresponding to I_c is filtered only by the neural modulation transfer function (P_{MTF}) of the visual pathways and left unaffected by the optical modulation transfer function of the eye because individual light quanta cannot be blurred by the point spread function of ocular optics. In other words, although ocular optics redistributes light so that high spatial frequencies in the image are attenuated more than low spatial frequencies, optics does not introduce correlations among neighbouring points, and therefore it does not attenuate the high spatial frequencies of quantal noise (Graham & Hood, 1992). Thus,

$$P_{MTF}^2(f)\, N_{qc} = N_i, \qquad (4.2)$$

where f is spatial frequency.

On the basis of equation (4.1) we can write equation (4.2) as

$$P_{MTF}^2(f) = (N_i / K)\, I_c, \qquad (4.3)$$

which means that I_c is only affected by the neural visual pathways. Thus, I_c remains independent of optical blur although contrast sensitivity at high spatial frequencies and in peripheral vision is reduced by ocular optics.

As shown in Section 3.2, for foveally viewed cosine gratings I_c is directly proportional to spatial frequency squared (Van Nes et al., 1967). Hence, on the basis of equation (4.3) the foveal P_{MTF} for cosine gratings is proportional to spatial frequency, confirming the finding of Rovamo et al. (1993). Thus, cosine gratings are relatively more attenuated at low than high spatial frequencies by the foveal $P_{MTF}(f)$.

For the sake of simplicity and without losing generality Rovamo et al. (1993) assumed that P_{MTF} (f) is proportional to f at the fovea. According to the foveal experiments of Chapter 3, $I_c = I_o F^2$, where the numerical value of I_o provides an estimate for I_c at 1 c/deg. Thus, $(N_i/K) = I_o^{-1}$ in equation (4.3).

4.2. Methods

4.2.1. APPARATUS, STIMULI, AND PROCEDURES

Again the apparatus, stimuli, and procedures are described in Chapter 2, General methods. Therefore only the special features are described here.

The stimuli consisted of vertical cosine gratings within sharp-edged circular apertures. The apertures used were 2 - 16 cm in diameter. Spatial frequencies were 2 and 0.5 c/cm on the screen. A table describing the spatial extent and location of the stimuli for each spatial frequency (c/deg) and eccentricity is provided in Appendix 5. The eccentricities studied were 3, 9, 20, and 37 deg in

the nasal visual field. Eccentricity refers to the angular distance between the point of fixation and the centre of the grating in the nasal visual field of the dominant eye. Thus, at the eccentricity of 37 deg the nearest edge of the largest grating was at the distance of 20 deg from the fovea. The stimulus field was always perpendicular to the line determined by the pupil and the centre of the grating. Both the fixation point and grating were always at the same viewing distance from the eye. Subject's head was stabilised using a chin rest. A small black dot served as a fixation point within the luminous screen, and a small, red LED - whose luminance was reduced by neutral density filters in accordance with the screen luminance - served as a fixation point outside the screen.

4.2.2. SUBJECTS

Four experienced subjects, aged 23-31 years, served as observers. All were corrected myopes: refractions in the dominant eye were T.H. (o.d) -1.75 DS, K.L. (o.d) -1.75 cyl -0.5 ax 90°, J.M. (o.d) -0.75 cyl -0.25 ax 90°, and S.U. (o.d.) -4.0 DS. Their accommodation had a range of at least 6 D. Hence, they were emmetropes at the viewing distances of 28.6 - 229 cm used in my experiments. With optimal refraction their monocular Snellen acuities at 5 m were within 1.2-1.6.

3.3. Results

In foveal vision the increase and saturation of contrast sensitivity as a function of retinal illuminance is similar for all grating areas, as was shown in Section 3.3. Thus, the critical illuminance (I_C) marking the transition between the increasing and saturated parts of the contrast sensitivity function is independent of grating area in foveal vision. According to the contrast detection model of human vision (Rovamo et al., 1993) extended to low light

levels in Section 3.3, I_c should be independent of grating area also in peripheral vision.

The above hypothesis is tested in Fig. 4.1, where I measured contrast sensitivity as a function of retinal illuminance for various grating areas at the eccentricity of 37 deg in the nasal visual field. Retinal illuminance varied across 4 logarithmic units from 3.83×10^{-2} to 6.28×10^{2} phot. td. Retinal illuminance is not affected by eccentricity because the retinal area per one solid degree of visual field and the effective pupillary area decrease similarly when eccentricity increases from 0 to 80 deg (Bedell & Katz, 1982; Rovamo, 1983). Spatial frequency was 1 c/deg. Test grating areas covered a range from 12.6 to 804 deg^2. Consequently the number of square cycles (Af^2) (Virsu & Rovamo, 1979), calculated by multiplying grating area (A) by spatial frequency (f) squared, ranged from 12.6 to 804.

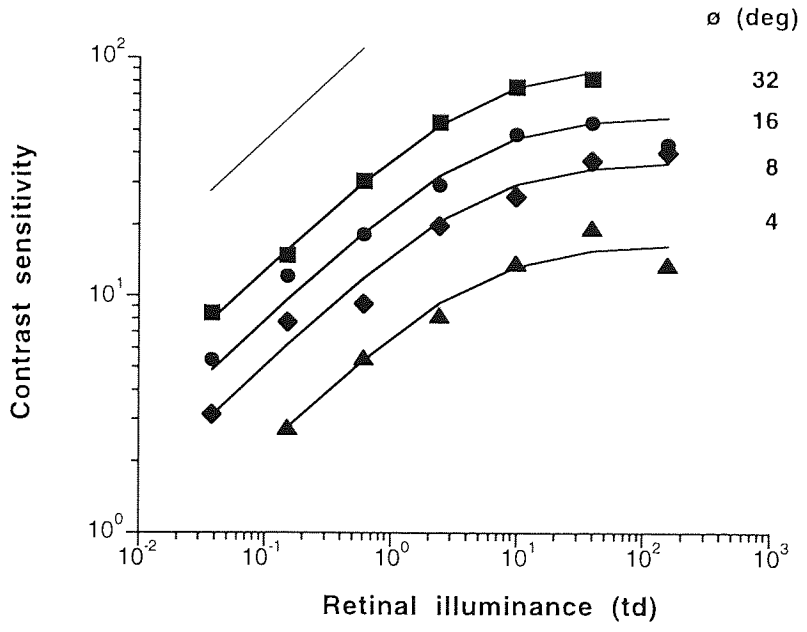

Fig. 4.1. *Contrast sensitivity as a function of retinal illuminance for various grating areas at the eccentricity of 20 deg in the nasal visual field.*

As Fig. 4.1 shows, contrast sensitivity first increased with retinal illuminance at all grating areas. The slope of increase was 0.5 at low levels of retinal

illuminance, obeying DeVries-Rose law (DeVries, 1943; Rose, 1948). The increase then saturated at high levels of retinal illuminance and contrast sensitivity became independent of luminance level, obeying Weber's law. Inspection of the data showed that critical retinal illuminance was independent of grating area, because the contrast sensitivity functions of Fig. 4.1 were parallel at all grating areas.

The contrast sensitivity functions of Fig. 4.1 were then averaged in vertical direction across grating areas at 0.15 - 39 phot. td and equation (3.3) was fitted to this geometrical average with the method of least squares in order to obtain the value for I_c. It was found to be 5.3 phot. td. Thereafter, on the basis of equation (3.3), the contrast sensitivity values measured for each grating area at various levels of retinal illuminance were first divided by the corresponding values of expression $(1+ I_c / I)^{-0.5}$ and then geometrically averaged in order to get the estimates of S_{max} for the grating areas used in Fig. 4.1. They were found to be 16.5, 36.9, 57.3, and 93.3 for areas of 12.6, 50.3, 201, and 804 deg^2, respectively. Smooth curves in Fig. 4.1 were then calculated by equation (3.3) fitted to the data of each grating area separately. Explained variance was 98%, when S_{max} was allowed to vary with grating area.

In the experiments of Fig. 4.2 the study was extended to other spatial frequencies and eccentricities in the nasal visual field. Monocular contrast sensitivity was measured as a function of retinal illuminance for vertical cosine gratings for spatial frequencies of 0.25 - 8 c/deg at 3 - 37 degrees of eccentricity. The number of square cycles (Af^2) was constant at 50. The upper limit of the spatial frequencies studied at each eccentricity was determined by the local grating acuity, and the lower limit was determined by the largest grating area available on the screen and the shortest practical viewing

distance. Retinal illuminance varied across 8 logarithmic units from 1.50×10^{-4} to 2.51×10^{3} phot. td.

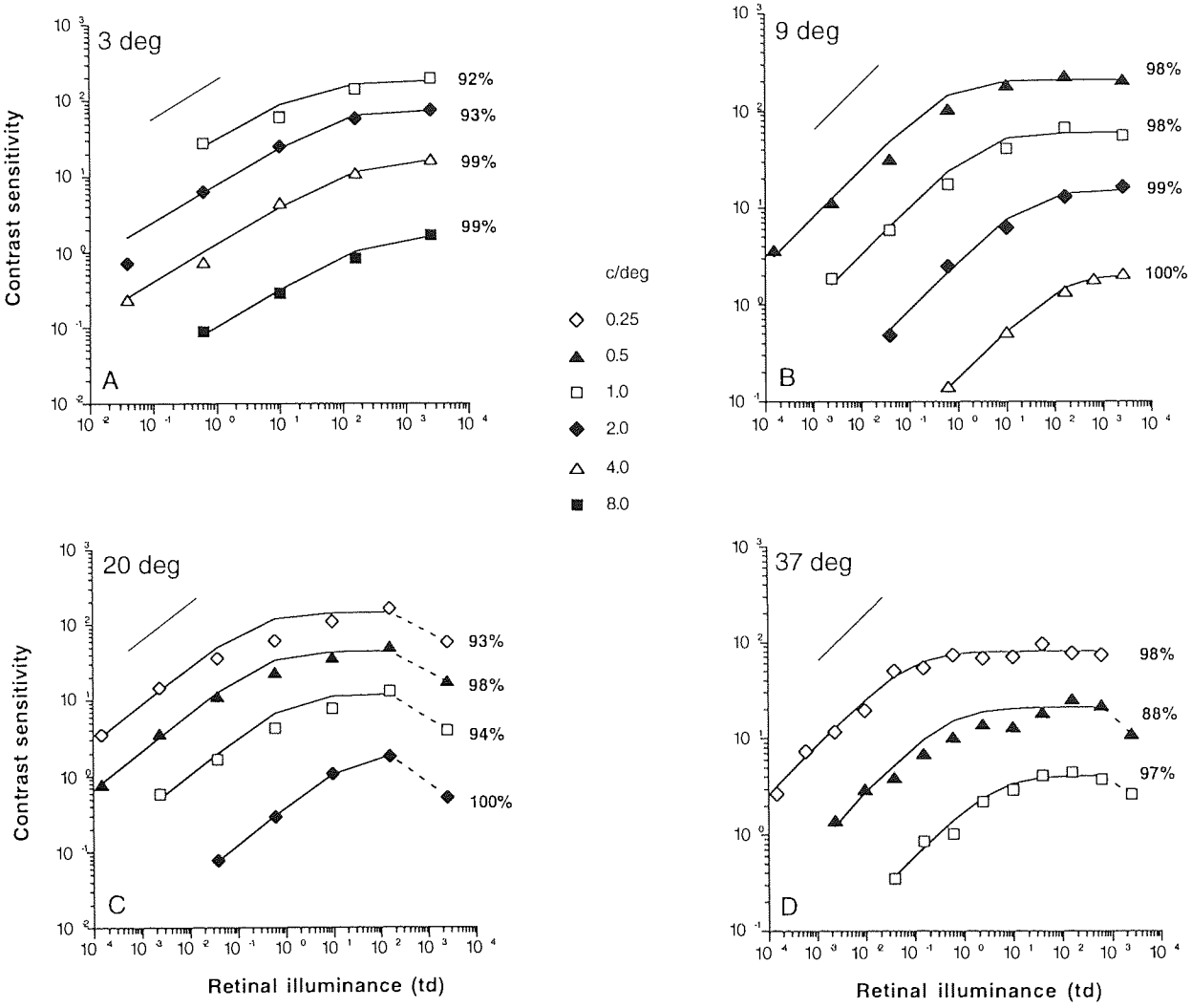

Fig. 4.2. *Contrast sensitivity as a function of retinal illuminance at eccentricities of 3, 9, 20, and 37 deg in the nasal visual field.*

Fig. 4.2 shows that at all spatial frequencies and eccentricities studied contrast sensitivity increased with retinal illuminance. The slope of increase was again 0.5 at lower levels of retinal illuminance, obeying DeVries-Rose law (Rose, 1948; DeVries, 1943). Again at higher levels of retinal illuminance the increase saturated and contrast sensitivity became independent of luminance level, obeying Weber's law. In addition, above 160 - 630 phot. td contrast

sensitivity at the eccentricities of 20-37 deg decreased with increasing retinal illuminance. A similar decrease was also found at the eccentricity of 37 deg in the experiments of Fig. 4.1 above 39 - 630 td, although not shown in the figure. Daitch and Green (1969) have also reported a similar phenomenon for 0.5-1 c/deg at the eccentricity of 12 deg in the nasal visual field.

From Fig. 4.2 it can be seen that the I_c marking the transition between DeVries-Rose and Weber's laws increased with spatial frequency, in agreement with Van Nes and Bouman (1967) and Chapter 3.2. Closer inspection of the data showed that at low spatial frequencies (≤1 c/deg) performance often fell between DeVries-Rose and Weber's laws at intermediate light levels, in agreement with Kelly (1972), Koenderink et al. (1978), and Savage and Banks (1992).

Equation (3.3) was fitted separately to the data of each spatial frequency at each eccentricity with the method of least squares. Smooth curves in Fig. 4.2 were then calculated by using equation (3.3) with corresponding parameters. The data points where contrast sensitivity decreased with increasing retinal illuminance were excluded from the least squares regression. Explained variance was on average 96%, with a range of 88 - 100% across spatial frequencies and eccentricities.

In Fig. 4.3.A the estimates of critical retinal illuminance (I_c) were plotted as a function of spatial frequency in double logarithmic co-ordinates. The estimates of I_c at 3-37 deg of eccentricity were obtained when equation (3.3) was fitted to the data of Fig. 4.2 whereas the foveal estimates of I_c were obtained from my previous study in Chapter 3.3.

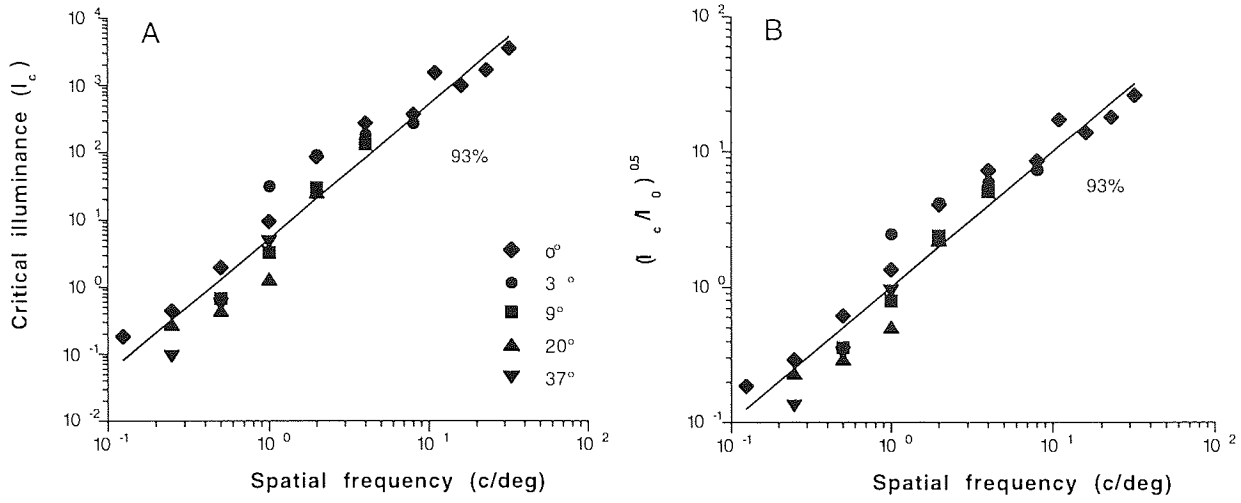

Fig. 4.3. *A) The estimates of critical retinal illuminance at various eccentricities as a function of spatial frequency. Foveal estimates from Chapter 2.3. B) The estimates of* $P_{MTF}(f) = (I_c/I_0)^{0.5}$ *at various eccentricities as a function of spatial frequency.*

As Fig. 4.3.A shows, all the estimates of critical retinal illuminance fell on a common straight line and in double logarithmic co-ordinates I_c increased linearly with spatial frequency of 0.125 to 32 c/deg. The deviations of the estimates of I_c from the straight line are similar in magnitude to those found for monochromatic foveal gratings (see Laming, 1991). However, the fact that my data has been collected from eight subjects at various spatial frequencies and eccentricities could contribute to the variability of I_c values across eccentricities at each spatial frequency. The slope of increase was 2, which means that I_c increased in direct proportion to spatial frequency squared, in agreement with the foveal results of Van Nes et al. (1967) and Section 3.2. This also means that critical retinal flux (If^{-2}), calculated now by dividing critical retinal illuminance by spatial frequency squared, was constant at all spatial frequencies and eccentricities. The straight line $I_c = I_0F^2$ in Fig. 4.3.A is a least squares fit to the data. The explained variance was 93%. The value of constant I_0 was found to be 5.22 phot. td. deg^2, in agreement with Fig. 4.1. It is

also an estimate for the critical retinal flux valid for all spatial frequencies and eccentricities.

In the foveal study of Section 3.2 the I_0 was found to be 21 phot. td deg^2 for spatial frequencies of 0.124 - 4 c/deg when grating areas varied within 0.785 - 201 deg^2. In the more extensive foveal study of Section 3.3 I_0 was found to be 7.93 phot. td deg^2 for spatial frequencies of 0.125 - 32 c/deg and grating areas varying between 0.785 - 804 deg^2.

In Fig. 4.3.B I have plotted $(I_c / I_0)^{0.5}$ as a function of spatial frequency, because according to equation (4.3) $P_{MTF}(f) = (I_c / I_0)^{0.5}$. And as $I_c = I_0F^2$, therefore $P_{MTF}(f) = F$, which provided a good fit to the data as Fig. 4.3.B. shows. The explained variance was 93%.

4.4. Discussion

These experiments have shown that for cosine gratings the increase of contrast sensitivity with retinal illuminance was similar at all eccentricities in the nasal visual field. Contrast sensitivity increased in proportion to the square root of retinal illuminance (I) in dim light, thus obeying DeVries-Rose law, but was independent of retinal illuminance in bright light, following Weber's law. The dependence of contrast sensitivity (S) on retinal illuminance was quantitatively described by equation (3.3) at all spatial frequencies. The explained variance was 96% on the average, and had a range of 88-100% across spatial frequencies and eccentricities. In equation (3.3) S_{max} is the maximum contrast sensitivity obtainable in bright light at the exposure duration and grating area used, and I_c is the critical retinal illuminance marking the transition between DeVries-Rose and Weber's laws.

At low spatial frequencies performance fell between DeVries-Rose and Weber's laws at intermediate light levels, in agreement with Kelly (1972), Koenderink et al. (1978), and Savage and Banks (1992). One explanation for the slow transition from Weber's to DeVries-Rose law with decreasing luminance is the fact that the increase in the effective spectral density of quantal noise with decreasing luminance is retarded by the increasing quantum efficiency that is due to transition from cone to rod vision. This slow transition between DeVries-Rose and Weber's laws at low spatial frequencies was not predicted by the contrast detection model introduced in the previous chapter. However, the quantitative differences between predicted and measured contrast sensitivities were small, as explained variance remained high at 88-98% even at low spatial frequencies.

Analysis of the experimental data showed that at all eccentricities and spatial frequencies studied critical retinal illuminance I_c was directly proportional to spatial frequency squared i.e. $I_c = I_0 f^2$, where I_0 = 5.22 phot. td. deg^2 and f is spatial frequency in c/deg. Explained variance was 93%. The finding means that my study extends the foveal result of Chapter 3.2 and Van Nes et al. (1967) throughout the visual field . The value of I_0, calculated by dividing critical retinal illuminance (I_c) by spatial frequency squared, indicates the critical retinal flux 5.22 phot. td deg^2 that is valid for all spatial frequencies and eccentricities. Thus, the previous foveal result that the transition between DeVries-Rose and Weber's laws takes place at the same retinal flux irrespective of spatial frequency can be generalised across the whole visual field.

Koenderink et al. (1978) concluded that the far retinal periphery is less affected by a decrease in the retinal illuminance than the foveal region so that at the same spatial frequency the transition point between DeVries-Rose and Weber's laws is lower for a peripheral grating. This clearly disagrees with our

findings. However, Koenderink et al (1978) used moving gratings, whose size was larger in the periphery than at the fovea. Based on the study described in the previous Section 3.3 and on the results of Fig. 4.1 in this chapter, it appears that critical retinal illuminance is independent of stimulus area for stationary gratings. Therefore, the probable reason for the discrepancy between my results and the finding of Koenderink et al. (1978) was grating movement.

Daitch and Green (1969) measured contrast sensitivity as a function of retinal illuminance for several spatial frequencies for gratings exposed for 0.2 sec at the eccentricity of 12 degs. Their contrast sensitivities were lower than those found at the eccentricity of 9 deg in the current study probably because of their short exposure duration. I fitted equation (3.3) to their data at 0.5 - 4 c/deg and found that critical retinal illuminance was proportional to spatial frequency squared with an explained variance of 79%.

In bright light visual acuity for symbols is far better (Mandelbaum & Sloan, 1947) and gratings are resolved at higher spatial frequencies (Rovamo & Raninen, 1990) in the fovea than periphery. Both visual acuity and grating resolution decrease with retinal illuminance but the reduction starts in the fovea at higher luminance levels than in the periphery (Mandelbaum & Sloan, 1947; Rovamo & Raninen, 1990). This phenomenon is conventionally explained by assuming that the fovea enters the DeVries-Rose region at higher luminance levels than the retinal periphery (Koenderink et al., 1978). However, according to my results high spatial frequencies enter the DeVries-Rose region at higher luminance levels than low spatial frequencies irrespective of retinal location, thus explaining the dependence of acuity on retinal illuminance and eccentricity.

All the equations used to fit and analyse the data were derived from the contrast detection model of human vision (Rovamo et al., 1993) extended to low light levels in Section 3.3. According to the extended model the modulation transfer function (P_{MTF}) of the neural visual pathways squared is directly proportional to critical retinal illuminance (I_c) at all spatial frequencies. Hence, my finding that I_c was similarly proportional to spatial frequency squared at all eccentricities means that up to the spatial cut-off frequency determined (Rovamo & Virsu, 1979) by the lowest local sampling density (cones at eccentricities 0 - 10 deg and ganglion cells above 10 deg), the modulation transfer function (P_{MTF}) of the neural visual pathways is similar (i.e. proportional to spatial frequency) at all visual field locations. Hence, according to the extended model the decrease of contrast sensitivity with increasing eccentricity at high spatial frequencies is due to deterioration in ocular optics or spatial summation. The latter alternative is supported by Banks, Sekuler & Anderson (1991), who concluded that the neural efficiency of detection at high spatial frequencies decreases with increasing eccentricity.

5. THE OPTICAL MODULATION TRANSFER FUNCTION ACROSS THE VISUAL FIELD

According to the extended contrast detection model described in Chapter 3, the human visual system in a detection task can be described as a simple image processor comprising (i) low-pass filtering due to the optical modulation transfer function (O_{MTF}) of the eye, (ii) addition of light-dependent noise at the event of quantal absorption, (iii) high-pass filtering (lateral inhibition) due to the neural modulation transfer function (P_{MTF}) of the visual pathways, (iv) addition of internal neural noise, and (v) detection by a local matched filter whose efficiency decreases with increasing grating area. During the course of this work, I have already studied the phases (ii), (iii), and (iv), and shown that spatial integration saturates at the same number of square cycles (Af^2) at all spatial frequencies ($f \geq 0.5$ c/deg) and levels of retinal illuminance (Chapter 3), and that the neural modulation transfer function is proportional to spatial frequency at all eccentricities (Chapter 4). The final experimental chapter of this thesis concentrates on phase (i), the human optical modulation transfer function (O_{MTF}) both in the fovea and the periphery.

5.1 Introduction

The image of any object in the visual field is formed on the retina by the optical system of the eye. The optics of the eye logically consists of all the structures between the first encounter of light quanta with the eye to the site of phototransduction, i.e. when light is transformed to neural impulses. Here I will briefly review the components and characteristics of the human eye that affect the quality of the image projected to the outer segments of retinal photoreceptors. However, the scope of this work is not extended to the role of binocular vision, although in normal vision visual signals are received in both

eyes. The optical modulation transfer function (O_{MTF}) is used to describe the loss in contrast caused by the eye optics. The previous methods that have been used to determine the O_{MTF} of the human eye will also be briefly reviewed here.

5.1.1. THE OPTICAL COMPONENTS AND CHARACTERISTICS OF THE HUMAN EYE

5.1.1.1. The preretinal factors

The cornea

The outermost structure of the eye is the cornea, which is a clear, transparent tissue combination covered by the tear film. The transparency arises from the relative constancy in size, orientation and spacing of the collagen fibres of each stromal lamella, which form the stroma, the main bulk of the cornea (Maurice, 1957, 1969, 1970 in Charman, 1983). On the anterior side the stroma is separated from the epithelium by Bowman's membrane, and Descement's membrane separates it from the posterior endothelium (e.g. Waltman & Hart, 1987). The cornea contributes approximately two thirds of the total 60 D of the refractive power of the eye. This great refracting power is due to the significant difference in refractive indices between air and the cornea/tear film. Consequently, irregularities on the corneal surface have a significant effect on the quality of the retinal image. The tear film smoothes out the small irregularities in the corneal surface, which is fairly spherical over the central region but flattens towards the periphery. The peripheral flattening serves to reduce spherical aberration (Charman, 1983).

Aqueous humour

Between the posterior surface of the cornea and the lens there is the anterior chamber, filled with clear and transparent aqueous humour. In a healthy eye the aqueous does not usually affect the image quality (Weale, 1963).

Pupil

The aperture stop of the optical system of the eye is the pupil, an opening in the iris. It has an important role in determining the image quality falling on the retina by assuming the size that is necessary for optimum sharpness of vision (Charman, 1991). The pupil thus regulates the balance between diffraction and aberrations, as well as the ocular depth of focus. The main determinant of the pupillary response is the light striking the retina (Bouma, 1965). The pupil consists of a circular muscle, the sphincter pupillae, and a radial muscle, the dilator pupillae, which constantly adjust the pupil size (e.g. Alexandridis, 1985). The posterior surface of the dilator is covered by the pigment epithelium of the iris. Both muscles act upon each other, and are innervated by both the sympathetic and parasympathetic pathways (Alexandridis, 1973). With monochromatic light the pupil constriction begins at luminance values at which the sensitivity of the rod mechanism begins to fall off (Aguilar & Stiles, 1954).

The lens

The crystalline lens provides refractive power by contributing maximally about 20 D to the optical system of the eye. One of the main functions of the lens is to provide accommodation, which means adjusting the refractive power of the eye to focus on objects either in infinity or at closer distances from the eye. This is performed in co-operation with the ciliary muscle (see e.g. Moses,

1987); The lens, which is made from fibres that are formed throughout life, is attached to ciliary processes by zonules. When the ciliary muscle contracts and the zonules relax, the lens becomes thicker thus increasing its refractive power. Likewise, the lens is flattened and the refractive power is reduced when the ciliary muscle is relaxed. Another function of the lens is to absorb ultra-violet light (Cotlier, 1987), which would increase the intraocular scattering and thus degrade the retinal image quality. The form of the lens also contributes to reduce aberration in the eye (Charman, 1983).

Vitreous body

The transparent gel filling the chamber between the retina and lens is called the vitreous body. It gives the eye its shape, and is almost clear and free of refractive irregularities in young people, but with advancing age these may become more common (Weale, 1963).

5.1.1.2. The retina

The retina is a derivative and an extension of the diencephalon and the optic nerve is structurally and functionally a tract of the central nervous system (Cohen, 1987). The vertebrate retina is inverted, thus receptors are facing the back of the eye rather than towards the light. Consequently light must traverse the layers of neural elements as well as the main body of the receptor before it reaches the photopigment in the receptor outer segments. Although the neurons lying in the optical path are transparent in principle, the numerous arteries, veins and capillaries, which form a rich plexus among the neural elements, are a significant source of light scatter in the eye (Retina, 1991). However, the pigment epithelium, which is the outer layer of the optic cup, contains melanin granules which absorb scattered light (Hewitt & Adler, 1989).

The retina itself is firmly attached to the pigment epithelium in only two areas, the optic disc (optic nerve) and the ora serrata by the ciliary body.

The retina is separated from the vitreous body by the inner limiting membrane. The nerve fibres from the retinal neurones travel towards the optic nerve above the three layers of retinal neurones. The innermost layer consists of the ganglion cells, which collect and process information from lower retinal layers. The information from other retinal cells is relayed via axons and synapses from the inner nuclear layer, where the amacrine, horizontal, and bipolar cell bodies are found (Blanks, 1989). The horizontal cells relay information between photoreceptors (Blanks, 1989) thus affecting the adaptive mechanisms (Shapley & Enroth-Cugell, 1984). The other means of lateral information flow is the amacrine cells, which synapse with rod and cone bipolar cells, and ganglion cells (Shapley & Enroth-Cugell, 1984), but the main link between photoreceptors and ganglion cells are the bipolar cells, which receive information from photoreceptors and relay it either directly to ganglion cells, or synapse with amacrine cells (Shapley & Enroth-Cugell, 1984). The ganglion cells can receive information from multiple lower-level cells, and have either ON or OFF -center receptive fields, which means that they are either depolarised of hyperpolarized in response to increased illumination in the receptive field center.

The quantal absorption, where the light energy is converted to neural impulses (electrical signals), takes place in the outer segments of visual photoreceptors. All photoreceptors have an outer segment which contains one of the four differently sensitive visual pigments, connected to an inner segment which contains the metabolic machinery, a perikaryal region containing the cell nucleus, and a synaptic terminal (Blanks, 1989). Although all photopigments absorb quanta of all wavelengths in the visual spectrum, they are not equally sensitive to light of all wavelengths. Rods contain a visual

pigment called rhodopsin providing great sensitivity, and absorbing maximally in the blue-green (500 nm) region of the spectrum. Cones, which provide visual acuity for pattern detection as well as colour vision, have one of the three visual pigments called iopsins, and are most sensitive to wavelengths at blue (450), green (530), or red (565) region of the electromagnetic spectrum.

The retinal topography is also of importance. The optic disc in the nasal retina is the site where the nerve fibres depart from the retina forming the optic nerve. The retinal arteries and veins also penetrate the retina at the optic disc. As there are no photoreceptors in that area, it causes a blind spot in the temporal visual field. In contrast, the best acuity is achieved at the centermost part of fovea, which is located on the visual axis of the eye. The foveola is about 0.1 mm in diameter, and free of cells except for densely packed red and green cones (Ogden, 1989). The nerve fibres, ganglion cells, and inner plexiform layers are absent from the fovea, which is composed entirely of tightly packed cones, comprising 10% of the cones of the retina (Ogden, 1989). The area, extending about 2 degs of visual angle, is also thought to be free of blue cones. The parafoveal and perifoveal regions form the peripheral zone of macula, extending about 2.75 mm from the centre of the fovea. As the cone density decreases sharply outside the fovea, the rod density increases, reaching maximum density at about 20 degrees of eccentricity.

The Stiles-Crawford effect and retinal fibre optics

The Stiles-Crawford effect (SCE) is a phenomenon related to the directional sensitivity of retinal cones. Parallel rays of light entering the pupil are more effective when striking foveal cones "head-on" than rays hitting the cones in an oblique angle, thus entering the pupil near the edge. The effect was accidentally found by Stiles and Crawford (1933), when they were attempting to develop an apparatus for measuring the area of the eye pupil. However,

they obtained strange results, implying that *"the apparent brightness of an object is not proportional to the pupil area because rays entering the pupil at points distant from the axis are not so effective visually as rays entering along or near to the axis"* . As a result they modified the apparatus and investigated their finding more thoroughly, making photometric matches by the flicker method both horizontally and vertically across the pupil. Peak sensitivity was found for rays entering the eye either in the center of the pupil or slightly displaced to the temporal side.

Already Stiles and Crawford suspected that their finding is of retinal origin. From histological studies it is now known that the retinal receptors tend to be oriented towards an anterior point, instead of the centre of the eye (e.g. Enoch & Tobey, 1981). Strong evidence of retinal origin is the fact that due to a trauma or an occlusion the peak of the SCE function shifts, being active throughout life (Bonds & MacLeod, 1978; Applegate & Bonds, 1980, Enoch & Birch, 1981). Apart from being a proof of retinal origin, the change in orientation also indicates to phototropic properties in the alignment mechanism. However, when light is not present, the receptors will tilt according to the tractional force (Enoch & Birch, 1981), although experiments with completely occluded eyes do not indicate any loss in the directionality (Enoch & Birch, 1985; Enoch, Hamer, Lakshminarayanan, Yasuma, Birch & Yamade, 1987), nor does the finding of an existing alignment of photoreceptors in an unborn rhesus monkey foetus" eye (Laties, in Enoch, 1972).

The receptor orientation has been described as waveguiding, as the light is guided by the receptor into the outer segments, where photopigment is located. As a waveguide accepts light incident within a solid angle about its axis, it is directional in its acceptance of light in order to avoid stray light entering the receptor, and it has to be selective with the acceptance of different

wavelengths to prevent crosstalk. Crosstalk is caused by exchange of energy between adjacent fibres, and it degrades the ability of the fibre to maintain contrast between image details, thus degrading also the resolution of an individual photoreceptor (Enoch & Lakshminarayan, 1991). In other words, the receptor has to posses fibre-optic properties, which in theory vertebrate photoreceptors do (Enoch & Lakshminarayan, 1991): They are transparent, and both rods and cones have refractive indices which are higher than the surrounding medium. The cross-talk is prevented as receptors are separated by a medium with lower refractive index, by a distance which is at least equal to the wavelength of light. The system of a large aperture pupil and small aperture photoreceptors enhances the light capture of quanta from the visual signal simultaneously minimising the stray light reaching the retinal image (Enoch & Lakshminarayanan, 1991).

The receptor fibre optic properties and SCE are consequently closely related phenomena. The main goal of the receptor orientation seems thus to be to reduce the deleterious effects of intraocular scatter. Although both cones and rods have been shown to exhibit fibre-optics properties (Sidman, 1957; Enoch & Tobey, 1978), in general SCE is considered to only affect cones. The variation in the SCE across the retina has also been studied (Stiles, 1939; Westheimer, 1967; Enoch & Hope, 1973; Bedell & Enoch, 1979) and the effect is strongest at approximately 2 deg, declining thereafter smoothly towards periphery so that at 35 deg the effect is similar in magnitude as in the fovea (Bedell & Enoch, 1979).

Crawford (1937) found that the foveal SCE does not depend on the background luminance. When he did the same experiment in the periphery, the effect was detected at high illuminance levels but at low light levels the SCE function was almost flat. However, there are some cases in the literature, where scotopic (low-light level) SCE has been reported with decentered

pupils (Bonds & MacLeod, 1978; Flamant & Stiles, 1948), and with achromats (Nordby & Sharpe, 1988). Consequently the directionality is not only a property of cones, but rods possess waveguide properties as well (Alpern 1983), although the magnitude of the SCE functions is much lower with peripheral rods than parafoveal cones (Van Loo & Enoch, 1975).

SCE is wavelength dependent as Stiles first reported in 1937. He discovered that directional selectivity was greater for short wavelength light than for wavelengths in the middle of the visible spectrum. The dependence increases again with long wavelengths, but not in the same magnitude as with short wavelengths (Enoch & Stiles, 1961).

Although the SCE is of retinal origin, it can be regarded as pupil apodization. Apodization is defined (Metcalf, 1965) as the occlusion of a pupil by a partially transmitting mask, which may have varying transmittance across its surface. An aperture stop is also an example of apodization. Light rays striking the fovea at an oblique angle are not absorbed into the receptors, but reflected back. Consequently, the increase in pupil size does not degrade the O_{MTF} in a manner that would be expected if there were no Stiles-Crawford effect.

5.1.2. DIFFRACTION

Due to the wave nature of light, a limited aperture causes a spread of light even in a fully focused aberration-free system. When the eye is diffraction limited, it means that the pupil has decreased to an extent where diffraction overcomes the improvement in the retinal image quality achieved by decreasing the pupil size, which reduces the spherical and chromatic aberration as well as other blur. The magnitude of diffraction is wavelength dependent, bending shorter wavelengths more. In general terms, the eye is

commonly assumed to be diffraction limited for pupil diameters of 2 mm or less.

5.1.3. METHODS USED TO DETERMINE THE O_{MTF} OF THE HUMAN EYE

The quality of the retinal image has been extensively studied by many researchers applying various techniques over the past decades. A common agreement between the researchers is that the eye optics is a low-pass filter, attenuating high spatial frequencies and thus preventing under-sampling, or aliasing in foveal vision. The peripheral optics has not been studied as much, but the common view is that the image quality filtered through the optics is not degraded enough in order to match the sampling limitations of the peripheral retina (Charman, 1991).

The most reliable way to determine the O_{MTF} of a human eye would of course include a recording device in the outer segments of the retinal photoreceptors. This, however, has not yet been possible, but the optical MTF of a freshly excised human retina has been measured by Ohzu & Enoch (1972). Their work provides a useful estimate of the magnitude of retinal scatter, but inevitably the total effect of eye optics remained unknown. Here I will go through the basics of the methods used to measure the optical transfer function of the human eye in vivo.

5.1.3.1 The double-pass method

The ophthalmoscopic double-pass method in its present form can be considered as the state of art in this field. As implied by its name, it follows the principles of an ophthalmoscope, i.e. an image is projected to the retina and the part of the light in the retinal image which is reflected back is used to

compute the O_{MTF} of the human eye. The main assumption in the double-pass technique is that the retinal reflection is diffuse, thus destroying all coherence in the reflected image. Being it so, the single-pass O_{MTF} of the eye is the square root of the O_{MTF} deduced from the measurement of the double-pass point spread function (Charman, 1991).

Most earlier studies (e.g. Campbell and Gubish, 1966; Jennings and Charman, 1981) measured the double-pass line-spread function by recording the reflection with photoelectric techniques. The Fourier transformation of the external line-spread function yields the double-pass O_{MTF}, which is then square rooted to give the single-pass O_{MTF}. The single-pass line-spread function is then obtained by the inverse Fourier transformation. More recent versions (e.g. Santamaria, Artal and Bescós, 1987; Artal, 1990; Artal and Navarro, 1994) utilise a television or video camera and image analysis systems to make direct measurements of the point spread function. The use of a point spread function enables the observations in all orientations, which is more precise than the unidimensional spread function owing to the asymmetries of the wave aberrations of the eye and the irregularities of the retina.

The fact that the double-pass method measures light which is discarded by the visual system poses a dilemma to its credibility. There is also some doubt with the double-pass method as to which retinal layer the reflection arises from. Santamaria et al. (1987) think that reflection takes place at all planes after the interior membrane, but assume in their calculations that the reflection originates from receptor surfaces. This would bias the obtained O_{MTF}s by ignoring part of the retinal light scatter, and even part of the eye optics. At larger pupil sizes the directionality of retinal cones plays an important role in foveal vision. According to Artal (1990) in the double-pass imaging process only the second pass is affected by the apodization, because of the

directionality in the reflection. In his calculations he included both the Stiles-Crawford effect and the retinal reflection directionality, obtaining clearly better estimates for the O_{MTF} than without introducing the corrections. However, some studies (Artal and Navarro, 1994) do not take into account the fact that light rays entering the pupil at different angles are not equally effective.

5.1.3.2. The interferometric method

The psychophysical interference method has been used to study the optical quality of the eye since 1935 (Le Grand). It is presumed that an interferometric grating projected to the retina completely bypasses the optics of the eye. The monochromatic O_{MTF} is then calculated as the ratio of contrast thresholds of the internal grating to a normal external grating.

In principle, the interference fringes are produced by imaging two point sources of coherent light close to the nodal points of the eye, forming a fringe on the retina. The commonly used light source is an He-Ne laser, which emits red light of 628.3 nm. Spatial frequency is varied by changing the distance between the point sources, and the contrast of the grating is varied by changing either the mean retinal illuminance or the relative intensity of the sources.

In the much cited work of Campbell and Green (1965) the external gratings were generated on the face of an oscilloscope with a green phosphor. The size of the external gratings was 6.5 deg^2 whereas the internal gratings covered a circular area of about 700 deg^2. This lead to an underestimation of the O_{MTF} at low and medium spatial frequencies, because the extensive spatial integration (Hoekstra, van der Goot, van den Brink & Bilsen, 1974; Howell & Hess, 1978; Virsu & Rovamo, 1979) across the internal gratings

yielded higher contrast sensitivities than would have been obtained if the gratings had occupied the same area.

The most recent paper utilising the interference method is by Williams, Brainard, McMahon and Navarro (1994). They used a dual interferometer, which could produce both the external and internal gratings simultaneously, and thus the two kinds of grating had the same wavelength and similar viewing conditions.

There are some weaknesses in the interference method, though. Intraocular scattering reduces the contrast of both the external and the internal gratings, although the internal grating is supposed to be unaffected by optical factors of the eye. This fact would neglect the effect of scatter, thus overestimating the O_{MTF} (Campbell and Gubisch, 1966). Some concern has also been raised over the difference in wavefronts in the two types of gratings (Van Meeteren, 1974) as well as over the possibility that retinal receptors are abnormally excited when the coherent beams have to come from two small areas in the pupil (Charman, 1991). Williams et al. (1994) compared the double-pass and interferometric O_{MTF}s under same experimental conditions. They argued that the assumption of Campbell and Gubisch (1966) was not correct, as the ocular scatter affects the two grating types differently, producing random variations in the internal contrast. The argument of Charman (1991) was also denied, as the observers were not able to distinguish the two types of grating when similar viewing conditions were used. Thus the interferometric O_{MTF} was not influenced by neural (receptoral) factors. Their monochromatic red O_{MTF}s gained by the interferometric method were higher than those they obtained by the double-pass method. They concluded that the true O_{MTF} would lie closer to the interferometric than the double-pass estimate.

5.1.3.3. Measurement of wavefront aberrations

The quality of eye optics has also been examined by ray tracing. As optical elements change the direction of individual light rays, so the curvature of the wavefront changes. The difference between a perfectly spherical and a distorted wavefront denotes the wavefront aberration (Freeman, 1990), which is usually categorised into the five Seidel aberrations (spherical aberration, coma, astigmatism, curvature of field, and distortion). However, as the refracting surfaces of the eye are neither regular nor spherical, the Seidel aberrations can be applied to the eye only in general terms.

The O_{MTF} is extracted in a form of pupil function, which tells the variation in phase and amplitude across the exit pupil. Each wavefront of aberration equals 2π of phase, so the local phase is deduced from the wavefront aberration (Charman, 1991). The amplitude can be assumed to be uniform across the pupil or estimated allowances for the Stiles-Crawford effect and lenticular absorption can be added in weighting functions. The retinal scatter is ignored with wavefront measurements and therefore the method renders an overestimation in the O_{MTF} (Charman, 1991).

The wavefront aberrations of the eye have been measured point by point across the pupil (Smirnov, 1962; Campbell, Harrison & Simonet, 1993), by the Foucault knife-edge technique (Berny & Slansky, 1969), and by aberroscope methods (Howland & Howland, 1977; Walsh, Charman & Howland, 1984). Berny & Slansky (1969) based their method on the principle of the Foucault test and photographed the reflection in the eye of an edge in two perpendicular orientations, from which they deduced the retinal point spread function and compared it with the ideal Airy disc. Howland & Howland (1977) measured monochromatic wave aberration with a crossed cylinder aberroscope, which consisted of $\pm$ 5 D crossed cylinder with interlaced grid.

The subjects did freehand drawings of their subjective impression of a distorted grid pattern. They concluded that comalike aberrations are an important factor in image distortion at all pupil sizes, and that spherical aberrations are often limited to one orientation. Walsh, Charman & Howland (1984) modified the method by obtaining the retinal images by direct photographic recording instead of subjective drawings and confirmed the findings of the subjective aberroscope. Campbell, Harrison & Simonet (1990) measured optical blur across the pupil, also confirming the finding of Howland & Howland (1977) that comatic aberrations play a dominant role in image degradation.

5.1.3.4. Theoretical calculations

Van Meeteren (1974) has estimated the ocular O_{MTF} in white light by using averaged typical estimates of individual aberrations and other causes for image degradation. He concluded that chromatic aberration is the predominant factor governing image quality. A two parameter fit, which was first suggested by Johnson (1970) has replaced the earlier propositions of single-parameter functions (Charman, 1991). For example, Deeley, Drasdo & Charman (1991) applied a two parameter fit for a polychromatic white light O_{MTF} when combining the calculations of Van Meeteren (1974) with the data of Campbell & Gubisch (1966) and Ohzu & Enoch (1972), who measured the MTF of an excised human retina.

In the following I will introduce two new psychophysical methods to estimate the human optical modulation transfer function. In the first experiment I used only one pupil size (ø8 mm), but Section 5.3 extends the study to various pupil sizes. Finally, in Section 5.4 the new methods were applied to measure peripheral O_{MTF} of the human eye.

5.2. Two new psychophysical methods to determine the O_{MTF}

5.2.1. RATIONALE OF THE METHODS

In the previous Chapters 3 and 4 it was explained that the inverse of the spectral density of external quantal noise (N_q) in the light entering the human eye through the pupil is proportional to retinal illuminance (I) in photopic trolands. Hence,

$$N_q^{-1} = k' I, \tag{5.1}$$

where k' is constant. It is probably worth noting that the effective quantal flux absorbed in the outer segments of photoreceptors is smaller than external luminous flux, because some light is lost in the ocular media and only part of light reaching the photoreceptors is absorbed by the photopigment.

In accordance with Pelli (1990) I define the critical spectral densities of quantal and spatial noises to be such that they reduce root-mean-square contrast sensitivity (S) by a factor of $\sqrt{2}$. I have already mentioned earlier that the spectral density of quantal noise (N_q) is not affected by the O_{MTF} of the eye. External added spatial noise, however, is part of the image and therefore the spectral density of external white spatial noise (N_s) added to the pixels of a grating image is affected by the O_{MTF} of the human eye. Therefore, the critical spectral density of spatial noise (N_{sc}) is comparable to the critical spectral density of quantal noise (N_{qc}) only at the event of quantal absorption, after which both types of noise become an integral part of the neural representation of the image. Thus, N_{sc} filtered by O_{MTF} is at each spatial frequency (f) proportional to N_{qc}. Hence,

$$O_{MTF}^2(f)\, N_{sc} = k'' N_{qc}, \tag{5.2}$$

where k'' is constant. Equation (5.1) is then modified by replacing N_q by N_{qc} and I by critical retinal illuminance (I_c). Then by combining equations (5.1) and (5.2) we get

$$k\, O_{MTF}(f) = (I_c N_{sc})^{-0.5}, \qquad (5.3)$$

where $k = (k'/ k'')^{-0.5}$.

By finding the values of critical retinal illuminance (I_c) and critical spectral density of spatial noise (N_{sc}) for each spatial frequency we can estimate the optical modulation transfer function with equation (5.3). I will call this method the noise comparison method. I assume O_{MTF} to be equal to unity at low spatial frequencies, but it would be possible to include the effect of ocular straylight as Ijspeert, van den Berg & Spekreijse (1993) did by assuming O_{MTF} to be equal to 0.87 at low spatial frequencies.

The rationale behind the second method for determining the O_{MTF} of the human eye is the following: The three principal factors affecting the human spatial contrast sensitivity function for stationary gratings with a constant long exposure time are stimulus area (A), retinal illuminance (I), and the optical modulation transfer function (O_{MTF}) of the human eye. In Section 3.2 I showed that the effect of retinal illuminance (I) can be equalised across spatial frequencies (f) by keeping the retinal flux (If^{-2}) constant, because then quantal noise reduces contrast sensitivity by a constant factor at all spatial frequencies (Van Nes, Koenderink, Nas & Bouman, 1967). Section 3.3 showed that the influence of grating area (A) can be equalised across spatial frequencies ($f \geq 0.5$ c/deg) at all luminance levels by keeping the number of square cycles (Af^2) constant, because then the effect of spatial integration on contrast sensitivity is similar at all spatial frequencies (Howell & Hess, 1978; Virsu &

Rovamo, 1979; Rovamo et al., 1993). On the basis of the above, contrast sensitivities measured for gratings with a constant retinal flux (If^{-2}) and constant number of square cycles (Af^2) are therefore directly proportional to O_{MTF} at all spatial frequencies. I will call this method the relative method.

The rationale of the relative method is in complete accordance with Banks, Geisler and Bennett (1987), who concluded that the decrease of contrast sensitivity with spatial frequency for gratings with a constant number of square cycles (Af^2) is solely due to the O_{MTF} at medium and high spatial frequencies if human vision is not limited by quantal noise i.e. Weber's law is valid. In the relative method quantal noise reduces contrast sensitivity by a constant factor at all spatial frequencies.

5.2.2. METHODS

5.2.2.1. Apparatus, Stimuli, and Procedures

Both the apparatus and the main features of the stimuli and procedures are described in General Methods. Hence, I will here briefly introduce only the special features of the stimuli and procedures. The stimuli were vertical cosine gratings (2 c/cm) in a square field of 8x8 cm^2 with sharply truncated edges. Black cardboard in front of the screen masked the equiluminous surround to a square field of 20x20 cm^2. The spatial frequency was varied by changing the viewing distance within a range of 28.6 - 659 cm. The external noise was one-dimensional. Higher levels of retinal illuminance were obtained by adding external light to the screen. The light source consisted of two defocused Liesegang Fantimat 250 AF slide projectors (Liesegang GmbH, Düsseldorf, Germany) directed obliquely towards the screen and located on both sides of the observer in order to achieve homogenous screen luminance. Different levels of light intensity were produced by changing the distance of the

projectors from the screen and by changing lamp brightness by means of a switch in each slide projector. The effect of additional light on the grating contrasts displayed was taken into account by multiplying the threshold contrasts by $L_o/(L_o+L_i)$, where L_o is the luminance of the screen without additional light and L_i is the amount of light added onto the screen.

5.2.2.2. Subjects

Two experienced subjects, aged 30 and 32 years, served as observers. Both were corrected myopes, -0.75D for JM in the right eye and -1.25D for OL in the right eye. The range of their accommodation was at least 6D and with optimal refraction their monocular Snellen acuities in the dominant eye at 5 m were 1.6.

5.2.2.3. The description of the O_{MTF}

According to Johnson (1972) the optical low-pass attenuation as a function of spatial frequency was modelled as

$$O_{MTF}(f) = \exp[-(f/f_c)^n], \qquad (5.4)$$

where f_c refers to the spatial frequency at which $O_{MTF}(f) = 1/e$, and exponent n indicates how quickly O_{MTF} decreases with increasing spatial frequency above f_c.

In my experiments contrast sensitivity S is directly proportional to the optical modulation transfer function. Hence,

$$K = K_0\, O_{MTF}(f). \qquad (5.5)$$

K_0 corresponds to the maximum sensitivity at spatial frequencies where O_{MTF} is equal to unity. The equations (5.4) and (5.5) can then be combined to obtain the following equation presented in logarithmic form:

$$\ln K = \ln K_0 - (f/f_c)^n, \qquad (5.6)$$

which was fitted to the data of Fig. 5.3.B with KaleidaGraph software package 3.0.1. (Synergy Software, Reading, PA). The goodness of the fit to the data of Fig. 5.3.B is r^2 given by the software.

5.2.3. RESULTS

Fig. 5.1 shows contrast sensitivity as a function of spatial frequency for vertical cosine gratings in three different conditions. In the bright light condition retinal illuminance was 2500, 25000, and 22000 phot. td at 1 - 11, 16, and 23 c/deg, respectively. As previous Chapters have shown the critical retinal illuminance (I_c) marking the transition from DeVries-Rose (DeVries, 1943; Rose, 1948) to Weber's law increases with spatial frequency (Van Nes & Bouman, 1967) higher levels of retinal illuminance were used at 16 - 23 c/deg. In the dim light condition retinal illuminance increased by 0.6 logarithmic units per octave from 0.63 phot. td at 1 c/deg to 320 phot. td at 23 c/deg. The retinal illuminances used were chosen so that contrast sensitivity was at all spatial frequencies reduced approximately by a factor of 3 from the sensitivities measured in the bright light condition. In the third, noise condition, retinal illuminance was 2500 phot. td at all spatial frequencies and the stimulus gratings were embedded in one-dimensional spatial noise. The spectral density of the one-dimensional external Gaussian noise, calculated by equation (2.4), decreased in proportion to increasing spatial frequency from 6.40×10^{-2} deg^2 at 1 c/deg to 2.30×10^{-7} deg at 23 c/deg^2. The range of spatial frequencies studied in all three conditions was 1 - 23 c/deg. Grating

area varied from 0.484 at 23 c/deg to 254 deg^2 at 1 c/deg. The number of square cycles (Af^2) was constant at 256.

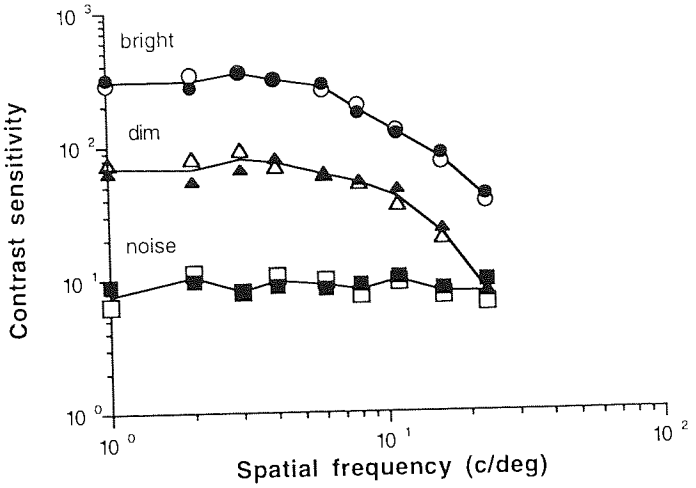

Fig. 5.1. *Contrast sensitivity as a function of spatial frequency in bright and dim light and in one-dimensional spatial noise. Open symbols JM, solid symbols OL.*

As Fig. 5.1 shows, in bright light contrast sensitivity was practically constant at 1 - 6 c/deg but decreased thereafter with increasing spatial frequency. The result is consistent with Virsu and Rovamo (1979) and Rovamo, Franssila and Näsänen (1992) who have shown that for a grating with a constant number of square cycles contrast sensitivity is constant at low and medium spatial frequencies decreasing thereafter with increasing spatial frequency. The same result was also obtained in the study of Section 3.3. The result is also in agreement with McCann (1978) who showed that contrast sensitivity is independent of the viewing distance provided that spatial frequency is not too high. In dim light contrast sensitivity was similarly constant at 1 - 6 c/deg and then decreased with increasing spatial frequency. At all spatial frequencies contrast sensitivity was lower by a factor of 3 - 5 in dim than bright light. The decrease at high spatial frequencies was steeper in dim light, probably because in bright light condition the retinal illuminance of 2500 phot td used at 1-11 c/deg was increased to 22000 - 25000 phot. td at 16 - 23 c/deg. Contrast

sensitivity for gratings embedded in one-dimensional spatial noise was independent of spatial frequency at all spatial frequencies studied, in agreement with the result of Rovamo et al. (1992) obtained in two-dimensional spatial noise. At 1 - 16 c/deg contrast sensitivity in noise was lower than contrast sensitivity in dim or bright light, whereas at 23 c/deg contrast sensitivity in noise was equal to contrast sensitivity in dim light. The results of both subjects were almost identical in all three conditions.

According to Chapter 3 the dependency of contrast sensitivity (S) on retinal luminance (I) can be described by the equation

$$S = S_{max} (1 + I_c/ I)^{-0.5}, \qquad (3.3)$$

which combines the DeVries-Rose and Weber's laws, as explained in Chapter 3. S_{max} is the maximum contrast sensitivity obtainable in bright light and I_c is the critical retinal illuminance at which $S = S_{max} / \sqrt{2}$. Using the contrast sensitivity values of Fig. 5.1 measured in bright and dim light at each spatial frequency it was possible to obtain estimates of I_c and S_{max} for 1-23 c/deg because equation (3.3) has only two parameters. For this purpose equation (3.3) was transformed to $S^{-2} = (S_{max}^{-2}) + (S_{max}^{-2} I_c) I^{-1}$, which is equivalent to the equation of a line, where S^{-2} is the dependent variable, I^{-1} is the independent variable, and (S_{max}^{-2}) and $(S_{max}^{-2} I_c)$ are the vertical intercept and slope of the line, respectively. By fitting a line of least squares to the two values of contrast sensitivity of which the other was measured in dim light and the other was obtained in bright light I got the estimates of vertical intercept and slope for each spatial frequency. The line of least squares is in fact an exact solution (explained variance 100%), because two pairs of dependent and independent variables can always be connected by a straight line. Hence, the unavoidable experimental inaccuracies in the two contrast sensitivities measured are not reflected in the above explained variance. I then calculated

the estimates of S_{max} and I_c for each spatial frequency by taking the inverse of the square root of the vertical intercept and by dividing the estimate of slope by the estimate of the vertical intercept.

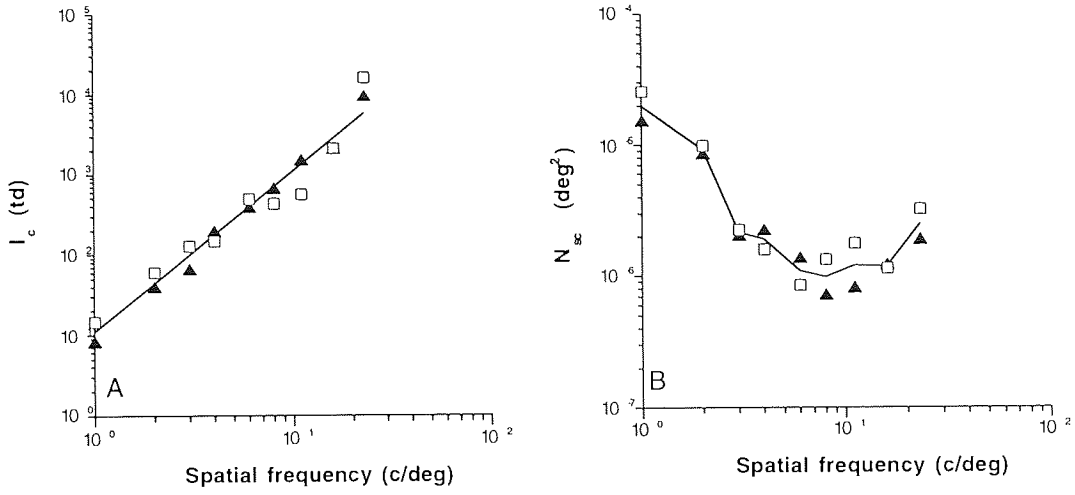

Fig. 5.2. *A) Critical retinal illuminance as a function of spatial frequency. B) the estimates of critical spectral density of external added spatial noise. Open and solid symbols refer to JM and OL, respectively.*

The fitting procedure revealed that the estimates of S_{max} (although not shown) at each spatial frequency were practically identical to the contrast sensitivities measured in bright light, which corroborates that in the bright light condition Weber's law was valid and contrast sensitivity was not limited by quantal noise.

The estimates of I_c were plotted in Fig 5.2.A as a function of spatial frequency in double logarithmic co-ordinates. As Fig. 5.2.A shows, I_c increased linearly as a function of spatial frequency with a slope of 2. The critical retinal illuminance (I_c) thus increased in proportion to spatial frequency squared, again in agreement with Van Nes et al. (1967) and Chapter 3. The equation fitted to the estimates of I_c was therefore $I_c = I_0F^2$. To obtain the value of I_0 the estimates of I_c were first divided by F^2 and then geometrically averaged. I_0

was found to be 11 phot td deg^2, in accordance with the earlier studies of this thesis. The values for I_0 were found to be 21, 7.93, and 5.22 phot td deg^2 in the studies of Sections 3.2 and 3.3 and Chapter 4, respectively. The numerical value of I_0 provides an estimate for critical retinal illuminance in phot td at 1 c/deg. The percentage of the total variance explained was 96%.

According to Rovamo, Luntinen & Näsänen (1996) the dependency of contrast sensitivity (S) on the spectral density (N_S) of external white two-dimensional spatial noise can be described by equation

$$S = S_{max} (1 + N_S / N_{sc})^{-0.5}, \quad (5.7)$$

where S_{max} is the maximum contrast sensitivity obtainable without external noise and N_{sc} is the critical spectral density of noise at which $S = S_{max} / \sqrt{2}$. Equation (5.7) is in agreement with Burgess, Wagner, Jennings & Barlow (1981) who showed that contrast energy threshold ($E = S^{-2}A$) increases as a linear function of N_S. On the basis of Fig. 3 in Stromayer and Julesz (1972) and Rovamo and Kukkonen (1995) equation (5.7) applies to one-dimensional noise, too.

The estimates of N_{sc} and S_{max} for 1 -23 c/deg were obtained by using equation (5.7) and the contrast sensitivity values of Fig. 5.1 measured in bright light and spatial noise at each spatial frequency. The procedure was similar to that applied to equation (3.3). The equation (5.7) was transformed to $S^{-2} = (S_{max}^{-2}) + (S_{max}^{-2} N_{sc}^{-1}) N_S$, which is equivalent to the equation of a line where S^{-2} is the dependent variable, N_S is the independent variable, and (S_{max}^{-2}) and $(S_{max}^{-2} N_{sc}^{-1})$ are the vertical intercept and slope of the line, respectively. By fitting a line of least squares to the two values of contrast sensitivity measured in spatial noise and bright light ($N_S = 0$) I got the estimates of vertical intercept and slope for each spatial frequency. I then

calculated the estimates of S_{max} and N_{SC} for each spatial frequency as (1/√vertical intercept) and (vertical intercept / slope).

Fig. 5.2.B. shows the estimates of N_{SC} plotted as a function of spatial frequency in double logarithmic co-ordinates. With increasing spatial frequency N_{SC} first decreased with a slope of -2 up to 6 c/deg reaching a minimum at about 8 c/deg and increased thereafter, in agreement with the result of Rovamo et al. (1996) obtained with two-dimensional white spatial noise.

The estimates of N_{SC} and I_C were used to calculate the estimates of expression $(\gamma I_C N_{SC})^{-0.5}$, which is plotted as a function of spatial frequency in Fig. 5.3.A. The estimates of $(\gamma I_C N_{SC})^{-0.5}$ were constant at 1 - 4 c/deg after which they started to decrease with spatial frequency. According to equation (5.3) the estimates of

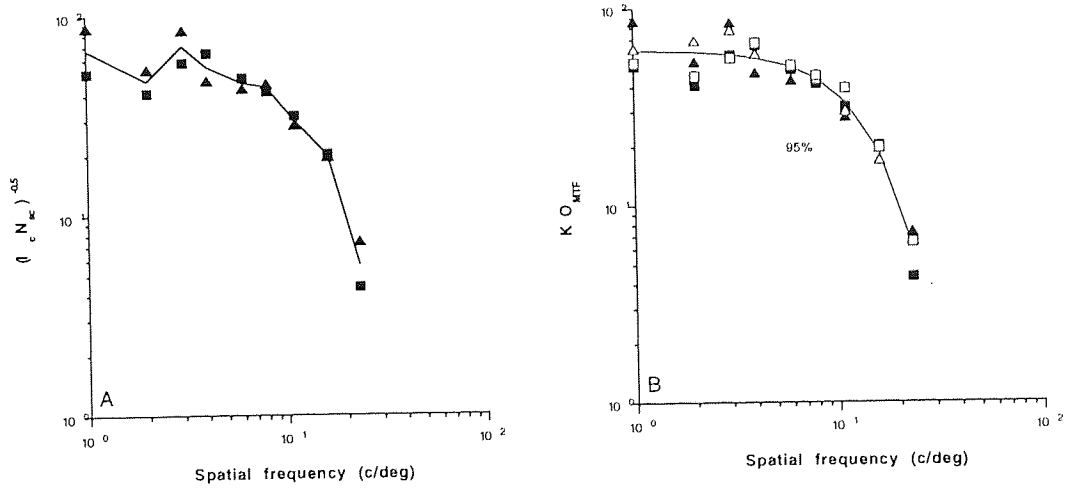

Fig. 5.3. *A) Optical modulation transfer function multiplied by a scaling constant, and obtained by the noise comparison method. B) Contrast sensitivity data obtained by the relative method and multiplied by 0.83, and plotted together with data from plot A) as a function of spatial frequency. The O_{MTF} is estimated by* $exp[-(f/13.8)^{1.45}]$

$(\gamma I_c N_{sc})^{-0.5}$ are directly proportional to the O_{MTF} of the human eye as If^{-2} and Af^2 were both kept constant across spatial frequencies.

The contrast sensitivities at 1 - 4 c/deg in dim light (Fig. 5.1) were then geometrically averaged as well as the estimates of $(\gamma I_c N_{sc})^{-0.5}$ at 1 - 4 c/deg (Fig. 5.3.A). The averaged values turned out to be 72.6 and 60.6, respectively. Their ratio 0.83 was used to superimpose the spatial contrast sensitivity function measured in dim light and the estimates of $(\gamma I_c N_{sc})^{-0.5}$ by multiplying the dim light contrast sensitivity data by 0.83. The vertically scaled contrast sensitivities are plotted in Fig. 5.3.B. together with the estimates of $(\gamma I_c N_{sc})^{-0.5}$.

After vertical scaling the spatial contrast sensitivity function measured in dim light was practically identical to the estimates of $(\gamma I_c N_{sc})^{-0.5}$ at all spatial frequencies as Fig. 5.3.B shows. This means that my two methods provided identical estimates of the foveal O_{MTF} for the human eye. The statistical independence of the two methods is not affected by the fact that the contrast sensitivity function measured in the dim light condition provided an estimate for the O_{MTF} and was also used to estimate the values of I_c at various spatial frequencies, because the estimate of I_c depends also on the contrast sensitivity in the bright light condition. In addition, the estimate of the foveal O_{MTF} determined by the noise comparison method was at each spatial frequency based on the product of I_c and N_{sc}, of which the latter was calculated from the contrast sensitivities measured in bright light and embedded in spatial noise.

Optical low-pass attenuation as a function of spatial frequency was modelled by a low-pass filter (Johnson, 1972). Hence, equation (5.6) was fitted to the data of Fig. 5.3.B. The value of the parameter f_c, indicating the spatial frequency at which S = 1/e, was 13.8 c/deg. The parameter n denoting how

steeply contrast sensitivity declines above f_c, was 1.45, and the proportionality constant K_0 was 66.2. Explained variance for the smooth curve was 94%.

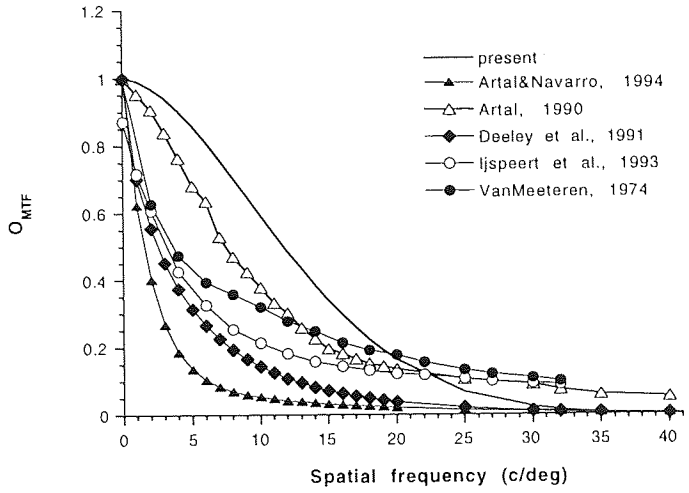

Fig. 5.4. *Foveal O_{MTF}s obtained by various methods as a function of spatial frequency on linear axis.*

The foveal O_{MTF} of the human eye for a pupil diameter of 8 mm was obtained by assuming that the optical attenuation is zero at 0 c/deg. In Fig. 5.4 the estimate for the O_{MTF} has been plotted in linear co-ordinates as a function of spatial frequency together with other, previously published estimates (Artal, 1990; Artal & Navarro, 1994; Ijspeert et al., 1993; Deeley et al., 1991; Van Meeteren, 1974) for pupil diameters of 5.8 - 8 mm.

My estimate gave the highest estimate for O_{MTF} at 1 - 18 c/deg. Artal's (1990) monochromatic O_{MTF} was obtained by an advanced version of the double-pass method for a 6 mm pupil, and it is closest to my estimate and similar in shape. Van Meeteren (1974) utilised the typical aberrations of the human eye and calculated the O_{MTF} in white light for a 7 mm pupil. Ijspeert et al. (1993) transformed the monochromatic O_{MTF} of Campbell & Green (1965), obtained by the laser interference method for a 5.8 mm pupil, to a white light O_{MTF}. The estimate also took into account stray light by assuming that O_{MTF} = 0.87 at 0

c/deg. Deeley et al. (1991) pooled the O_{MTF}s from Campbell & Gubisch (1966), obtained by the double-pass method, and from Van Meeteren (1974) combined with the retinal scatter data of Ohzu & Enoch (1972), and calculated the O_{MTF} of the human eye for an 8 mm pupil. The lowest estimate is by Artal & Navarro (1994), which was also determined by the advanced double-pass method.

5.2.4. DISCUSSION

My experiments showed that under the assumption that the optical attenuation of contrast at 0 c/deg is zero, the foveal optical modulation transfer function of the human eye measured with two new psychophysical methods for an 8 mm pupil is $O_{MTF} = \exp [-(f/13.8)^{1.45}]$. The equation means that O_{MTF} is reduced to 1/e at 13.8 c/deg, after which it decreases with a slope of -1.45 when plotted in double logarithmic co-ordinates. The O_{MTF} measured represents now contrast attenuation between the anterior surface of the cornea and the absorption of light quanta in the outer segments of photoreceptors. It thus includes, for example, all the optical aberrations, pupil-location dependent lenticular absorption, intraocular and retinal scatter as well as the Stiles-Crawford (1933) effect.

The noise comparison method used light-dependent quantal noise and external added white spatial noise, and compared their effects on grating contrast sensitivity across spatial frequencies. The spatial noise was attenuated by O_{MTF} whereas quantal noise by-passed the optical blur. Hence, the method resembles to the laser interference method (e.g. Westheimer, 1960; Campbell & Green, 1965; Williams et al., 1994). The estimates of I_c were obtained from the experimental contrast sensitivity data by means of equations (3.3), which combines the DeVries-Rose and Weber's laws valid in dim and bright light, respectively. The estimates of N_{sc} were similarly obtained by

means of equation (5.7), which is equivalent to the well established fact that contrast energy threshold increases as a linear function of the spectral density of external noise (Burgess et al, 1981; Legge, Kersten & Burgess, 1987; Pelli, 1990). Equations (3.3) and (5,7) describe the dependence of contrast sensitivity on retinal illuminance and on the spectral density of external spatial noise quite accurately: the explained variance is typically over 95% (Chapter 3; Luntinen et al., 1994).

The relative method utilised the equalization of the effect of grating area and retinal illuminance on contrast sensitivity across spatial frequencies. The equalization was based on two solid experimental findings of the foveal vision, which have been shown in Chapter 3. First, critical retinal illuminance (I_c) marking the cessation of the DeVries-Rose law resulting from quantal noise is proportional to spatial frequency squared at 0.125 - 32 c/deg (Van Nes et al., 1967) and second, critical area marking the cessation of the Piper's law of spatial integration is inversely proportional to spatial frequency squared at 0.5 - 32 c/deg (Howell & Hess, 1978; Virsu & Rovamo, 1979; Rovamo et al., 1993b). For both relationships the explained variance is typically over 95% (Section 3.3; Rovamo et al., 1993).

The relative method could have been affected by (i) involuntary fixational eye movements that could improve and reduce contrast sensitivity at low and high spatial frequencies, respectively (see Van Nes et al., 1967), by (ii) exposure time, because the effect of exposure duration on contrast sensitivity varies with spatial frequency (e.g. Legge, 1978), and by (iii) uncontrolled accommodation (Green & Campbell, 1965). However, in agreement with Rovamo et al. (1993), the combined effect of these factors seems to be negligible in my experiments, because both the relative and noise comparison methods gave similar results. Besides, the noise comparison method was independent of exposure duration, eye movements, and natural accommodation, as it was based on the

comparison of the effects of quantal (unaffected by O_{MTF}) and spatial (attenuated by optical blur) noises on contrast sensitivity across spatial frequencies.

My estimate for polychromatic foveal O_{MTF} of the human eye was found to be better at 1-18 c/deg than any foveal O_{MTF} previously reported for pupils of 5.8-8 mm (Artal, 1990; Deeley et al., 1991; Ijspeert et al., 1993; Van Meeteren, 1974; Artal & Navarro, 1994). One possible explanation for the various O_{MTF}s could be individual differences. The foveal O_{MTF} for a 5 mm pupil at 5-20 c/deg has been reported to vary by a factor of 2-4 between 55 observers (Howland & Howland, 1977). Artal, Ferro, Miranda and Navarro (1993) have proposed that interindividual differences are mainly due to refraction and ageing. Artal and Navarro (1994) also concluded rather constant image quality for the eight subjects used in their study. The number of observers was only two in Artal (1990), Campbell and Green (1965), and the current study whereas Van Meeteren (1974) utilised the typical aberrations of the human eye and Deeley et al. (1991) pooled together the data of Van Meeteren (1974) and Campbell & Gubisch (1966).

Artal (1990) used an advanced version of the double pass method and produced a monochromatic foveal O_{MTF} for a 6 mm pupil. His estimate is closest to ours and similar in shape. However, the other estimate provided by the same method (Artal & Navarro, 1994) was a lot worse than my estimate or the estimate of Artal's. Artal and Navarro (1994) discussed the difference concluding that the better estimate of Artal (1990) was caused by uncorrected refraction. Also, the effect of Stiles-Crawford effect (SCE) was taken into account in Artal's (1990) study, but not in the Artal & Navarro (1994) study. I will discuss the SCE more thoroughly in the following experiment, where comparison with Artal and Navarro's study is made for several pupil sizes. Nevertheless, the major assumption in the

double-pass technique is that coherence is destroyed when the image is reflected at the retina, so that it is valid to take the O_{MTF} of the eye as being the square root of the O_{MTF} deduced from the measurement of a double-pass, external point/line-spread function (Charman, 1991). However, the reflected light is exactly the light that has not been absorbed in the photoreceptors (or elsewhere), whereas from the point of view of visual perception it would, instead, be relevant to know the optical spread of the light that is subsequently absorbed in the photoreceptors.

Ijspeert et al. (1993) transformed the monochromatic foveal O_{MTF} of Campbell and Green (1965) measured by the laser interference method to a white light O_{MTF} for a 5.8 mm pupil. They also took into account the effect of straylight by assuming that $O_{MTF} = 0.87$ at 0 c/deg, which reduced O_{MTF} by 13% i.e. 0.06 logarithmic units at all spatial frequencies. In the experiments of Campbell and Green (1965) the diameter of the red interference grating was 30 deg whereas the green grating on the screen was considerably smaller, because the aperture in front of the oscilloscope was only 1.3 x 2 deg^2. Thus, the extensive spatial integration (Hoekstra, van der Goot, van den Brink & Bilsen, 1974; Savoy & McCann, 1975; Howell & Hess, 1978; Virsu & Rovamo, 1979) across the internal grating explains why contrast sensitivity in Fig. 9 of Campbell and Green (1965) is at low and medium spatial frequencies clearly better for internal than external grating. This results in an underestimation of the O_{MTF} of the human eye, because in the interference method O_{MTF} is at each spatial frequency calculated as the ratio of the external to internal contrast sensitivity. The difference between external and internal grating sizes in the experiment of Campbell and Green (1965) thus provides an explanation why the O_{MTF} of Ijspeert et al. (1993) is lower than mine at low and medium spatial frequencies.

Van Meeteren (1974) utilised the typical aberrations of the human eye, took into account the Stiles-Crawford (1933) effect, and calculated the O_{MTF} of the human eye for a 7 mm pupil in white light. It is, however, quite possible, that all the typical aberrations never occur in the same human eye and the existing aberrations tend to cancel each other resulting in an O_{MTF} better than the O_{MTF} based on the typical aberrations. This could explain why the O_{MTF} of Van Meeteren (1974) is lower than mine at 1-23 c/deg.

Deeley et al. (1991) pooled together the O_{MTF}s of Campbell & Gubisch (1965) obtained by the double-pass method and Van Meeteren (1974) combined with the retinal scatter data of Ohzu and Enoch (1972) and calculated the polychromatic O_{MTF} of the human eye for an 8 mm pupil. Thus, it is understandable that the O_{MTF} of Deeley et al. (1991) was lower than the O_{MTF} of Van Meeteren (1974).

In conclusion, the foveal optical modulation transfer functions (O_{MTF}) of the human eye, determined in white light for an 8 mm pupil by two new independent psychophysical methods based on (i) the comparison of the effects of quantal and spatial noise and (ii) the equalization of the effect of grating area and retinal illuminance on contrast sensitivity across spatial frequencies, were found to be identical across the spatial frequency range of 1 - 23 c/deg used in my study, and to have higher values at 1 - 18 c/deg than any foveal O_{MTF} previously reported in the literature for 5.8 - 8 mm pupils.

5.3. O_{MTF} at various pupil sizes

Section 5.2 studied the O_{MTF} of the human eye only at one pupil size (ø 8mm). In the following Section the effect of pupil size will be examined by using the relative method (constant retinal flux (If^{-2}) and constant number of square cycles (Af^2) across spatial frequencies) introduced in Section 5.2.

5.3.1. METHODS

The methods used in this study are almost identical to those in the previous Section 5.2.

The stimuli were vertical cosine gratings (2 c/cm) in a square field of 8 x 8 cm^2 with sharply truncated edges. Different spatial frequencies were obtained by changing the viewing distance within the range of 28.6 - 917 cm. The pupil size was varied by using soft black opaque contact lenses (Madden & Layman Ltd., St. Leonards-on-Sea, U.K.) with transparent pupils of various sizes. The pupil sizes used were 1.5, 2, 4 and 6 mm in diameter. For a pupil size of 8 mm an otherwise similar, but clear contact lens was used. The contact lenses with zero refractive power were fitted optimally to both of the subjects, who were the same as in the previous study. Both had experience in using contact lenses.

5.3.2. RESULTS

In the experiments I measured contrast sensitivity for vertical cosine gratings as a function of spatial frequency in order to determine the foveal O_{MTF} of the human eye for various pupil sizes. According to the relative method described in Section 5.2. the screen luminance increased with spatial frequency in steps of 0.6 logarithmic units per octave from 0.049 cd/m^2 at 1 c/deg to 50 cd/m^2 at

32 c/deg. Retinal flux (If^{-2}) was thus kept constant across spatial frequencies (f) at each pupil size. However, as retinal illuminance (I) depends on the aperture, retinal flux also varied with pupil size. Hence, retinal flux (If^{-2}) was 0.0863, 0.153, 0.614, 1.38, and 2.45 phot td deg^2 at the pupil sizes of 1.5, 2, 4, 6 and 8 mm, respectively.

The number of square cycles (Af^2) was always equal to 256, as spatial frequency (f) and grating area (A) were varied by changing the viewing distance from 28.6 cm at 1 c/deg up to 917 cm at 32 c/deg.

Preceding the actual experiments, the O_{MTF} of the contact lenses was to be determined. Thus, in the experiment of Fig. 5.5 I measured spatial contrast sensitivity functions for a pupil of 8 mm in diameter with and without a clear contact lens. The O_{MTF} can now be calculated as the ratio of the spatial contrast sensitivity functions measured. However, as Fig. 5.5 shows, the two contrast sensitivity functions were identical being independent of spatial frequency from 1 to 6 c/deg and decreasing thereafter. The similarity of the two

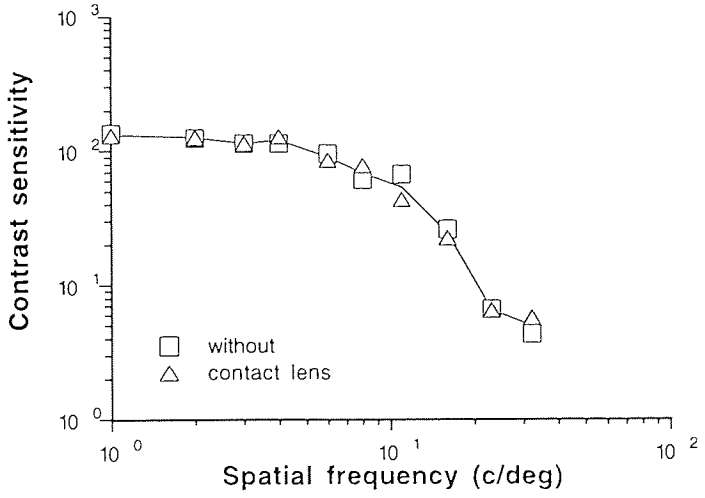

Fig. 5.5. Contrast sensitivity as a function of spatial frequency with and without a clear contact lens. Pupil diameter was 8 mm and subject JM.

contrast sensitivity functions indicates that the O_{MTF} of the clear contact lens with zero refractive power was equal to unity across 1 - 32 c/deg.

Fig. 5.6 shows contrast sensitivity as a function of spatial frequency measured for the pupil diameters of 1.5, 2, 4, 6 and 8 mm. The spatial contrast sensitivity functions were similar for the two subjects. Irrespective of pupil size contrast sensitivity remained practically constant at low and medium spatial frequencies (≤6 c/deg) but decreased then at higher spatial frequencies.

The smooth curve at each pupil size describes the optical low-pass attenuation as a function of spatial frequency. It was calculated by equation (3.21) fitted to the combined contrast sensitivity data of the two subjects at each pupil size. The explained variance was on average 92% with a range of 88 - 95%. The maximum contrast sensitivity (S_0) obtainable at each luminance level was found to be 50, 63, 117, 147, and 174 at the pupil diameters of 1.5, 2, 4, 6, and 8, respectively. The increase of S_0 with pupil diameter is due to the increase of contrast sensitivity with retinal illuminance (Van Nes & Bouman, 1967).

The dashed curve in each frame represents the O_{MTF} of the diffraction limited system with a circular aperture at the wavelength of 550 nm. It was calculated (see Appendix 4) according to Johnson (1972) and multiplied by the value of S_0 corresponding to each pupil size. The dotted curve shows the O_{MTF} when the inevitable retinal light scatter (Ohzu & Enoch, 1972) has been taken into account by multiplying the diffraction limited system of each pupil size by the optical modulation transfer function of the foveal retina, which is independent of pupil size and calculated (Appendix 4) according to Deeley et al. (1991).

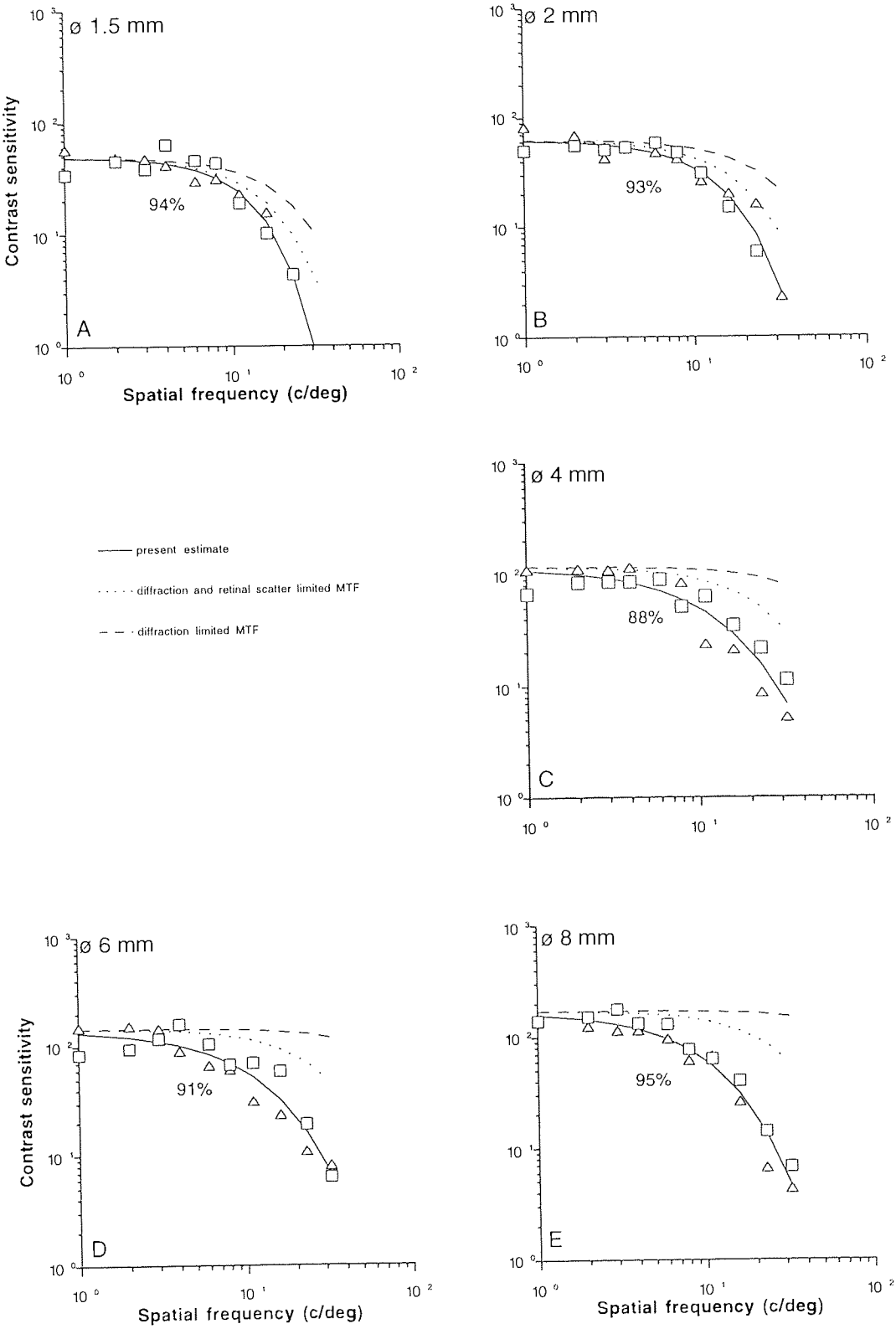
ø 1.5 mm
94%
A
ø 2 mm
93%
B
ø 4 mm
88%
C
ø 6 mm
91%
D
ø 8 mm
95%
E
Contrast sensitivity
Spatial frequency (c/deg)
present estimate
diffraction and retinal scatter limited MTF
diffraction limited MTF

Fig. 5.6. Spatial contrast sensitivity functions at various pupil sizes. With each pupil diameter the retinal flux and the number of square cycles were kept constant across spatial frequencies.

Fig. 5.6 shows that the estimate of O_{MTF} at the pupil diameter of 1.5 mm is quite close to the circular aperture system limited by diffraction and retinal light scatter.

At the pupil diameters of 2 - 8 mm the O_{MTF} of the human eye progressively deviates from the O_{MTF} of the diffraction and retinal light scatter limited system.

The values of the parameters of the estimates of O_{MTF}, i.e. f_c and n, have been plotted as a function of pupil size in Fig. 5.7. The solid triangles in both of the frames of Fig. 5.7 refer to the fit of equation (5.6) to the $(I_c N_{sc})^{-0.5}$ data of the previous study (noise comparison method in Section 5.2), which was conducted with an 8 mm pupil. The error bars show the standard errors, as given by the software.

The values of f_c as a function of pupil size are shown in Fig. 5.7.A. They were found to be 13.3, 14.3, 11.8, 10,7 and 9.7 (12.6) c/deg at pupil diameters 1.5, 2, 4, 6 and 8 (8) mm, respectively, suggesting that there is a rapid change between pupil diameters 2 and 4 mm. The horizontal lines estimate the values of f_c at different pupil diameters, and were calculated as the geometrical means of the values of f_c at 1.5 - 2 mm and 4 - 8 mm. The oblique part of the estimate is an interpolation between 2 and 4 mm.

According to Johnson (1972) the f_c of a diffraction limited system can be described as $f_c = 0.48\ f_0$, where f_0 is the cut-off frequency (Appendix 4). The corresponding dashed line has been drawn in Fig. 5.7.A. As the retinal light scatter is independent on the pupil size, another, but smoothly curving dotted

line has been added to the frame describing the O_{MTF} of the diffraction and retinal light scatter (Ohzu & Enoch, 1972) limited eye. The dotted curve was obtained as follows: First the O_{MTF}s calculated for diffraction limited systems with small apertures (0.25 - 1.75 mm) were multiplied by the O_{MTF} due to retinal light scatter, which is independent of pupil size. The equation (5.4) was then fitted to the calculated values, providing theoretical values of f_c for a diffraction and retinal light scatter limited eye. The intersection of the dotted function describing the theoretical dependence of parameter f_c on pupil size, with the average of experimental estimates of f_c at small pupil sizes indicate that ocular optics would be limited only by diffraction and retinal light scatter when pupil diameter ≤ 1.1 mm. Diffraction would be the only limiting factor at the pupil sizes ≤ 0.9, where the horizontal and dashed lines intersect.

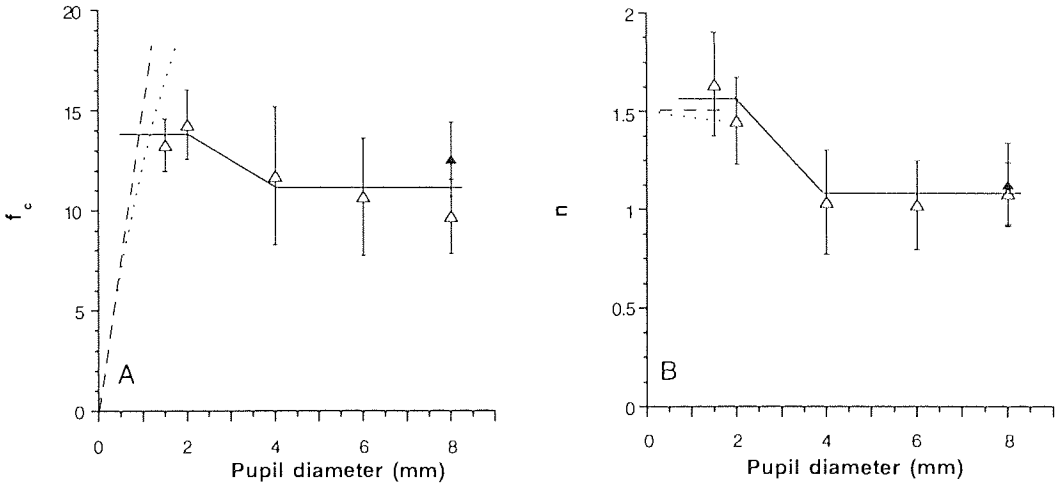

Fig. 5.7. *The values of fc (A) and n (B) as a function of pupil diameter. The dashed curves show the pupil size dependency of the parameters of the O_{MTF} of the diffraction limited system, and the dotted curves show the pupil size dependency of the parameters of the O_{MTF} of the diffraction limited system affected by retinal scatter.*

Fig. 5.7.B .shows the values of n indicating the steepness of the decrease of O_{MTF} at higher spatial frequencies. At pupil sizes of 1.5 - 2 mm the value of n was about 1.55, which deviates only little from the value of n = 1.5 valid for the

totally diffraction limited system at circular apertures ≤ 1.5 mm (Johnson, 1972). At 4 - 8 mm the value of n was about 1.05, implying again a swift change between diameters of 2 and 4 mm.

A comparison of the present estimates of human foveal O_{MTF} with other previously published estimates obtained with various methods is presented in Fig. 5.8. The recent estimates from Van Meeteren (1974), Deeley et al. (1991), Ijspeert et al. (1993) and Artal & Navarro (1994) together with the results of the present study at various pupil sizes have been plotted on semilogarithmic co-ordinates. Ijspeert et al. (1993) represents the laser interference method, as they converted the monochromatic data of Campbell & Green (1965) into white light O_{MTF}. They also took into account the effect of intraocular light scatter so that their O_{MTF} at zero frequency is 0.87. For pupil sizes 2 and 4 mm I have used their most recent estimates (Van den Berg, Ijspeert & Spekreijse, 1994). Artal & Navarro (1994) represent a very sophisticated double-pass method with monochromatic 632.8 nm light. Van Meeteren (1974) used averaged individual aberrations, took into account the Stiles-Crawford effect (1933), and calculated O_{MTF} in white light. Deeley et al. (1991) calculated their O_{MTF} in white light by combining the data of Campbell & Gubisch (1966), Van Meeteren (1974) and Ohzu & Enoch (1972).

As very few estimates of O_{MTF} are available for the pupil size of 1.5 mm, I averaged the estimates for 1 and 2 mm by Van Meeteren (1974) to approximate an estimate for 1.5 mm. All estimates of white-light O_{MTF} at 1.5 mm (Van Meeteren, 1974; Deeley et al., 1991; current) showed similar attenuation and were found to be equivalent to the monochromatic diffraction and retinal light scatter limited system at low and intermediate (≤ 10 c/deg) spatial frequencies. At spatial frequencies above 10 c/deg the current estimate decreased slightly more rapidly than the estimates of Van Meeteren (1974)

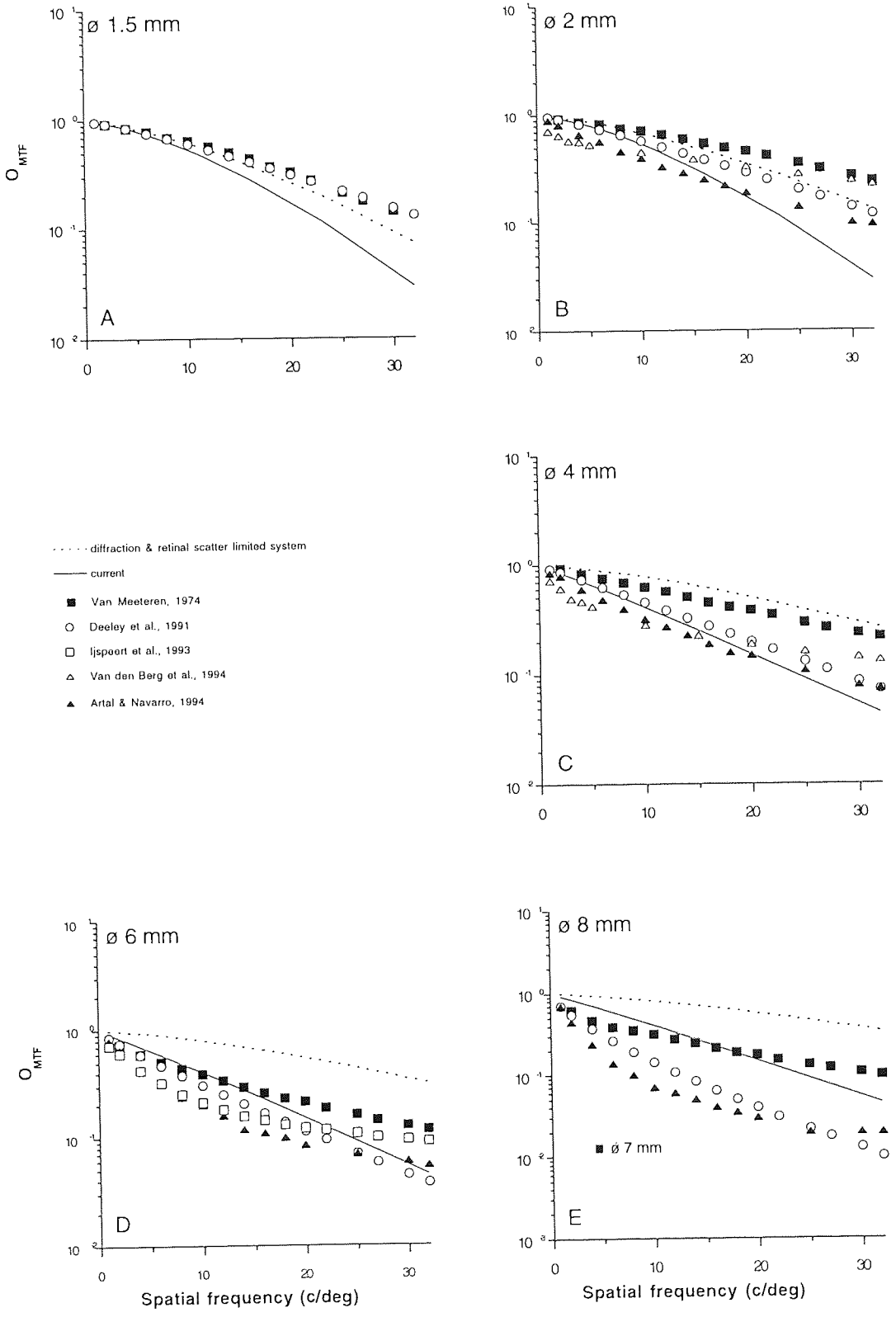
ø 1.5 mm
A
ø 2 mm
B
ø 4 mm
C
ø 6 mm
D
ø 8 mm
ø 7 mm
E
O_{MTF}
Spatial frequency (c/deg)
diffraction & retinal scatter limited system
current
Van Meeteren, 1974
Deeley et al., 1991
Ijspeert et al., 1993
Van den Berg et al., 1994
Artal & Navarro, 1994

Fig. 5.8. Comparison of the previously published O_{MTF}s with the current estimates at various pupil diameters.

and Deeley et al. (1991), which both still followed the theoretical upper limit of the O_{MTF} up to 15 c/deg. However, at spatial frequencies above 15 c/deg both Van Meeteren (1974) and Deeley et al. (1991) seem to exceed the monochromatic O_{MTF} of the diffraction and retinal light scatter limited system.

For the pupil size of 2 mm the estimates of Van den Berg et al. (1994) and Artal & Navarro (1994) are at low and medium spatial frequencies ($\leq$ 10 c/deg) lower than the estimates of Van Meeteren (1974), Deeley et al. (1991), and the current study, which all follow the theoretical upper limit of the O_{MTF}. Between 10 - 20 c/deg the estimate of the current study fell between Deeley et al. (1991) and Artal & Navarro (1994). At higher spatial frequencies Van Meeteren (1974) and Van den Berg et al. (1994) exceed the monochromatic O_{MTF} of the diffraction and retinal light scatter limited system, whereas the current estimate goes below Artal & Navarro (1994).

At the pupil size of 4 mm the estimate of Van Meeteren (1974) for O_{MTF} showed practically no deviation from the monochromatic (550 nm) O_{MTF} of the diffraction and retinal light scatter limited system. However, Deeley et al. (1991) agreed well with the present study, while Artal & Navarro (1994) and Van den Berg et al. (1994) were slightly lower below 20 c/deg. At higher spatial frequencies the current estimate still agrees well with Deeley et al. (1991) and also with Artal & Navarro (1994), whereas Van den Berg et al. (1994) shows a slight tendency towards the O_{MTF} of the diffraction and retinal light scatter limited eye.

At the pupil size of 6 mm all estimates are well below the O_{MTF} of the system limited by diffraction and retinal light scatter. Below 15 c/deg only Artal &

Navarro (1994) and Ijspeert et al. (1993) are lower than the other estimates. At higher spatial frequencies the decrease of the estimates of Van Meeteren (1974) and Ijspeert et al. (1993) slows down while other estimates remain in good agreement with the current estimate.

The O_{MTF} estimates of Deeley et al. (1991) and Artal & Navarro (1994) for an 8 mm pupil decreased quickly with increasing spatial frequency. Above 10 c/deg Deeley et al. (1991) is parallel to the current estimate. Artal & Navarro (1994) slow down above 20 c/deg and approach the current estimate exceeding it at f > 30 c/deg. Van Meeteren's (1974) estimate for a 7 mm pupil was worse below 15 c/deg but then became better than the current estimate. At higher spatial frequencies his O_{MTF} seems to approach the O_{MTF} of the retinal scatter and diffraction limited system.

5.3.3. DISCUSSION

The foveal O_{MTF} of the human eye was determined by measuring contrast sensitivity at various pupil sizes for gratings with constant retinal flux and number of square cycles. This simple psychophysical method yielded estimates which are in general agreement with other but more arduous techniques. The human foveal O_{MTF} was modelled as $O_{MTF} = \exp [-(f/f_c)^n]$, where f refers to spatial frequency in c/deg and parameters f_c and n depend on pupil size. At small pupil sizes (1.5 - 2 mm) f_c = 13.8 c/deg and n = 1.55, whereas at pupil sizes 4 - 8 mm f_c = 11.1 c/deg and n = 1.07. There is bound to be a rapid change between 2 and 4 mm pupil diameters.

The fact that in the previous study (Section 5.2) I obtained higher values for parameters f_c and n with an 8 mm pupil than would be predicted by this study exposes the sensitivity of my fit. I realise that the spacing of spatial frequencies measured should be more dense, as now individual datapoints affect the

fitting procedure significantly. In the study of Section 5.2 the highest spatial frequency used was 23 c/deg compared to 32 c/deg in this study. However, the more results I obtained (more estimates in Section 5.4) they tend to support the values presented here.

Diffraction and retinal light scatter set the upper limit for the eye's performance at small pupil diameters. My results show that the human eye at pupil diameter of 1.5 - 2 mm behaves like the diffraction limited system with the circular aperture of 0.9 mm in diameter, and assuming that retinal light scatter is as Ohzu & Enoch (1972) have proposed, its pupil diameter would be 1.1 mm. The difference in pupil diameter is due to intraocular light scatter and aberrations of ocular optics. With increasing pupil size the contribution of these factors increases which explains the progressive deviation of the O_{MTF} of the human eye from the circular aperture diffraction and retinal light scatter limited system at pupil diameters of 2 - 8 mm.

The basic differences between the methods which have been used to estimate the human O_{MTF} has already been discussed in the Introduction (5.1) and Section 5.2, thus now I will only review the differences between the previous estimates and the current one at various pupil sizes.

Van Meeteren (1974) based his calculations on averaged individual aberrations, and obtained estimates of the O_{MTF} for polychromatic white light. With pupil sizes $\leq$ 4 mm his estimates exceed the present ones at all spatial frequencies. As a matter of fact, his estimates seem to follow the theoretical O_{MTF} of the diffraction and retinal light scatter limited eye, and even exceeding it at high spatial frequencies with 1.5 mm pupil. With a 6 mm pupil his estimate is coinciding with the present estimate below 15 c/deg, but exceeds it at high spatial frequencies. At an 8 mm pupil the present estimate is better than Van Meeteren's (1974) at $\leq$ 10 c/deg, but again at high spatial frequencies his

estimate shows less image degradation than suggested in this study, although his estimate is for a 7 mm pupil aperture.

Deeley et al. (1991) calculated their analytical approximation for polychromatic white light. They actually combined the data of Campbell & Gubish (1966) and Ohzu & Enoch (1972) as well as the calculations of Van Meeteren (1974). The estimates of Deeley et al. (1991) for the pupil sizes of 4 and 6 mm are in good agreement with the present estimate at all spatial frequencies. At smaller pupil diameters they estimate the O_{MTF}s to be higher than the current one, exceeding the O_{MTF} of the diffraction and retinal scatter limited eye at 1.5 mm pupil size. At an 8 mm pupil size, however, their approximation indicates more optical deterioration than my estimate.

Both Ijspeert et al. (1993) and Van den Berg et al. (1994) based their estimates on the interferometric results of Campbell & Green (1965). At all pupil sizes available (2, 3.8, 5.8) the estimates fall below mine at low and medium spatial frequencies in a manner that the smaller the pupil size, the lower the spatial frequency where their estimates become better than the current ones.

The current estimate agrees to a great degree with the estimates obtained by the double-pass technique (Artal & Navarro, 1994) at pupil sizes of 2 and 4 mm (see also Fig. 5.15.A). However, at medium spatial frequencies with a 6 mm pupil Artal & Navarro estimate the image degradation caused by ocular optics to be worse than the current estimation. With an 8 mm pupil the current estimate is above Artal & Navarro (1994) to a considerable degree at spatial frequencies below 30 c/deg, but then the relationship seems to be reversed.

The most likely reason for the discrepancy between the O_{MTF}s of Artal & Navarro (1994) and the proposed O_{MTF}s at large pupil sizes is the pupil

apodization (Metcalf, 1965). The Stiles-Crawford effect (1933) is automatically counted for in the present method. However, the double-pass method ignores it. Furthermore, the double-pass technique utilizes the light which is not used, but rejected and reflected back from various parts of the eye. According to Van Meeteren (1974), who did allow for the Stiles-Crawford effect (1933) by including an apodizing function, SCE affects medium spatial frequencies most. This is logical because high spatial frequencies are seen by the fovea, where the receptors are oriented approximately along the visual axis (Enoch & Lakshminarayan, 1991). On the other hand, low spatial frequencies are not attenuated by the O_{MTF}. The effect of SCE on medium spatial frequencies inevitably gets stronger with increasing pupil aperture. Therefore, at least part of the differences between the current estimate and the double-pass method would be expected.

In conclusion the foveal O_{MTF} of the human eye, measured by using the relative method, was described with an explained variance of 92% by $O_{MTF} = \exp [-(f/f_c)^n]$, where f is spatial frequency in c/deg. The parameter n indicates the steepness of the decrease in contrast sensitivity at high spatial frequencies. The values were n = 1.07 when pupil size was 4 - 8 mm, and n = 1.55 with 1.5 - 2 mm diameter. The parameter f_c is the spatial frequency when $O_{MTF} = 1/e$. It was found to be 11.1 c/deg at pupil diameters 4 - 8 mm, and 13.8 c/deg at 1.5 - 2 mm.

5.4. The O_{MTF} at various eccentricities

In this section both the relative and noise comparison methods introduced in Section 5.2 are applied in the peripheral optics.

5.4.1. INTRODUCTION

There are numerous studies concerning the optical quality of human foveal vision, but only a few concentrate on peripheral optics. A general agreement concerning the foveal vision is that optics is a low-pass filter and a major factor limiting visual acuity so that the receptor mosaic is roughly matched with the quality of optics in the fovea (Williams, 1985). In the peripheral vision contrast sensitivity decreases towards the periphery, declining more rapidly at high spatial frequencies (Robson & Graham, 1981). Consequently also the visual acuity declines towards the periphery (Sloan, 1968). An important factor limiting the peripheral resolution seems to be post-receptoral mechanism (Anderson & Hess, 1990; Thibos, Walsh & Cheney, 1987) because receptor density is higher than the sampling density of e.g. ganglion cells in the peripheral retina. In addition, corrected peripheral optics offers better image quality than the underlying receptor mosaic or neural system can utilise (Jennings & Charman, 1978, 1981; Navarro, Artal & Williams, 1993).

Because of the nature of visual information being transmitted by discrete neurones, the human visual system samples the retinal image at spatially discrete locations, and is therefore potentially susceptible to sampling artefacts, or aliasing (Anderson & Hess, 1990). In the fovea the visual system precludes aliasing by low-pass filtering of the eye optics, thus eliminating potentially aliased high spatial frequencies. Preventing spatial frequencies above the local cut-off frequency from reaching the sampling site would be the optimum solution in the periphery as well. Nevertheless, the optimum

irregularity in the cone mosaic (Yellott, 1982), or averaging over the receptor aperture (Miller & Bernard, 1983) have been suggested as the mechanisms which prevent aliasing, and thus to be the limiting factors for visual acuity. On the other hand, Anderson, Mullen and Hess (1991) concluded that peripheral spatial resolution is limited by post-receptoral mechanisms instead of optical or receptoral properties of the eye. The prevailing idea is that optics is not sufficiently poor to accomplish the task when peripheral correction is used. However, it is possible that peripheral optics is an important limiting factor for peripheral visual acuity when it is left uncorrected, as is the case in everyday life, when necessary correction is based only on the foveal refraction.

As has been mentioned in Section 5.1 of this thesis, the eye optics is plagued by aberrations distorting the image at large pupil sizes and by diffraction at small pupil sizes, as well as by intraocular light scatter, which is independent of pupil size. The oblique astigmatism has been shown to increase with eccentricity (Millodot, 1981) as much as several dioptres, showing large individual variation along different meridians. However, correcting for the oblique astigmatism does not improve static visual acuity (Millodot, Johnson, Lamont & Leibovitz, 1975), although motion thresholds seem to benefit from peripheral refractive correction (Leibovitz, Johnson & Isabel, 1972). A recent study (Artal, Derrington & Colombo, 1995) indicates, however, that spherical correction for simple gratings in the periphery also improves detection. The actual studies measuring the optical modulation transfer function in the periphery show approximately constant optical quality across an area covering about 25 deg around the optical axis (Jennings & Charman, 1978, 1981; Navarro et al., 1993) with the peripheral optics corrected for each eccentricity. On the other hand, studies comparing uncorrected peripheral visual acuities for gratings either affected by the optics or bypassing it by the interference method show deterioration in the optical quality with increasing eccentricity (Green, 1967; Frisén & Glansholm, 1975).

I will now apply the relative method and noise comparison method from Section 5.2 to measure for the first time the peripheral O_{MTF} with foveal refraction, but with uncorrected peripheral optics, which is the natural viewing condition.

5.4.2 METHODS

5.4.2.1 Apparatus, Stimuli and Procedures

The apparatus, stimuli and procedures are described in detail in General Methods, and therefore only the special features are described here.

The stimuli were square-shaped vertical cosine gratings with sharply truncated edges, whose area and spatial frequency was varied on the screen together with the viewing distance. Black cardboard in front of the screen masked the equiluminous surround to a square field of 20x20 cm^2. Two-dimensional white added spatial noise was used in the second method. The experiments were performed in a dark room, the only light sources being the display and a self-luminous fixation point. Eccentricity within 5 - 20 deg refers to the angular distance between the point of fixation and the nearest edge of the grating in the nasal visual field of the dominant eye, except for subject OL, the angular distance was between the point of fixation and the centre of the grating. The stimulus field was always perpendicular to the line determined by the pupil and the centre of the grating. Both the fixation point and grating were always at the same viewing distance from the eye. A small black dot served as a fixation point within the luminous screen, and a small red LED - whose luminance was reduced by neutral density filters in accordance with the screen luminance - served as a fixation point outside the screen.

5.4.2.2 Subjects

Four experienced subjects, aged 24 - 34 years, served as observers. All wore foveal refractive correction in their dominant eye; SU od. -4.0, KT od. -6.0, JM od. -0.75, and OL od. -1.25. None of the subjects needed astigmatic correction. Their range of accommodation was at least 6D, and with optimal refraction their foveal monocular Snellen acuities at 5 m were at least 1.6.

5.4.3 RESULTS

As explained in previous Chapters, in foveal vision the effect of grating area can be equalised across spatial frequencies ($f \geq 0.5$ c/deg) by keeping the number of square cycles (Af^2) constant, as then the influence of spatial integration on contrast sensitivity is similar at all spatial frequencies (Howell & Hess, 1978; Virsu & Rovamo, 1979; Rovamo, Luntinen & Näsänen, 1993). The Af^2 -rule breaks down at spatial frequencies below 0.5 c/deg, because the critical area for spatial integration is then constant in solid degrees (Rovamo et al., 1993). This means that the maximal area of spatial integration projected onto the striate cortex is also constant in mm^2 (Daniel & Whitteridge, 1961). In the peripheral visual field this cortical area corresponds to a much larger area in the visual field (Drasdo, 1977; Rovamo, Virsu & Näsänen, 1978). This makes it feasible that spatial integration takes place at a constant number of square cycles even at spatial frequencies below 0.5 c/deg. Because in peripheral vision the decrease of grating acuity with increasing eccentricity (Mandelbaum & Sloan, 1947; Sloan, 1968; Rovamo & Raninen, 1990) causes the maximal contrast sensitivity to be shifted to low spatial frequencies (Hilz & Cavonius, 1974; Rovamo et al., 1978) by progressively reducing contrast sensitivity at high spatial frequencies, the use of very low spatial frequencies is necessary in this work.

In order to find out whether saturation of spatial integration in periphery occurs at a constant number of square cycles, the experiment of Fig. 5.9 was carried out at an eccentricity of 20 deg in the nasal visual field. The viewing distance was 28.6 cm, whilst the spatial frequencies on the screen were 0.25, 0.5, 1, and 2 c/cm, thus yielding 0.125, 0.25, 0.5, and 1 c/deg. The grating areas covered a range of 64 - 1024 deg^2 at 0.125 c/deg, 16 - 1024 deg^2 at 0.25 c/deg, 4 - 1024 deg^2 at 0.5 c/deg, and 1 - 1024 deg^2 at 1 c/deg. Consequently, the relative grating area (Af^2) varied between 1 and 1024 square cycles, depending on the spatial frequency. The average retinal illuminance produced by the display with a 4 mm natural pupil was 630 phot td, corresponding to 1600 scot td.

In Figs. 5.9 A and B contrast sensitivity has been plotted as a function of grating area (A). In general, the curves are similar in shape, contrast sensitivity increasing with grating area and spatial frequency. Inspection of the frames also shows a tendency towards saturation at large grating areas, whilst the increase at small grating areas follows a slope of approximately 0.5. At spatial frequencies $f \geq 0.5$, the dependence of contrast sensitivity on grating area is in agreement with the foveal results of Rovamo et al. (1993).

In Figs. 5.9.C and D the data was plotted as a function of the number of square cycles (Af^2). The range of square cycles studied was 1 - 16 at 0.125 c/deg, 1 - 64 at 0.25 c/deg, 1 - 256 at 0.5 c/deg, and 1 - 1024 at 1 c/deg. The contrast sensitivity functions now collapsed together so that contrast sensitivity increased with the number of square cycles (Af^2), until the increase saturated and contrast sensitivity became independent of Af^2 at larger number of square cycles.

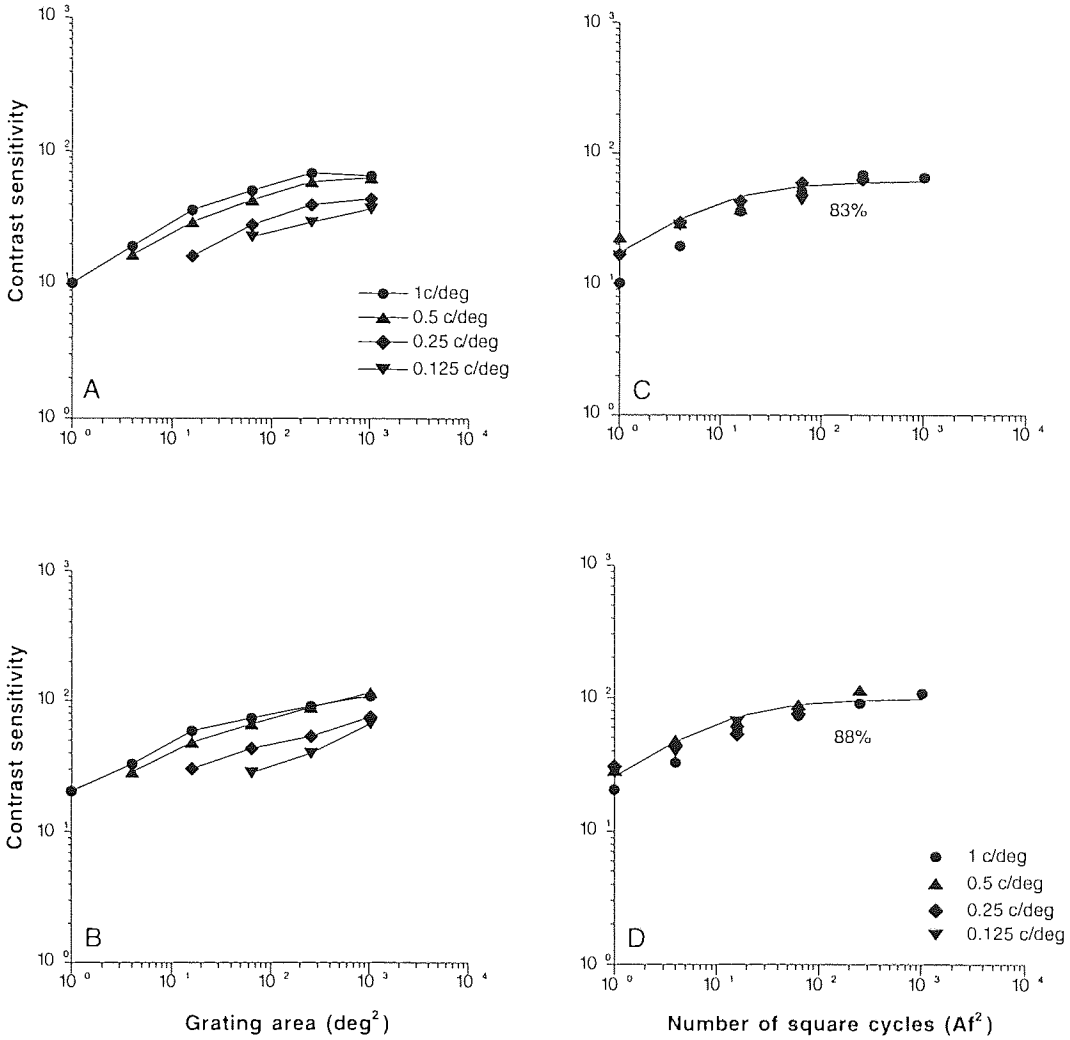

Fig. 5.9. *Contrast sensitivity measured at the eccentricity of 20 deg in the nasal visual field. A and B) plotted as a function of grating area, C and D) plotted as a function of the number of square cycles*

According to the contrast detection model (Rovamo et al., 1993), contrast sensitivity as a function of the number of square cycles was modelled by equation

$$S = S_{max} (1+Z_C/Z)^{-0.5} \qquad (5.8),$$

where S is the experimentally measured contrast sensitivity, S_{max} is the maximum contrast sensitivity obtainable by spatial integration at the exposure duration (500 msec) used, Z is the number of square cycles, and Z_c is the critical number of square cycles marking the saturation of spatial integration. Equation (5.8) was fitted to the data of Figs. 5.9.C and D with the method of least squares that minimises the relative error. For further details see Rovamo, et al. (1993).

The smooth curves in Fig. 5.9.C and D were calculated by using equation (5.8) fitted separately to the contrast sensitivity data of each subject. The contrast sensitivity functions of different spatial frequencies and grating areas follow a single curve when plotted as a function of the number of square cycles (Af^2). This means that spatial integration saturates at a constant number of square cycles (Af^2) irrespective of spatial frequency. In frame C, the critical number of square cycles (Z_c), marking the saturation of spatial integration, is 11, and in D it is 14. The values of S_{max} were 61 and 99, respectively. The explained variances were 83% and 88% for the two subjects tested.

In the foveal data of Rovamo et al. (1993) the value of Z_c increased from 4 to 80 c^2, and the value of S_{max} increased from 140 to 600, when spatial frequency increased from 0.125 to 1 c/deg, but at an eccentricity of 20 deg, Z_c and S_{max} were independent of spatial frequency. This implies that spatial integration is less extensive in peripheral than foveal vision. However, in the present study viewing was monocular and grating area increased only in the nasal direction, whereas in the foveal study of Rovamo et al. (1993) grating size increased symmetrically around the fovea in the binocular visual field.

The foveal spatial contrast sensitivity for stationary gratings with long exposure time is determined by grating area, retinal illuminance and the optical modulation transfer function (O_{MTF}). When two of these principal factors are

neutralized across spatial frequencies, contrast sensitivity is dependent only on the third determinant. Therefore the foveal O_{MTF} can be estimated by the relative method as introduced in Section 5.2.

Chapter 4 shows that critical retinal illuminance $I_c = I_0F^2$ up to the local retinal cut-off frequency (Rovamo & Virsu, 1979) at all eccentricities in the nasal visual field. The value of I_0 indicates the critical retinal illuminance at 1 c/deg. The above equation also means that retinal flux (If^{-2}) is independent of spatial frequency at all spatial frequencies. In the experiment of Fig. 5.9 I showed that the saturation of spatial integration takes place at a constant number of square cycles also in the periphery, even at spatial frequencies below 0.5 c/deg. Therefore, I was able to apply the relative method in the periphery, too.

The dominant eye was dilated to 8 mm, producing 2500 phot td on the retina at all eccentricities, because retinal illuminance remains fairly constant to about 80 deg visual angle (Bedell & Katz, 1982; Rovamo, 1983). Each time as spatial frequency was decreased by an octave, luminance was reduced to one fourth by a 0.6 log unit neutral density filter. At each eccentricity retinal flux (If^{-2}) was thus kept constant at all spatial frequencies, being 2.44, 39.1, 156, and 625 phot td deg^2 at the eccentricities of 0, 5, 10, and 20 deg, respectively. Likewise, the number of square cycles (Af^2) was kept constant across spatial frequencies at each eccentricity by varying either the grating size on the screen or the viewing distance (for details see Appendix 6). The number of square cycles was 16 at eccentricities 0 - 10 deg, and 4 at 20 deg.

In Fig. 5.10 the spatial contrast sensitivity functions measured with a constant number of square cycles (Af^2) and with constant retinal flux (If^{-2}) at each eccentricity are directly proportional to the O_{MTF}. At all eccentricities of 0 - 20 deg contrast sensitivity was practically constant at low spatial frequencies, and

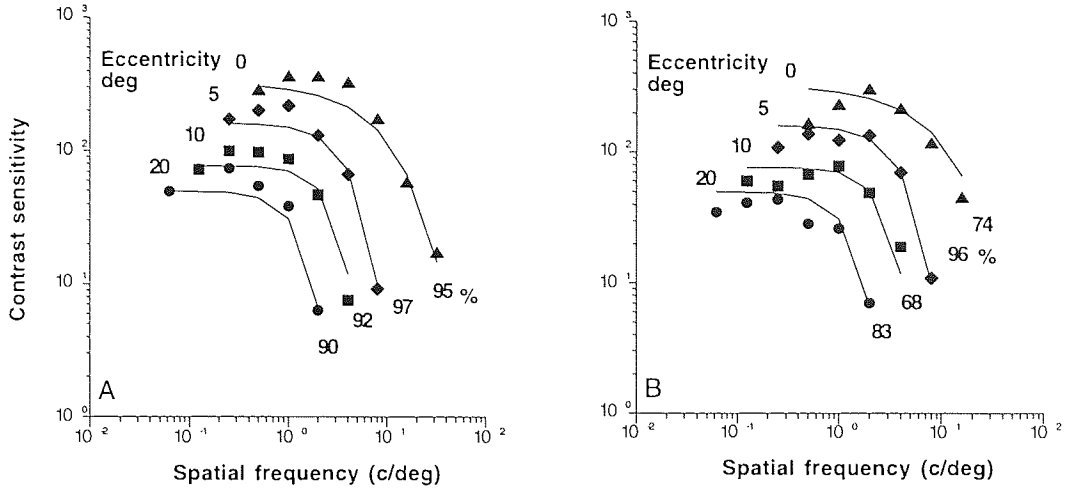

Fig. 5.10 *Contrast sensitivity measured according to the relative method, i.e. contrast sensitivity functions are directly proportional to O_{MTF}. The results of 0 and 5 deg have been shifted upwards by factors 4 and 2, respectively.*

then declined with increasing spatial frequency. The smooth curves represent the optical low-pass attenuation, calculated by equation (3.21) fitted to the combined data of both subjects at each eccentricity tested. The explained variances ranged between 68 - 97 %. With increasing eccentricity the value of parameter f_c decreased from 9.97 to 1.43 c/deg whereas the value of n increased from 0.97 to 2.09. The values of the two parameters are plotted as a function of eccentricity in Fig. 5.14.

The noise comparison method is based on the fact that individual light quanta cannot be blurred by the eye optics (Graham & Hood, 1992). Therefore, the effect of quantal noise on contrast sensitivity is comparable to the effect of added spatial noise only in the event of quantal absorption, when both noises have become an integral part of the neural representation of the image. Thus,

$$N_{qc} = O_{MTF}^2(f)\, N_{sc}, \qquad (5.9)$$

where N_{qc} and N_{sc} are the critical quantal and spatial noises, respectively. They are here defined to reduce r.m.s. contrast sensitivity by a factor of $\sqrt{2}$, in accordance with Pelli (1990). In addition,

$$N_{qc} = K/I_c \qquad (3.17)$$

on the basis of the following reasoning: Let retinal illuminance (I) correspond to n quanta on the average. One standard deviation from the mean is then equal to $\sqrt{n}$, because light quanta obey Poisson distribution. By definition, r.m.s. contrast of noise is equal to standard deviation divided by the mean, i.e. contrast = $\sqrt{n}/n = 1/\sqrt{n} = 1/\sqrt{I}$. In addition, quantal noise is white, because the number of quanta incident on neighbouring retinal locations at any time are uncorrelated. Therefore, by definition (Legge, Kersten & Burgess, 1987) the spectral density of quantal noise (N_q) is proportional to its r.m.s. contrast squared, which is equal to I^{-1}. By combining equations (5.9) and (3.17), we can therefore write:

$$K'' O_{MTF}(f) = (N_{sc} \times I_c)^{-0.5} \qquad (5.10),$$

where $K'' = 1/\sqrt{K'}$. At all eccentricities up to the local retinal cut-off frequency (Rovamo & Virsu, 1979) $I_c = I_0 F^2$ (Rovamo et al., 1995), where F = f / (c/deg) and the value of I_0 indicates I_c at 1 c/deg. Hence, equation (5.10) can be rewritten as

$$K O_{MTF}(f) = (N_{sc} \times F^2)^{-0.5} \qquad (5.11),$$

where $K = \sqrt{I_0} \times K''$.

The critical spectral density of added spatial noise for each spatial frequency and eccentricity was determined by measuring contrast sensitivity for gratings

of various spatial frequencies embedded in two-dimensional external white noise and for similar gratings without external added noise. Eccentricities covered were again 0, 5, 10, and 20 deg in the nasal visual field.

The dependency of contrast sensitivity on the spectral density of added white spatial noise (N_S) can be described by equation (Rovamo et al., 1996)

$$S = S_{max} (1+N_S/N_{SC})^{-0.5}, \qquad (5.7)$$

where S_{max} is the maximum contrast sensitivity obtainable without external noise, and N_{SC} is the critical spectral density of the noise, where $S = S_{max}/\sqrt{2}$.

The grating area in deg^2 was constant at each eccentricity, but the number of square cycles extended from 1 at the lowest to 1024 at the highest spatial frequency at each eccentricity. The spectral density of external noise (N_S) calculated according to equation (5.3) varied between 3.66×10^{-1} and 8.93×10^{-5} deg^2 (see Appendix 6) and reduced contrast sensitivity at each spatial frequency to about one third of the value obtained without external noise. Natural pupils (ø 5 mm) were used. Hence, retinal illuminance was constant at 980 phot td at all eccentricities and spatial frequencies.

In Fig. 5.11 the contrast sensitivity functions measured both with and without added spatial noise for the two observers have been plotted as a function of spatial frequency at each eccentricity. The functions have bandpass shape at all eccentricities studied, but the peak sensitivity shifts towards lower frequencies with increasing eccentricity. The shape of the curves with and without noise was also similar. Interindividual differences between the two subjects were quite small, although the eccentricity was calculated from the grating edge for JM but from the centre of the grating for OL. For eccentricities of 0, 5, 10, and 20 deg measured from the nearest edge of the stimulus the

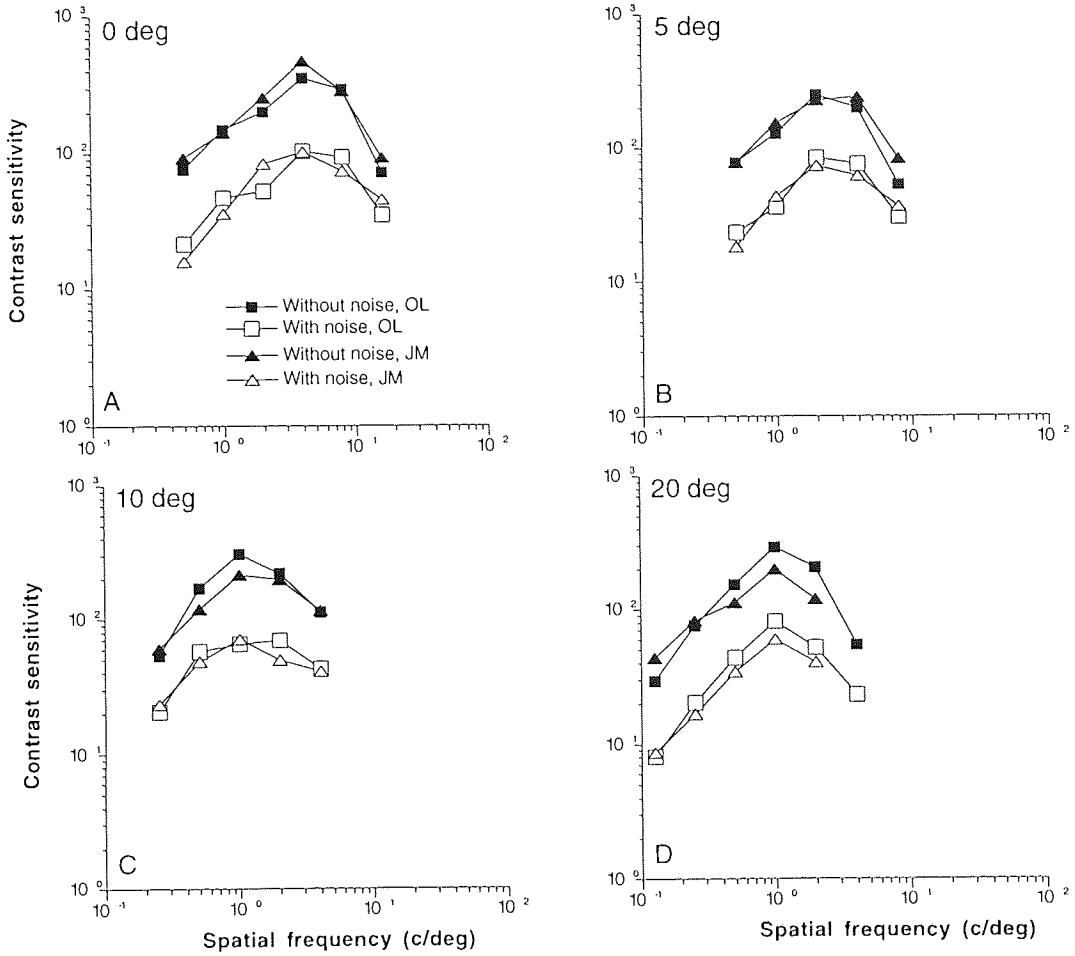

Fig. 5.11 *Contrast sensitivity at eccentricities of 0 - 20 deg with and without added spatial noise*

corresponding eccentricities measured from the stimulus centre were 1, 7, 14, and 28 deg. Only at the eccentricity of 20 deg grating resolution was better when eccentricity was measured from the stimulus centre than from its nearest edge. Hence, when the difference in eccentricity was small (1 - 4 deg), contrast sensitivity functions for the two subjects were quite similar.

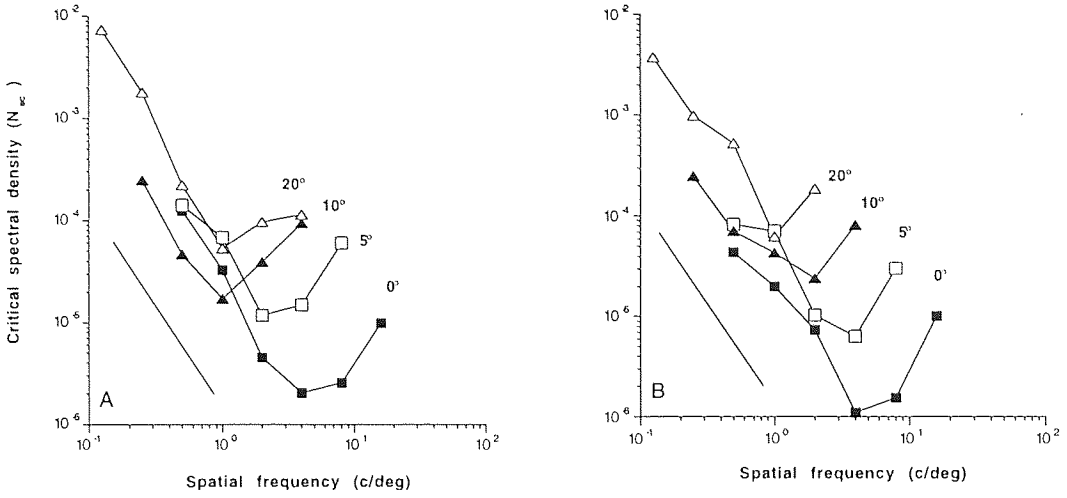

Fig. 5.12 *The critical spectral densities of external added noise determined from the data of 5.11 and plotted as a function of spatial frequency. A reference line indicates the slope of -2.*

The critical values of the spectral density of added spatial white noise (N_{SC}) for the two subjects were found by fitting equation (5.7) separately to their contrast sensitivity data at each spatial frequency and eccentricity. Fig. 5.12 shows the values of N_{SC} as a function of spatial frequency at each eccentricity. As external added spatial noise is affected both by the low-pass filtering of the O_{MTF} and by the high-pass filtering of the neural visual pathways (Section 5.2), the curves resemble contrast threshold functions i.e. the inverses of the functions shown in Fig. 5.11. Because of the MTF of the neural visual pathways reflecting lateral inhibition, stronger noise is required to mask the grating at low spatial frequencies. In fact, N_{SC} is approximately equal to f^{-2} at low spatial frequencies, because low spatial frequencies are attenuated relatively more by the neural modulation transfer function of the visual pathways ($P_{MTF}(f) = F$) than high spatial frequencies (Chapter 4). In accordance with the shift of the maximum contrast sensitivity towards low spatial frequencies with increasing eccentricity, the minimum of the critical

spectral density of added spatial noise is also shifted towards lower spatial frequencies with increasing eccentricity. The spatial noise is also attenuated by the O_{MTF}, and consequently stronger noise is required to mask the grating at high spatial frequencies.

Fig. 5.13 shows the values of $(N_{sc}\ F^2)^{-0.5}$ plotted as a function of spatial frequency at each retinal eccentricity studied. In Fig. 5.13 $K_0\ O_{MTF} = (N_{sc}\ F^2)^{-0.5}$, so the data points of Fig. 5.13 were fitted by an equation

$$\ln K = \ln K_0 - (f/f_c)^n\ , \qquad (5.12)$$

where K_0 is the proportionality constant similar to S_0 in equation (3.21). According to equation (5.11) the values are directly proportional to O_{MTF} at each eccentricity. Hence, at low spatial frequencies the attenuation due to the eye optics is approximately similar at all eccentricities. Then attenuation increased markedly causing O_{MTF}s to decline rapidly at spatial frequencies close to the grating acuity at each retinal location. Scrutiny of Fig. 5.13 reveals that the decrease starts earlier at greater eccentricities. Smooth curves were calculated by equation (5.12) fitted to the data points at each eccentricity. The explained variance ranged within 79 - 97 %.

The values of the parameters n and f_c of the equation describing the low-pass attenuation of ocular optics were obtained by the two techniques described in this paper. They are shown in Fig. 5.14 as a function of eccentricity together with the values obtained in sections 5.2 and 5.3. Parameter f_c refers to the spatial frequency at which O_{MTF} (f) = 1/e, and exponent n indicates how rapidly O_{MTF} decreases as spatial frequency increases above f_c. The results acquired with the two different methods provided similar values for the

parameters f_c and n, although in the relative method the pupil size used was 8 mm in comparison to 5 mm in the noise method.

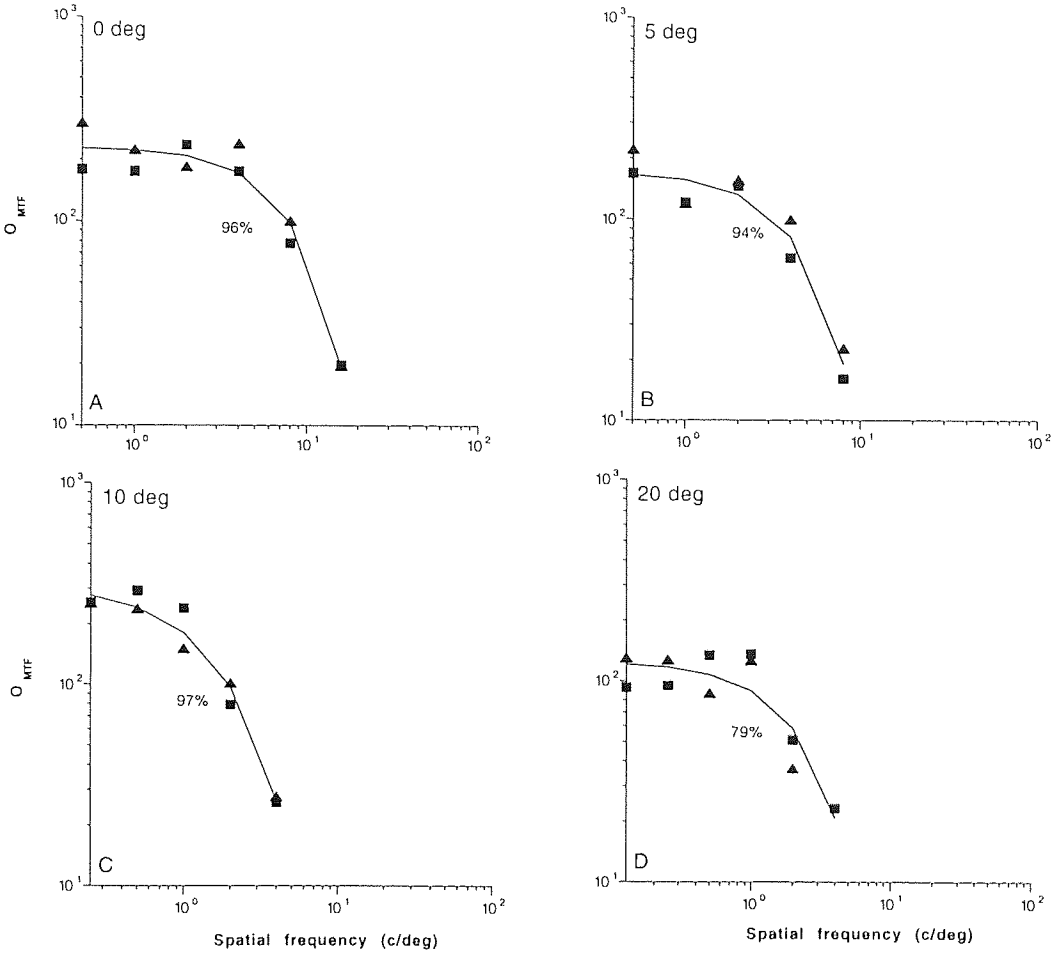

Fig. 5.13 *The estimates of $(N_{sc}F^2)^{-0.5}$ calculated from the data of Fig. 5.11 are directly proportional to the O_{MTF}*

With increasing eccentricity, the value of f_c decreases rapidly from the foveal value of about 10 c/deg to 5 c/deg at 5 deg eccentricity. Thereafter the decrease is more shallow, f_c approaching 2 c/deg at the eccentricity of 20 deg. The values of n increase from about 1 at fovea to about 1.5 at the eccentricity of 20 deg, indicating a more rapid decline in O_{MTF} at spatial frequencies above f_c in the periphery than at the fovea.

As the values of the parameters of O_{MTF} obtained with these two methods are similar, I use their means for estimating the O_{MTF}s at retinal eccentricities of 0 - 20 deg. Hence, according to my results the O_{MTF} as a function of retinal eccentricity can be described as exp $[-(f/f_c)^n)]$, where the parameters f_c and n vary with eccentricity. The geometrical means of the values were 10, 4.7, 2.3, and 1.9 for f_c and 1.2, 1.7, 1.6, and 1.6 for n at eccentricities of 0, 5, 10, and 20 deg, respectively.

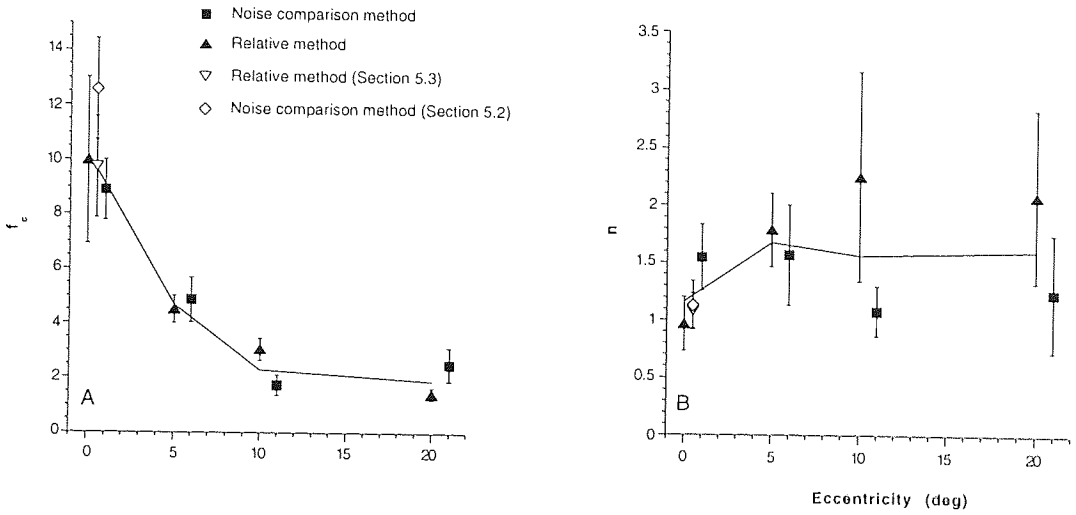

Fig. 5.14 *The values of parameters f_c and n. The line segments connect the geometrical means of the values of both parameters. For easier inspection the values at each eccentricity have been spread over two eccentricities.*

Finally, a comparison with earlier estimates of the O_{MTF} at various retinal eccentricities from Navarro et al. (1993) is shown in Fig. 5.15. They used natural pupils of 4 mm in diameter and corrected the spherical refractive error at each eccentricity. My estimates were similar for 5 and 8 mm pupils. Therefore, a comparison between the estimates for a ø4 mm pupil and the present ones is adequate.

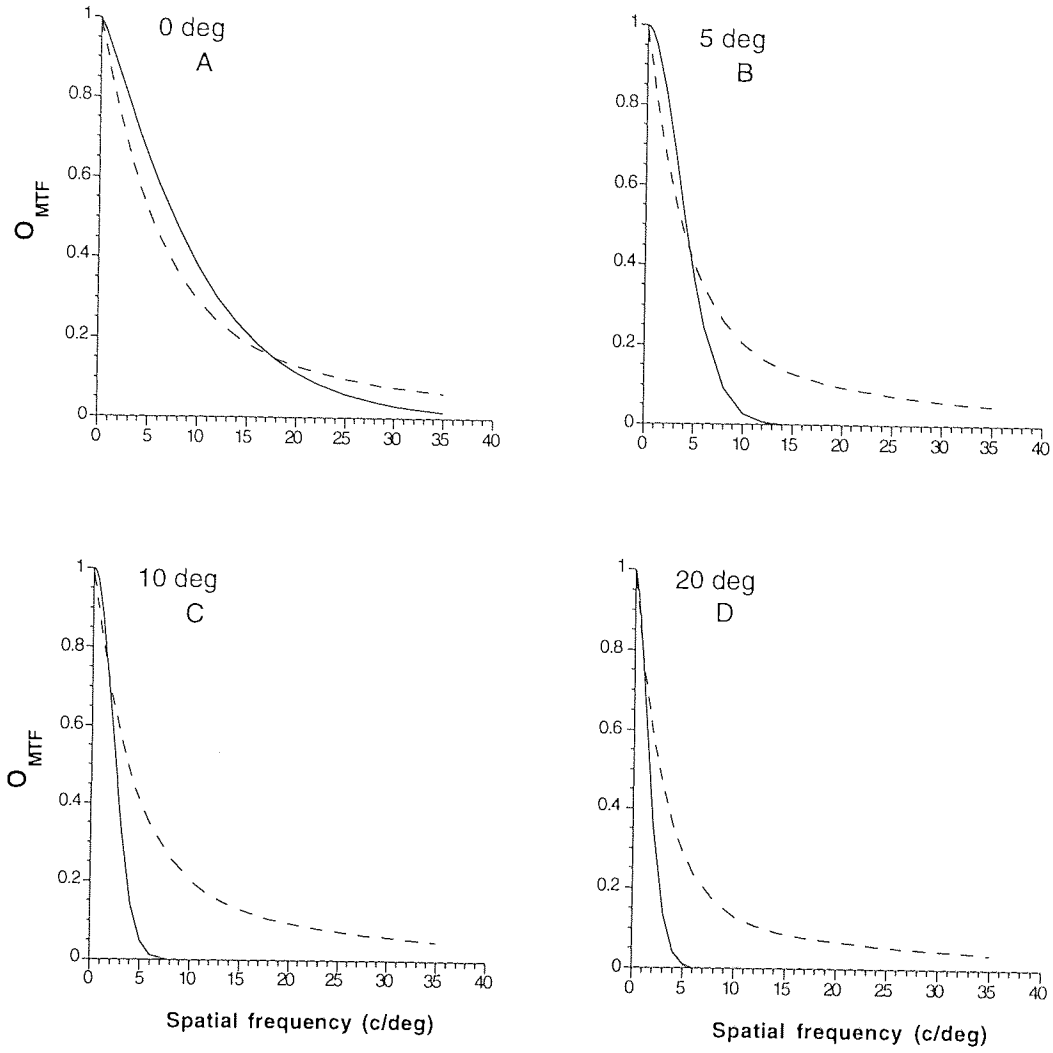

Fig. 5.15 *Comparison between my estimates of O_{MTF} and the estimates of Navarro et al.(1993) at various eccentricities.*

The foveal estimates of Navarro et al. (1993) and the present study are pretty similar, enforcing my earlier result that pupil size does not affect the O_{MTF} when it is at least 4 mm in diameter. At spatial frequencies below 17 c/deg the current estimate indicates less optical attenuation than that of Navarro et al. (1993), but at higher spatial frequencies the situation is reversed. At all other eccentricities the general trend is that the current estimate of O_{MTF} is lower than the estimate of Navarro et al. (1993). At 5 deg the present estimate still

implies less degradation at spatial frequencies below 5 c/deg, but thereafter the estimate of Navarro et al. indicates better image quality. The difference is notably larger at the eccentricity of 10 deg, when my estimate drops quite straightforwardly from 0.7 at 2 c/deg to near zero at 5 c/deg whereas the estimate of Navarro et al. has only decreased to 0.4 at 5 c/deg. At the eccentricity of 20 deg the estimates of Navarro et al. and the present one are similar only up to 1 c/deg, our estimate dropping again quickly to near zero, as theirs decreases more smoothly to 0.1 at 14 c/deg. The difference between the estimates is about 10-fold around 5 c/deg.

5.4.4. DISCUSSION

Using adequate foveal refraction but without correcting peripheral refractive errors I measured the optical modulation transfer function across the nasal visual field with two different psychophysical methods. In the relative method, the retinal flux (If^{-2}) and the number of square cycles (Af^2) were kept constant across spatial frequencies, thus yielding a contrast sensitivity function determined only by the optics of the eye. The noise comparison method is based on the comparison of the effects of quantal and added external white spatial noises on contrast sensitivity. The spectral density of added external white spatial noise is affected by the O_{MTF}, because spatial noise is an integral part of the image, but the spectral density of quantal noise is not affected by the O_{MTF}, because single quanta cannot be blurred by ocular optics.

Both methods gave similar estimates for the O_{MTF}s, which can be described as $O_{MTF}(f) = \exp [-(f/f_c)^n]$. Spatial frequency (f) is in c/deg, parameter f_c refers to spatial frequency at which O_{MTF} (f) = 1/e, and exponent n indicates how rapidly O_{MTF} decreases with increasing spatial frequency above f_c. The value of f_c declines with increasing eccentricity, whereas the value of n rises towards

periphery. The foveal result is in agreement with my earlier estimates shown in Sections 5.2 and 5.3. In the periphery the estimates of O_{MTF} showed significant deterioration at high spatial frequencies, which became more detrimental with increasing eccentricity. My O_{MTF}s of the peripheral optics are worse than previously reported O_{MTF}s measured with peripheral correction.

The fact that I used dilated pupils in the relative method, while natural 5 mm pupils were used in the noise comparison method, did not affect my results. In the fovea I have shown in Section 5.3 that the contribution of marginal rays of a pupil larger than 4 mm is negligible to distortion of retinal image quality, mainly because of the Stiles-Crawford effect (Stiles & Crawford, 1933). In addition, although the Stiles-Crawford effect is not as powerful in the periphery than it is in the parafovea (Bedell & Enoch, 1979), the highest spatial frequencies detectable in peripheral vision seem to be too low to be affected by the deleterious effect introduced by a large pupil size. At the eccentricity of 5 deg the highest spatial frequency detected was 8 c/deg, while at 20 deg it was 4 c/deg.

The finding that peripheral correction improves grating detection (Artal et al., 1995) beyond the local cut-off frequency determined by the sampling density of retinal ganglion cells (Rovamo & Virsu, 1979) implies that under normal foveally emmetropic viewing conditions, i.e. without local peripheral correction, low-pass filtering by the eye optics in the periphery is a determinant of traditional visual acuity, in agreement with the current study and Frisén and Glansholm (1975). Artal et al. (1995) also pointed out that each retinal location requires different correction, after which they found similar visual acuity for grating detection in the fovea and at the periphery. However, no peripheral correction can be used in everyday life without impairing the foveal vision.

Jennings & Charman (1981) used a double-pass method and found that up to an eccentricity of 20° the quality of eye optics is fairly constant and close to the optical quality in the fovea. Another and more recent study also using the double-pass method is by Navarro et al. (1993). They found an even better peripheral image quality. However, in these studies the peripheral image was focused at each eccentricity on the peripheral retina by spherical lenses. This abolishes the natural low-pass filtering of peripheral optics that serves to prevent aliasing (Galvin & Williams, 1992). Similarly, aliasing can be found in motion detection tasks with corrected peripheral optics (Anderson, Drasdo & Thompson, 1995).

As a further support to our result, studies using the interference method imply that the eye optics is well matched with peripheral retinal cone mosaic (Green, 1967, 1970) or subsequent neural structures, and is even responsible for the decreasing image quality towards the periphery (Frisén & Glansholm, 1975). Green (1967) obtained higher contrast sensitivities for internal interferometric gratings up to an eccentricity of 5 deg than he obtained for external gratings blaming the optical aberrations of the eye for the loss of sensitivity. In a later paper (Green, 1970) he extended the study up to 8 deg of eccentricity, but did not find any difference for grating acuities beyond 5 deg. However, Frisén & Glansholm (1975) studied two emmetropic subjects with no peripheral optical correction and found consistently better acuity for interference gratings than external gratings across the visual field up to the eccentricity of 80 deg. The difference increased with increasing eccentricity, suggesting an increasingly important image-degrading effect of the dioptric apparatus of the eye, in agreement with Artal et al. (1995).

Another factor contributing to the difference between the current O_{MTF}s and the O_{MTF}s of Navarro et al. (1993) could be the fact that the double-pass method is based on the measurements of light which is discarded by the

visual system. The main assumption is that the retina is a diffuse reflector destroying all coherence, and that the single-pass spread function is equivalent to the square-root of the double-pass spread function (Charman, 1991). However, an important factor is the origin of the retinal reflection, which determines the extent of the O_{MTF}. Unlike in the fovea, the peripheral photoreceptors are situated underneath several retinal layers, which vary in thickness as a function of eccentricity. For example, retinal ganglion cell density is greatest at the parafoveal ridge, declining rapidly only at about 15 deg in the temporal retina (Curcio & Allen, 1990). Even if neural layers could be considered to be transparent, the retinal veins and arteries form a plexus between the neural elements, and are a significant source of light scatter in the eye. The tentative assumption that the reflecting surface is in fact somewhere close to the internal membrane (Santamaría, Artal & Bescos, 1987) could thus be a factor contributing to the good image quality achieved by the double-pass method across the visual field.

Within the framework of the contrast detection model of Chapter 3 the decrease of contrast sensitivity with increasing eccentricity could in principle result from the deterioration of three factors: i) the optical modulation transfer function of the eye, ii) the neural modulation transfer function of the visual pathways, or iii) the efficiency of the detection filter in the brain. However, the decrease cannot be due to the second factor, because the neural modulation transfer function of the visual pathways is independent of retinal location, as shown in Chapter 4, up to the spatial cut-off frequency determined by the lowest neural sampling density at each retinal location (Rovamo & Virsu, 1979). My current results indicate that one reason for the decrease in contrast sensitivity with increasing eccentricity is the decline in the O_{MTF}. However, further experiments are required to determine whether the efficiency of the detection filter in the brain remains constant or also decreases with increasing eccentricity.

6. CONCLUDING SUMMARY

This thesis studied the effect of retinal illuminance on contrast sensitivity, and extended the Van Nes-Bouman law, i.e. that critical retinal illuminance (I_c) marking the transition between Weber's and DeVries-Rose law is proportional to spatial frequency squared, to low spatial frequencies in Section 3.2 and across the visual field in Chapter 4. Furthermore, in Section 3.2 it was shown that the effect of retinal illuminance (I) can be equalised across spatial frequencies (f) by keeping the retinal flux (If^{-2}) constant.

Section 3.3 extended the contrast detection model of Rovamo et al. (1993) to low light levels by showing that spatial integration is independent of retinal illuminance and that the effect of retinal illuminance on contrast sensitivity is independent of grating area. The human spatial contrast detection can thus be modelled as a simple image processor comprising low-pass filtering of the eye optics, addition of light-dependent noise at the event of quantal absorption, high-pass filtering due to the neural visual pathways, addition of internal neural noise, and detection by a local matched filter, whose efficiency decreases with grating area.

Based on the extended contrast detection model of Section 3.3. and on the results of Section 3.2. the neural modulation transfer function of the human eye was shown to be proportional to spatial frequency in Chapter 4.

Moreover, Chapter 5 included an extensive study of the optical modulation transfer function of the human eye. In Section 5.2 two new psychophysical methods to estimate the O_{MTF} were introduced. The methods were applied in the subsequent Sections 4.3 and 4.4, where the O_{MTF} was measured for different pupil sizes and retinal eccentricities. The results of Section 4.3

suggest that the Stiles-Crawford effect is more significant than assumed on the basis of previously published articles, and that previous estimates for O_{MTF} therefore overestimate the attenuation of eye optics at large pupil sizes. Section 4.4. implies that uncorrected peripheral optics is an important limiting factor for visual acuity and powerful enough to prevent aliasing in every-day life.

PUBLICATIONS AND PRESENTATIONS

PUBLICATIONS

Papers:

1) Mustonen, J., Rovamo, J. & Näsänen, R. (1993). The effects of grating area and spatial frequency on contrast sensitivity as a function of light level. *Vision Research, 33*, 2065-2072.

2) Rovamo, J., Mustonen, J.K. & Näsänen, R. (1994a). Modelling contrast sensitivity as a function of retinal illuminance and grating area. *Vision Research, 34*, 1301-1314

3) Rovamo, J.M., Mustonen, J.K. & Näsänen, R. (1994). Two simple psychophysical methods for determining the optical modulation transfer function of the human eye. *Vision Research, 34*, 2493-2502.

4) Rovamo, J.M., Mustonen, J.K. & Näsänen, R. (1995). Neural modulation transfer function of the human visual system at various eccentricities. *Vision Research, 35*, 767-774.

5 Mustonen, J.K. & Rovamo, J.M. (1995). Foveal optical modulation transfer function of the human eye at various pupil sizes. *Vision Research*, submitted.

6) Mustonen, J.K., Rovamo, J.M. & Uusinarkaus, S. (1995). The human optical modulation transfer function at various eccentricities. *Vision Research*, submitted.

Abstracts:

7) Mustonen J., Rovamo J., Näsänen R. (1991)
Contrast sensitivity as a function of luminance: effects of area and spatial frequency.; Optics and Photonics News Vol. 2 No. 9.

8) Mustonen J., Rovamo J., Näsänen R.(1992)
A combination of the DeVries-Rose and Weber's laws explains the increase of contrast sensitivity with retinal illuminance at all grating areas and spatial frequencies.; Investigative Ophthalmology & Visual Science, Vol.33, no 4

9) Mustonen J., Rovamo J., Näsänen R. (1992)
Contrast sensitivity as a function of grating area and retinal illuminance.: Optics and Photonics News, Vol. 3, No. 7

10) Mustonen J, Rovamo J, Näsänen R. (1993),
A psychophysical technique for determining the optical transfer function of the human eye. Investigative Ophthalmology & Visual Science, Vol.34, no 4

11) Rovamo J, Mustonen J, Näsänen R. (1993),
Contrast sensitivity as a function of exposure time and retinal illuminance. Investigative Ophthalmology & Visual Science, Vol.34, no 4

12) Mustonen J, Rovamo J, Näsänen R. (1993),
A simple psychophysical method for measuring the human optical transfer function. Perception, Vol 22 supplement

13) Mustonen, J. & Rovamo, J.
Neural modulation transfer function across the visual field. Investigative Ophthalmology & Visual Science., Vol 35, no 4

14) Rovamo, J. & Mustonen, J.
The foveal optical modulation transfer function at various pupil sizes. Investigative Ophthalmology & Visual Science, Vol 35, no 4.

PRESENTATIONS

Papers:

1) Mustonen J., Rovamo J., Näsänen R. (1992)
Contrast sensitivity as a function of grating area and retinal illuminance. Optical Society of America (OSA) 1992 Annual Meeting, Albuquerque, New Mexico, U.S.A.

2) Mustonen J, Rovamo J, Näsänen R. (1993),
A psychophysical technique for determining the optical transfer function of the human eye. IAssociation for Research in Vision and Ophthalmology (ARVO), 1993 Annual meeting, Sarasota, Florida, U.S.A.

3) Mustonen J, Rovamo J, Näsänen R. (1993),
A simple psychophysical method for measuring the human optical transfer function. European Congress for Visual Perception (ECVP), 1993 Annual meeting, Edinburgh, U.K.

Posters:

4) Mustonen J., Rovamo J., Näsänen R. (1991)
Contrast sensitivity as a function of luminance: effects of area and spatial frequency.; The Optical Society of America, San José, 1991.

5) Mustonen J., Rovamo J., Näsänen R.(1992)
A combination of the DeVries-Rose and Weber's laws explains the increase of contrast sensitivity with retinal illuminance at all grating areas and spatial frequencies.; Association for Research in Vision and Ophthalmology (ARVO), 1992 Annual meeting, Sarasota, Florida, U.S.A.

LIST OF REFERENCES

Alexandridis, E. (1972). *The Pupil,* Springer-Verlag, New York

Anderson, P.A. & Movshon, J.A. (1989). Binocular combination of contrast signals. *Vision Research, 29*, 1115-1132.

Anderson, S.J., Drasdo, N, & Thompson, C.M. (1995). Parvocellular neurons limit motion acuity in human peripheral vision. *The Proceedings of the Royal Society of London*, B, 261, 129-138.

Anderson, S.J. & Hess, R.F. (1990). Post-receptoral undersampling in normal human peripheral vision. *Vision Research, 10*, 1507-1515.

Anderson, S.J., Mullen, K.T. & Hess, R.F. (1991). Human peripheral spatial resolution for achromatic and chromatic stimuli: limits imposed by optical and retinal factors. *The Journal of Physiology, 442*, 47-64.

Artal, P., Derrington, A.M. & Colombo, E. (1995). Refraction, aliasing, and the absence of motion reversals in peripheral vision. *Vision Research*, 35, 939-947.

Applegate, R.A. & Bonds, A.B. (1980). Induced movement of receptor alignment toward a new pupillary aperture. *Investigative Ophthalmology and Visual Sciences, 21*, 869-873.

Artal, P. (1990). Calculations of two-dimensional foveal retinal images in real eyes. *The Journal of Optical Society of America A, 7*, 1374-1381.

Artal, P., Derrington, A.M. & Colombo, E. (1995). Refraction, aliasing, and the absence of motion reversals in peripheral vision. *Vision Research, 35*, 939-947.

Artal, P. Ferro, M., Miranda, I. & Navarro, R. (1993). Effects of aging in retinal image quality. *The Journal of Optical Society of America A, 10*, 1657-1663.

Artal, P. & Navarro, R. (1992). Simultaneuous measurement of two-point-spread functions at different locations across the human fovea. *Applied Optics, 31*, 3646-3656.

Artal, P. & Navarro, R. (1994). Monochromatic modulation transfer function of the human eye for different pupil diameters: an analytical expression. *The Journal of Optical Society of America A, 11*, 246-249.

Banks, M.S., Geisler, W.S. & Bennett, P.J. (1987). The physical limits of grating visibility. *Vision Research, 27*, 1915-1924.

Banks, M.S., Sekuler, A.B. & Anderson, S.J. (1991). Peripheral spatial vision: Limits imposed by optics, photoreceptors, and receptor pooling. *The Journal of Optical Society of America A., 8* , 1775-1787.

Barlow, H.B. (1977). Retinal and central factors in human vision limited by noise. In *Vertebrate photoreceptions*. Eds. Barlow, Fatt. London: Academic Press.

Barlow, H.B. & Levick, W.R. (1969). Three factors limiting the reliable detection of light by retinal ganglion cells of the cat. *Journal of Physiology, 200*, 1-24.

Baron, W.S. & Enoch, J.M. (1982). Calculating photopic illuminance. *American Journal of Optometry & Physiological Optics, Vol. 59*, 338-341.

Bedell, H.E. & Enoch, J.M. (1979). A study of the Stiles-Crawford (S-C) function at 35 degrees in the temporal field and the stability of the foveal S-C function peak over time. *The Journal of Optical Society of America, 69,* 435-441.

Bedell, H.E. & Katz, L.M. (1982). On the necessity of correcting peripheral target luminance for pupillary area. *The American Journal of Optometry and Physiological Optics, 59*, 767-769.

Berny, F. & Slansky, S. (1969). Wavefront determination resulting from Foucalt Test as applied to the human eye and visual instruments. In *Optical Instruments and Techniques*. Ed. Dickson, Oriel Press, England.

Blanks, J.C. (1989). Morphology of the retian. In *Retina*, Vol 1, Eds Ogden, Schachat, The Mosby Company, St Louis, Missouri

Bonds, A.B. & MacLeod, D.I.A. (1978). A displaced Stiles-Crawford effect associated with an eccentric pupil. *Investigative Ophthalmology and Visual Sciences, 17*, 754-761

Bour, L.J. (1980). MTF of the defocused optical system of the human eye for incoherent monochromatic light. *The Journal of Optical Society of America*, *70*, 321-328.

Burgess, A.E. (1990). High level visual decision efficiencies. In Blakemore, C. (Ed.), *Vision: Coding and efficiency* (pp.431-440). Cambridge: University Press.

Burgess, A.E., Wagner, R.E., Jennings, R.J. & Barlow, H.B. (19981). Efficiency of human visual signal discrimination. *Science, 214*, 93-94.

Campbell, F.W. & Green, D.G. (1965). Optical and retinal factors affecting visual resolution. *The Journal of Physiology, 181*, 576-593.

Campbell, F.W. & Gubisch, R.W. (1966). Optical quality of the human eye. *The Journal of Physiology*, *186*, 558-578.

Campbell, F.W. & Robson, J. G (1968). Application of Fourier analysis to the visibility of gratings. *The Journal of Physiology, 197,* 551-566.

Campbell, M.C.W., Harrison, E.M. & Simonet, P. (1990). Psychophysical measurement of the blur on the retina due to optical aberrations of the eye. *Vision Research, 30*, 1587-1602.

Charman, W.N. (1983). The retinal image in the human eye. In Osborne, N.N & Chader, G.J. (eds.) *Retinal Research*, Pergamon Press.

Charman, W.N. (1991) Limits on visual performance set by the eye's optics and the retinal cone mosaic. In *Vision and Visual Dysfunction*, Vol 5. Eds Kulikowski, Walsh & Murray, MacMillan Press, London.

Cohen, R.W. (1978). Applying psychophysics to display design. *Photographic Science and Engineering, 22*, 56-59.

Cohen, A.I. (1987). *The retina*. In Adler's Physiology of the eye. Eds Moses & Hart, C.V. Mosby Company, St Louis.

Cotlier, E. (1987) *The lens*. In Adler's Physiology of the eye. Eds Moses & Hart, C.V. Mosby Company, St Louis.

Crawford, B.H. (1937). The luminous efficiency of light entering the eye pupil at different points and its relation to brightness threshold measurements. *Proceedings of the Royal Society of London, B, 124*, 81-95.

Curcio, C.A. & Allen, K.A. (1990). Topography of ganglion cells in human retina. *The Journal of Comparative Neurology*, 300, 5-25.

Daitch, J.M. & Green, D.G. (1969). Contrast sensitivity of the human peripheral retina. *Vision Research, 9,* 947-952.

Daniel, P.M. & Whitteridge, D. (1961). The representation of the visual field on the cerebral cortex in monkeys. *The Journal of Physiology*, 159, 203-221.

Davila, K. & Geisler, W.S. (1991). The relative contributions of pre-neural and neural factors to areal summation in the fovea. *Vision Research, 31*, 1369-1380.

Deeley, R.J., Drasdo, N. & Charman, W.N. (1991). A simple parametric model of the human ocular modulation transfer function. *Ophthalmic and Physiologic Optics, Vol 11*, 91-93.

DeValois, R.L. & DeValois, K.K. (1990). In *Spatial Vision*, Oxford University Press, Oxford

Drasdo, N. (1977). The neural representation of visual space. *Nature, 266,* 554-556.

Elliott, P. (1964). Forced choice tables (Appendix 1). In Swets J.A. (Ed.), *Signal Detection and Recognition by Human Observers* (pp. 679-684), New York: Wiley

Enoch, J.M. (1972). Retinal receptor orientation and the role of fiber optics in vision. *Am. J. Optom. Arch. Am. Acad. Optom.*, 49, 455-470.

Enoch, J.M. & Bedell, H.E. (1979). Specification of the directionality of the Stiles-Crawford function. *American Journal of Optometry and Physiology, 56*, 341-344.

Enoch, J.M. & Birch, D.G. (1981). Inferred positive phototropic activity in human photoreceptors. *Phil. Trans.R.Soc.Lond.B.*, 291, 293-303.

Enoch, J.M. & Birch, D.G. (1985). comment on inferred positive phototropic activity in human photoreceptors. *Phil. Trans.R.Soc.Lond.B.*, 309, 611-613.

Enoch, J.M., Hamer, R.D., Lakshminarayanan, V., Yasuma, T., Birch, D.G. & Yamade, S. (1981). Effect of monocular light exclusion on the Stiles Crawford function. *Vision Research*, 27, 507-510.

Enoch, J.M. & Hope, G.M. (1973). Directional sensitivity of the foveal and parafoveal retina. *Investigative Ophthalmology* , 12, 497-503.

Enoch, J.M. & Lakshminarayanan, V. (1991). Retinal fibre optics. In *Vision and Visual Dysfunction*, Vol 1, Ed. Charman, MacMillan Press, London.

Enoch, J.M. & Stiles, W.S. (1961). The colour change of monochromatic light with retinal angle of incidence. *Optica Acta*, 8, 329-358.

Enoch, J.M. & Tobey, F.L. (1978). Differences in the index of refraction between the rat rod oouter segment and the interstitial matrix, *The Journal of the Optical Society of America, 68*, 1130-1134.

Enoch, J.M. & Tobey, F.L. (1981). *Vertebrate Photoreceptor Optics*. Vol 23, Springer-Verlag, Berlin.

Enroth-Cugell, C & Shapley, R.M. (1973). Flux, not retinal illumination, is what cat retinal ganglion cells care about. *The Journal of Physiology, 233*, 311-326.

Flamant, F. & Stiles, W.S. (1948). The directional sensitivities of the retinal rods to adapting of different wavelengths. *The Journal of Physiology, 107*, 187-202.

Freeman, M.H. (1990). *Optics*, Butterworths, London

Frisén, L. & Glansholm, A. (1975). Optical and neural resolution in peripheral vision. *Investigative Ophthalmology, 14*, 528-536.

Galvin, S & Williams, D (1992). Vision Research

Graham, N.V.S. (1989). *Visual pattern analyzers.* New York: Oxford University Press.

Graham, N. & Hood, D.C. (1992). Quantal noise and decision rules in dynamic models of light adaptation. *Vision Research, 32*, 779-787.

Green, D.G. (1967). Visual resolution when light enters the eye through different parts of the pupil. *The Journal of Physiology, 190*, 583-593.

Green, D.G. (1970). Regional variations in the visual acuity for interference fringes on the retina. *The Journal of Physiology, 207,* 351-356.

Green, D.G. & Campbell, F.W. (1965). Effect of focus on the visual response to a sinusoidally modulated spatial stimulus. *The Journal of Optical Society of America*, *55*, 1154-1157.

Hilz, R. & Cavonius, C.R. (1974). Functional organisation of the peripheral retina: sensitivity to periodic stimuli. *Vision Research*, 14, 1333-1337.

Hoekstra, J., van der Goot, D.P.J., van den Brink, G. & Bilsen, F.A. (1974). The influence of the number of cycles upon the visual contrast threshold for spatial sine wave patterns. *Vision Research, 14*, 365 - 368.

Howell, E.R. & Hess, R.F. (1978). The functional area for summation to threshold for sinusoidal gratings. *Vision Research, 18*, 369 - 374.

Howland, H.C. & Howland, B. (1977). A subjective method for the measurement of monochromatic aberrations of the eye. *The Journal of Optical Society of America*, *67*, 1508-1518.

Ijspeert, J.K., van den Berg, T.J.T.P. & Spekreijse, H. (1993). An improved mathematical description of the foveal visual point spread function with parameters for age, pupil size and pigmentation. *Vision Research, 33*, 15-20.

Jennings, J.A.M. & Charman, W.N. (1978). Optical image quality in the peripheral retina. *American Journal of Optometry and Physiological Optics, 55*, 582-590.

Jennings, J.A.M. & Charman, W.N. (1981). Off-axis image quality in the human eye. *Vision Research*, *21*, 445-455.

Johnson, C.B. (1972). Circular aperture diffraction limited MTF: Approximate expressions. *Applied Optics, 11*, 1875-1876.

Kelly, D.H. (1972). Adaptation effects on spatio-temporal sine-wave thresholds. *Vision Research, 12,* 89-101.

Kelly, D.H. (1977). Sisual contrast sensitivity. *Optica Acta, 24*, 107-129.

Koenderink, J.J., Bouman, M.A., Bueno de Mesquita, A.E. & Slappendel, S. (1978). Perimetry of contrast detection thresholds of moving spatial sine wave patterns. IV. The influence of the mean retinal illuminance. *The Journal of Optical Society of America, 68,* 860-865-955.

Krauskopf, J. (1962). Light distribution in human retinal images. *The Journal of Optical Society of America*, *52*, 1046-1050.

Kukkonen, H.T. & Rovamo, J.M. (1995). The effect of noise pixel size and shape on grating detectability. *Vision Research*, in press.

Laming, D. (1991) Contrast sensitivity. In Kulikowski, J.J., Walsh, V. & Murray, I.J. (eds), *Limits of Vision*, London: Macmillan Press

Legge, G.E. (1978). Sustained and transient mechanisms in human vision: Temporal and spatial properties. *Vision Research*, *18*, 69-81.

Legge, G.E., Kersten, D. & Burgess, A.E. (1987). Contrast discrimination in noise. *The Journal of Optical Society of America, A, Vol. 4*, No. 2, 391-404.

Leibovitz, H.W., Johnson, C.A. & Isabelle, E. (1972). Peripheral motion detection and refractive error. Science, 177, 1207-1208.

Lillywhite, P.G. (1981). Multiplicative intrinsic noise and the limits to visual performance. *Vision Research, 201*, 291-296.

Luntinen, O., Rovamo, J. & Näsänen, R. (1992). Modelling contrast sensitivity for vertical gratings as a function of grating area. *Supplement to Investigative Ophthalmology and Visual Science, 33*, 1347.

Mandelbaum, J. & Sloan, L.L. (1947). Peripheral visual acuity. *The American Journal of Ophthalmology, 30*, 581-588.

McCann J.J. (1978) Visibility of gradients and low spatial frequency sinusoids: Evidence for a distance constancy mechanism. *Society of Photographic Scientists and Engineers, 22*, 64-68

Metcalf, H. (1965). Stiles-Crawford apodization. *The Journal of Optical Society of America, 55*, 72-74.

Miller, W.H. & Bernard, G.D. (1983). Averaging over the foveal receptor aperture curtails aliasing. *Vision Research, 23*, 1365-1369.

Millodot, M. (1981). Effect of ametropia on peripheral refraction. *The American Journal of Optometry and Physiological Optics, 58*, 691-695.

Millodot, M., Johnson, C.A., Lamont, A. & Leibovitz, H.W. (1975). Effect of dioptrics on peripheral visual acuity. *Vision Research, 15*, 1357-1362.

Mäkelä, P., Whitaker, D. & Rovamo, J. (1992) Modelling of orientation discrimination across the visual field. *Vision Research, 33*, 723-730.

Nachamias, J. (1968). Visual resolution of two-bar patterns and square-wave gratings. *The Journal of Optical Society of America, 58,* 10-13.

Nagaraja, N.S. (1964). Effect of luminance noise on contrast thresholds. *The Journal of Optical Society of America, 54*, 950-955.

Navarro, R., Artal, P. & Williams, D.R. (1993). Modulation transfer of the human eye as a function of retinal eccentricity. *The Journal of the Optical Society of America, A, 10*, 201-212.

Nordby, K. & Sharpe, L.T. (1988). The directional sensitivity of the photoreceptors in the achromat. *The Journal of Physiology, 399*, 267-281.

Näsänen, R. (1989). Effects of halftoning and noise on visual perception of spatial signals. *Thesis*, Tekninen Korkeakoulu, Espoo, Finland.

Näsänen, R., Kukkonen, H & Rovamo, J. (1993). Spatial integration of band-pass filtered patterns in noise. *Vision Research, 33*, 903-911.

Ogden, T.E. (1989). Topography of the retina. In *Retina, Vol. 1*, Eds Ogden, Schachat, The Mosby Company, St Louis, Missouri

Ohzu, H. & Enoch, J.M. (1972). Optical modulation by the isolated human fovea. *Vision Research, 12*, 245-251.

Patel, A.S. (1966). Spatial resolution by the human visual system. The effect of mean retinal illuminance. *The Journal of the Optical Society of America, 56,* 689-694.

Pelli, D.G. (1990). The quantum efficiency of vision. In Blakemore, C. (ed.) *Vision: Coding and efficiency.* Cambridge: University Press.

Pelli, D.G. & Zhang, L. (1991). Accurate control of contrast on microcomputer displays. *Vision Research, 31*, 1337-1350.

Piper, H. (1903). Die Abhängigkeit des Reizwertes leuchtender Objeckte von ihrer flächenbesw. winkelgröfse. *Zeitschrift für Psychologie und Physiologie der Sinnesorgane, 32*, 98-112.

Pointer, J. S. & Hess, R. F. (1989) The contrast sensitivity gradient across the human visual field: with emphasis on the low spatial frequency range. *Vision Research, 29*, 1133-1151.

Polyak, S. (1957). In *The vertebrate visual system.* Chicago: Chicago University Press.

Robson, J.G. & Graham, N. (1981). Probability summation and regional variation in contrast sensitivity across the visual field. *Vision Research, 21*, 409-418.

Rose, A. (1948). The sensitivity performance of the human eye on an absolute scale. *The Journal of the Optical Society of America, 38*, 196-208.

Rovamo, J. (1983). Cortical magnification factor and contrast sensitivity to luminance-modulated chromatic gratings. *Acta Physiologica Scandinavica, 119*, 365-371.

Rovamo, J., Franssila, R., & Näsänen, R. (1992). Contrast sensitivity as a function of spatial frequency, viewing distance and eccentricity with and without spatial noise. *Vision Research, 32*, 631-637.

Rovamo, J.M. & Kukkonen, H.T. (1995). The effect of noise pixel size and shape on grating detectability. *Vision Research*, in press.

Rovamo, J., Kukkonen, H., Tiippana, K. & Näsänen, R. (1993). Effects of luminance and exposure time on contrast sensitivity in spatial noise. *Vision Research, 33*, 1123-1129.

Rovamo, J., Luntinen, O. & Näsänen, R. (1993). Modelling the dependence of contrast sensitivity on grating area and spatial frequency. *Vision Research, 33*, 2773-2788.

Rovamo, J. & Raninen, A. (1984). Critical flicker frequency and M-scaling of stimulus size and retinal illuminance. *Vision Research, 24*, 1127-1131.

Rovamo, J. & Raninen, A. (1990). Cortical acuity and the luminous flux collected by retinal ganglion cells at various eccentricities in human rod and cone vision. *Vision Research, 29*, 11-21.

Rovamo, J. & Virsu, V. (1979). An estimation and application of the human cortical magnification factor. *Experimental Brain Research, 37*, 495-510.

Rovamo, J.M., Virsu, V. & Näsänen, R. (1978). Cortical magnification factor predicts the photopic contrast sensitivity of peripheral vision. *Nature, 271*, 54-56.

Santamaria, J., Artal, P. & Bescos, J. (1987). Determination of the point-spread function of human eyes using a hybrid optical-digital method. *The Journal of Optical Society of America A, 4*, 1109-1114.

Savage, G.L. & Banks, M.S. (1992). Scotopic visual efficiency: Constraints by optics, receptor properties, and rod pooling. *Vision Research, 32,* 645-656.

Savoy, R.L. & McCann, J.J. (1975). Visibility of low-spatial-frequency sine-wave targets; Dependence on number of cycles. *The Journal of Optical Society of America, 65*, 343-350.

Shapley, R. (1991). Neural mechanisms of contrast sensitivity. In *Vision and Visual Dysfunction*, Vol 10. Ed. Regan, MacMillan Press, London.

Shapley, R. & Enroth-Cugell, C. (1984). Visual adaptation and retinal gain controls. In Osborne, N.N. & Chader, G.J. (Eds), *Progress in Retinal Research*, Vol 3 (pp. 263 - 343). Oxford: Pergamon Press.

Sidman, R. (1957). The structure and concentration of solids in photoreceptor cells studied by refractometry and interference microscopy. *J. Biophys. Biochem. Cytol., 3*, 15-30.

Sloan, L.L. (1968). The photopic acuity-luminance function with special reference to parafoveal vision. *Vision Research, 8*, 901-911.

Smirnov, M.S (1962). Measurement of the wave aberration of the human eye. *Biophysics, 6*, 766-795.

Stiles, W.S. (1939). The luminous efficiency of monochromatic rays entering the eye pupil at different points and a new color effect. *Proceedings of the Royal Society of London, B 123*, 90-118.

Stiles, W.S. & Crawford, B.H. (1933). The luminous efficiency of rays entering the eye pupil at different points. *The Proceedings of The Royal Society of London, B112*, 428-450.

Stromayer, C.F. & Julesz, B. (1972). Spatial-frequency masking in vision: Critical bands and spread of masking. *The Journal of Optical Society of America*, *62*, 1221-1232.

Tanner, W.P. & Birdsall T.G. (1958). Definitions of d' and h as Psychophysical Measures. *The Journal of the Acoustical Society of America, 30*, 922-928.

Thibos, L.N., Walsh, D.J. & Cheney, F.E. (1987). Vision beyond the resolution limit: Aliasing in the periphery. *Vision Research, 27*, 2193-2197.

Van den Berg, T.J.T.P., Ijspeert, J.K. & Spekreijse, H. (1994). Discrepancies in high frequency optical modulation transfer of the human eye, reply to Drasdo, Thompson and Charman. *Vision Research, 34*, 1251-1253.

Van Loo, J.A. & Enoch, J.M. (1975). The scotopic Stiles Crawford effect. *Vision Research, 15*, 1005-1009.

Van Meeteren, A. (1974). Calculations on the optical modulation transfer function of the human eye for white light. *Optica Acta*, *21*, 395-412.

Van Nes, F.L. & Bouman, M.A. (1967). Spatial modulation transfer in the human eye. *Journal of Optical Society of America, 57*, 401-406.

Van Nes, F.L., Koenderink, J.J., Nas, H. & Bouman, M.A. (1967). Spatiotemporal modulation transfer in the human eye. *Journal of Optical Society of America, 57*, 1082-1088.

Verghese, P. & Pelli, D.G. (1992). The information capacity of visual attention. *Vision Research, 32*, 983-995.

Virsu, V. & Rovamo, J. (1979). Visual resolution, contrast sensitivity, and the cortical magnification factor. *Experimental Brain Research, 37*, 475-494.

de Vries, H. (1943). The quantum character of light and its bearing upon threshold of vision, the differential sensitivity and visual acuity of the eye. *Physica, 10*, 553-564.

Walsh, G., Charman, W.N. & Howland, H.C. (1984). Objective technique for the determination of monochromatic aberrations of the human eye. *The Journal of Optical Society of America A*, *1*, 987-992.

Watson, A.B., Barlow, H.B. & Robson, J.G., (1983) What does the eye see best? *Nature, 302*, 419-422.

Westheimer, G. (1960). Modulation thresholds for sinusoidal light distributions on the retina. *The Journal of Physiology*, *152*, 67-74.

Westheimer, G. (1967). Dependence of the magnitude of the Stiles Crawford effect on retinal location. *Journal of Physiology, 192*, 309-315.

Wetherill, G.B. & Levitt, H. (1965). Sequential estimation of points on a psychometric function. *The British Journal of Mathematical and Statistical Psychology*, *18*, 1-10.

Williams, D.R. (1985). Aliasing in human foveal vision. *Vision Research, 25*, 195-205.

Williams, D.R., Brainard, D.H., McMahon, M.J. & Navarro, R. (1994). Double-pass and interferometric measures of the optical quality of the eye. *The Journal of Optical Society of America A*, 11, 3123-3135.

Yellott, J.I.Jr (1982). Spectral analysis of spatial sampling by photoreceptors: topological disorder prevents aliasing. *Vision Research, 22*, 1205-1210.

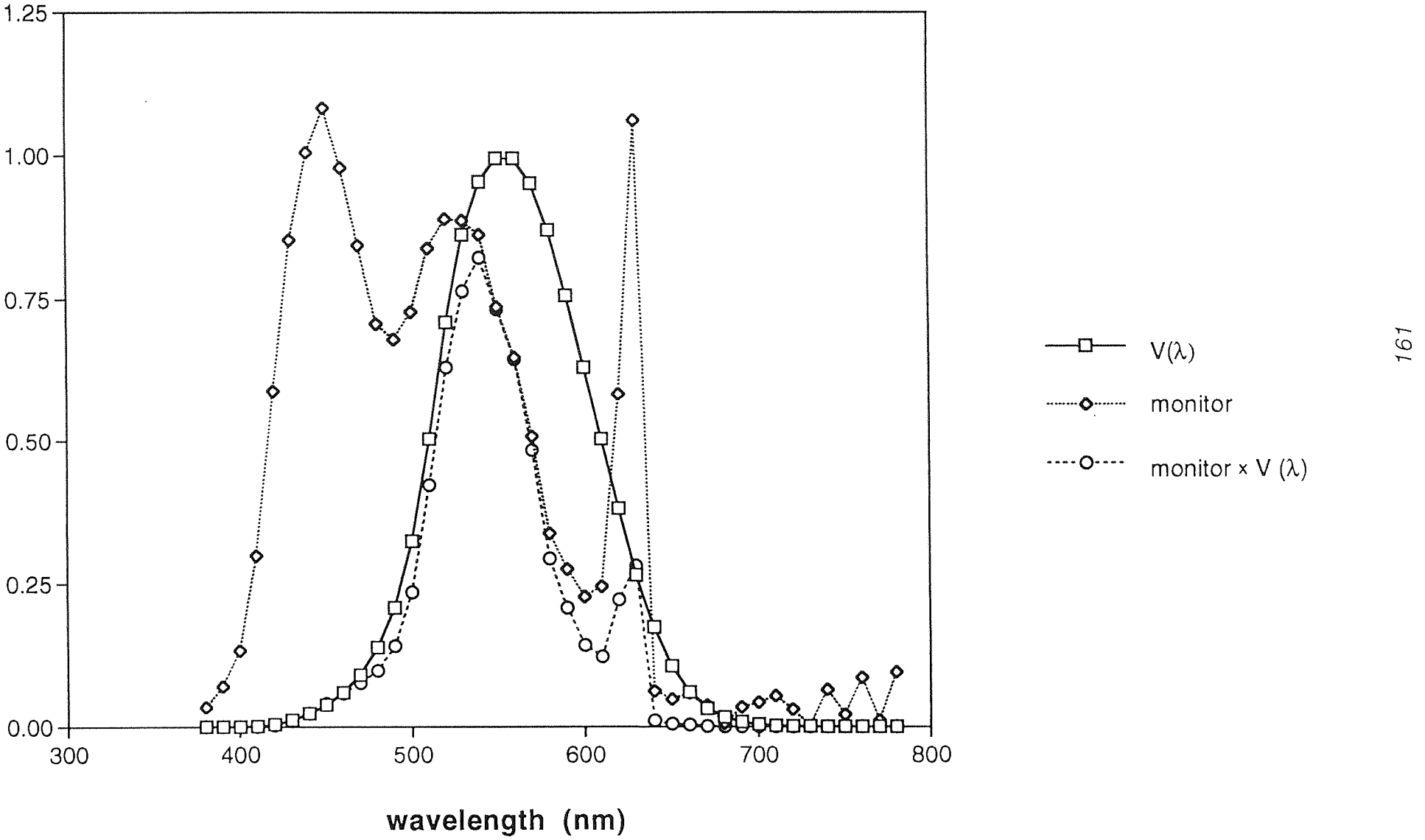
1.25
1.00
0.75
0.50
0.25
0.00
300
400
500
600
700
800
wavelength (nm)
V(λ)
monitor
monitor × V (λ)

Appendix 2

Explained variance

The goodness of the fit of an equation to the data was estimated as follows: First I calculated error variance $n^{-1}\Sigma(\log Y-\log Y_{est})^2$ of the experimental data (Y) from the predicted values (Y_{est}) and the total variance $n^{-1}\Sigma (\log Y-Y_{ave})^2$of the data, where $Y_{ave}= n^{-1}\Sigma \log Y$ is the average of logY. The explained proportion was then calculated as:

$$r^2 = 1 - \Sigma(\log Y-\log Y_{est})^2/\Sigma(\log Y-Y_{ave})^2. \qquad (A.1)$$

The values of Y_{est} were calculated by means of the relevant equation. We used logY instead of Y, because Y is plotted on a logarithmic scale. The explained proportion (r^2) is usually given as the percetage of the variance explained, which is obtained by multiplying the proportion by 100.

Appendix 3

The least squares curves

Contrast sensitivity as a function of retinal illuminance was modelled by fitting equation (3.2) to the contrast sensitivity data of Fig 3.1 at each spatial frequency and eccentricity separately. This was obtained by finding the minimum of the following:

$$G = \sum_{j=1}^{n} [\ (S_j^{-2} - k_1 - k_2/I_j) / S_j^{-2}\ ]^2, \qquad (A.2)$$

where $k_1 = S_{max}^{-2}$, $k_2 = I_c\, S_{max}^{-2}$, and S_j are contrast sensitivities corresponding to retinal illuminances I_j in Fig 3.1. As the range of S_j^{-2} is several logarithmic units, it is necessary to calculate the relative least squares curves by minimising the percentage error, as in equation (A.2). Otherwise the deviations of the large values of S_j^{-2} from the least squares curve would dominate the fitting procedure. Equation (A.2) was next transformed to

$$G = \sum_{j} [1 - k_1 S_j^2 - k_2 S_j^2 / I_j\ ]^2. \qquad (A.3)$$

The values of k_1 and k_2 that minimize G were then found by the method described in Mäkelä, Whitaker & Rovamo (1993). Thereafter I calculated $S_{max} = 1/\sqrt{k_1}$ and $I_c = k_2/k_1$.

Appendix 4

Diffraction and retinal light scatter limited O_{MTF}

According to Johnson (1972) the diffraction limited MTF of a circular aperture is

$$T_e(f) = (2/\pi) \{\arccos (f/f_0)-(f/f_0)[1-(f/f_0)^2]^{0.5}\}, \quad (A.4)$$

and can be very closely approximated as

$$T_a(f) = e\,[-(f/0.48f_0)^{1.5}]. \quad (A.5)$$

Spatial frequency (f) is in cycles per mm, f_0 is the cut-off frequency. The cut-off frequency is given by $f_0 = P/F\lambda$ c/mm, where P is the pupil diameter in mm, F is the focal length, i.e. the posterior nodal distance of the unaccommodated 60D schematic eye equal to 16.7 mm, and λ is the wavelength of monochromatic light. In our experiments we used white light, but when the O_{MTF} for the diffraction limited system was calculated for the precise spectral composition of "white" light produced by our monitor, and for a wavelength (550×10^{-6} mm) corresponding to the centre of the visible spectrum, only a hairbreadth distinction was found. For simplicity, the diffraction limit is shown for monochromatic 550 nm light, which can be considered equal to the diffraction limit calculated for the exact spectral composition of our computer display at 380-780 nm. Equation (A.4) gives spatial frequency in c/mm. To transform c/mm to c/deg of the visual field we assumed that 1 mm on the retina is equivalent to 3.4364 deg (Polyak, 1957).

In order to take into account the effect of retinal light scatter (Ohzu & Enoch, 1972), which is independent of pupil size, I applied the equation (A.5) of

Deeley et al., (1991). They used the data of Ohzu & Enoch (1972) to derive the equation $\ln T_s = -(f/33.2)^{1.38}$, where T_s refers to the effect of retinal light scatter on the modulation transfer. The optical MTF for a diffraction limited human eye attenuated by the inevitable retinal light scatter is thus described by equation

$$T_e(f)\, T_s = (2/\pi) \{\arccos (f/f_0) - (f/f_0) [1-(f/f_0)^2]^{0.5}\} \{\exp [-(f/33.2)^{1.38}]\}. \qquad (A.6)$$

Appendix 5

The spatial extent and location of stimuli in the experiment of Chapter 4

Eccentricity 3 deg

c/deg	viewing distance	c/cm	diameter (cm)	area (deg^2)	Af^2	fixation (cm) temp
1.0	114	0.5	16	50.6	50	6
2.0	229	0.5	16	12.6	50	12
4.0	114	2	4	3.14	50	6
8.0	229	2	4	0.785	50	12

Eccentricity 9 deg

c/deg	viewing distance	c/cm	diameter (cm)	area (deg^2)	Af^2	fixation (cm) temp
0.5	57.3	0.5	16	198	50	9
1.0	114	0.5	16	50.6	50	18
2.0	57.3	2	4	12.6	50	9
4.0	114	2	4	3.14	50	18

Eccentricity 20 deg

c/deg	viewing distance	c/cm	diameter (cm)	area (deg^2)	Af^2	fixation (cm) temp	fixation forward
0.25	28.6	0.5	16	767	50	10	2
0.5	57.3	0.5	16	198	50	20	4
1.0	28.6	2	4	50.6	50	10	2
2.0	57.3	2	4	12.6	50	20	4

Eccentricity 37 deg

c/deg	viewing distance	c/cm	diameter (cm)	area (deg^2)	Af^2	fixation (cm) temp	fixation forward
0.25	28.6	0.5	16	767	50	17	6
0.5	57.3	0.5	16	198	50	34	12
1.0	28.6	2	4	50.6	50	17	6

Appendix 6

The spatial extent of the stimuli in Chapter 5.4

Eccentricity 0 deg

retinal spatial frequency c/deg	viewing distance cm	grating area deg^2	screen spatial frequency c/cm	retinal area deg^2
0.5	114	16*16	0.25	64
1.0	114	8*8	0.5	16
2.0	114	4*4	1	4
4.0	114	2*2	2	1
8.0	229	2*2	2	0.25
16.0	458	2*2	2	0.0625
32.0	915	2*2	2	0.016

Eccentricity 5 deg

retinal spatial frequency c/deg	viewing distance cm	grating area deg^2	screen spatial frequency c/cm	retinal area deg^2
0.25	57.2	16*16	0.25	254
0.5	57.2	8*8	0.5	64
1.0	57.2	4*4	1	16
2.0	57.2	2*2	2	4
4.0	458	8*8	0.5	1
8.0	458	4*4	1	0.25

Eccentricity 10 deg

retinal spatial frequency c/deg	viewing distance cm	grating area deg^2	screen spatial frequency c/cm	retinal area deg^2
0.125	28.6	16*16	0.25	977
0.25	28.6	8*8	0.5	244
0.5	28.6	4*4	1	64
1.0	28.6	2*2	2	16
2.0	229	8*8	0.5	4
4.0	229	4*4	1	1

Eccentricity 20 deg

retinal spatial frequency c/deg	viewing distance cm	grating area deg^2	screen spatial frequency c/cm	retinal area deg^2
0.064	57.2	16*16	0.125	977
0.125	57.2	8*8	0.25	244
0.25	57.2	4*4	0.5	64
0.5	57.2	2*2	0.25	16
1.0	458	8*8	0.5	4
2.0	458	4*4	1	1

The spectral densities of the added spatial noise used in the experiments of Fig. 5.11

c/deg	0 deg	5 deg	10 deg	20 deg
0.125				9.14e-02
0.25			1.43e-03	2.29e-02
0.5	1.43e-03	1.43e-03	3.57e-04	2.54e-03
1.0	3.00e-04	8.04e-04	3.57e-04	6.35e-04
2.0	6.20e-05	8.93e-05	3.57e-04	1.43e-03
4.0	2.23e-05	8.93e-05	5.58e-04	
8.0	2.25e-05	1.30e-04		
16.0	3.25e-05			

Appendix 7

The experimental data

Chapter 3.2
Number of square cycles 3.14,
subjects JM and OU

td	0.785 deg^2, 2 c/deg	12.6 deg^2, 0.5 c/deg	201 deg^2, 0.125 c/deg	0.785 deg^2, 2 c/deg	12.6 deg^2, 0.5 c/deg	201 deg^2, 0.125 c/deg
2513	190.38	155.36	163.82	48.550	110.17	75.046
628	157.73	184.75	133.62	43.919	89.843	77.245
157	109.47	149.48	177.58	42.906	79.569	73.740
39.3	98.533	104.37	116.78	28.682	63.867	63.473
9.82	58.064	74.559	95.153	22.443	60.692	50.736
2.45	22.943	51.252	83.231		31.966	31.386
0.614		30.735	58.367		19.400	32.202
0.153		16.287	54.567			23.119
0.0383			28.126			23.699
0.00959			20.746			16.645

Number of square cycles 12.6
subjects JM and HK

td	0.785 deg^2, 4 c/deg	12.6 deg^2, 1 c/deg	201 deg^2, 0.25 c/deg	0.785 deg^2, 4 c/deg	12.6 deg^2, 1 c/deg	201 deg^2, 0.25 c/deg
2513	132.97	221.75	208.41	128.92	178.96	166.93
628	136.51	186.54	207.54	93.637	189.06	152.85
157	116.93	139.31	163.79	96.149	166.56	152.40
39.3	59.046	113.88	143.81	59.220	149.76	119.34
9.82	40.520	97.194	117.69	33.244	90.943	122.62
2.45	15.546	76.801	97.604	11.480	53.912	89.232
0.614		31.415	72.691		32.601	72.439
0.153		13.317	46.008		14.407	57.544
0.0383			33.367			31.528
0.00959			18.516			25.319

Number of square cycles 50.3
Subjects JM and OL

td	12.6 deg^2, 2 c/deg	50.3 deg^2, 1 c/deg	201 deg^2, 0.5 c/deg	12.6 deg^2, 2 c/deg	50.3 deg^2, 1 c/deg	201 deg^2, 0.5 c/deg
2513	346.86	432.63	273.32	364.23	433.51	317.86
628	312.15	309.72	284.45	321.15	377.37	306.56
157	248.10	284.54	301.68	269.16	266.40	307.93
39.3	214.58	191.30	246.31	207.74	191.75	206.75
9.82	135.45	166.67	208.37	152.62	151.13	158.57
2.45	71.195	96.004	141.75	66.973	127.04	102.57
0.614	37.695	80.941	99.419	30.459	62.845	77.201
0.153	13.855	52.852	85.237	12.688	32.263	76.013
0.0383		35.201	56.369		18.793	40.672
0.00959		21.005	37.319		14.142	28.062
0.00240		11.597	15.022			19.993

Number of square cycles 201
Subjects JM and KT

td	12.6 deg^2, 4 c/deg	50.3 deg^2, 2 c/deg	201 deg^2, 1 c/deg	12.6 deg^2, 4 c/deg	50.3 deg^2, 2 c/deg	201 deg^2, 1 c/deg
2513	379.51	588.58	476.18	314.51	395.83	406.21
628	316.80	443.47	510.05	249.75	340.23	385.63
157	203.34	375.79	453.60	186.00	266.60	241.27
39.3	180.15	314.17	316.65	120.50	167.84	181.12
9.82	112.85	174.07	288.82	86.109	98.213	131.45
2.45	43.580	112.72	199.89	31.063	64.764	83.748
0.614	22.191	51.779	151.94		28.861	84.361
0.153		25.689	70.123			52.377
0.0383			37.496			
0.00959			20.737			
0.00240			15.052			

The experimental data of Chapter 3.3.

0.25 c/deg

td	804 deg^2	201 deg^2	50.3 deg^2	12.6 deg^2
2513	212.77	187.34	77.042	55.895
157	194.19	127.53	72.881	53.948
9.82	138.91	83.345	54.919	39.069
0.614	92.944	46.512	32.626	17.050
0.0383	42.002	33.609	15.053	6.1108
0.0024	19.148	13.028	5.7247	2.2345

1 c/deg

td	804 deg^2	201 deg^2	50.3 deg^2	12.6 deg^2	3.14 deg^2	0.785 deg^2
2513	441.11	312.80	216.00	132.50	87.130	40.892
157	327.89	302.86	235.63	133.87	82.304	52.375
9.82	229.39	234.76	138.96	75.915	51.179	27.999
0.614	98.661	80.979	67.080	29.059	19.508	7.5279
0.0383	43.562	23.902	14.933	7.5236	4.5283	2.2557

4 c/deg

td	50.3 deg^2	12.6 deg^2	3.14 deg^2	0.785 deg^2	0.196 deg^2	0.049 deg^2
2513	409.16	334.82	260.26	208.69	120.05	51.319
157	242.66	236.90	173.17	95.438	78.175	34.471
9.82	98.736	79.268	55.154	32.755	25.249	13.073
0.614	18.296	12.162	8.7526	6.1603	3.8085	2.4141

11 c/deg

td	6.65 deg^2	1.66 deg^2	0.415 deg^2	0.104deg^2	0.026 deg^2	0.0065 deg^2
2513	197.66	130.54	80.795	59.883	36.621	15.944
628	140.31	92.583	59.868	26.911	15.630	9.5954
157	73.026	52.151	29.771	19.160	11.201	3.4846
39.2	47.834	29.184	22.479	10.853	6.3696	
9.82	18.953	13.415	8.5249	4.1479	2.8072	

Data of Fig. 2.7
(the addition of external light has been compensated at 23 and 32 c/deg)

td	0.125 c/deg	0.5 c/deg	2 c/deg	8 c/deg	16 c/deg	23 c/deg	32 c/deg
25000						44.252	
10000						47.934	13.651
2513	5042.9	2114.9	1466.2	334.41	69.769	25.605	8.9428
628				385.31	36.734	24.343	4.5682
157	5901.5	1941.3	918.75	194.64	26.745	14.621	3.4381
39.3				153.17	13.262	7.0937	
9.82	4122.4	1085.8	518.49	46.406	8.6219	3.5242	
2.45				12.308			
0.614	2191.6	471.40	125.12				
0.0383	1228.2	221.66	26.316				
0.00960			12.603				
0.00240	541.90	70.258					
0.00015	166.31						

deg^2	0.125 c/deg	0.5 c/deg	2 c/deg	8 c/deg	16 c/deg	23 c/deg	32 c/deg
804	42334						
201	37822	16704	3790.6				
50.3	32563	9517.2	3410.4				
12.6		6083.5	2515.7	476.52			
6.65						25.605	
3.14		3847.4	1493.7	445.88	81.129		8.9428
1.66						23.725	
0.787			667.84	309.55	69.769		8.8975
0.415						21.496	
0.196				174.12	55.641		7.2357
0.104						17.779	
0.0490				99.255	29.404		5.5118
0.0260						9.7053	
0.0120					18.016		3.6241

The experimental data of Chapter 4

Data of Fig. 4.1, subject JM
(partly replotted in Fig 4.2.D)

td	12.6 deg2	50.3 deg2	201 deg2	804 deg2
157	13.663	40.336	43.586	
39.3	19.450	37.239	53.900	82.386
9.82	13.823	26.388	48.104	75.974
2.45	8.2944	19.858	29.445	53.836
0.614	5.4772	9.2737	18.188	30.561
0.153	2.7789	7.7404	12.094	14.861
0.0383		3.1472	5.3486	8.4386

The data of Fig. 4.2
Eccentricity 3 deg, subject KL

td	1 c/deg	2 c/deg	4 c/deg	8 c/deg
2513	201.09	76.432	17.007	1.7040
157	145.39	58.666	11.252	0.83890
9.82	61.291	25.576	4.5168	0.28824
0.614	27.794	6.2992	0.74155	0.089202
0.0383		0.70777	0.23309	

Eccentricity 9 deg, subjects JM and TH

td	0.5 c/deg	1 c/deg	2 c/deg	4 c/deg
2513	207.89	55.437	16.268	2.0627
628				1.8069
157	227.70	66.700	13.015	1.3670
9.82	183.84	40.791	6.2481	0.51870
0.614	103.08	17.485	2.4630	0.14249
0.0383	31.882	5.8815	0.48066	
0.002397	11.292	1.8366		
0.000150	3.6270			

Eccentricity 20 deg, subject SU

td	0.25 c/deg	0.5 c/deg	1 c/deg	2 c/deg
2513	58.845	17.891	4.0088	0.52611
157	166.31	51.115	13.265	1.8451
9.82	111.81	37.153	7.7352	1.0798
0.614	61.818	23.136	4.3221	0.29254
0.0383	35.868	11.281	1.6512	0.078358
0.002397	14.600	3.6859	0.58060	
0.000150	3.5317	0.79260		

Eccentricity 37 deg, subject JM

td	0.25 c/deg	0.5 c/deg	1.0 c/deg
2513		11.191	2.6174
628	73.234	21.970	3.7681
157	77.458	25.563	4.4818
39.3	96.557	18.564	4.1377
9.82	70.984	13.260	2.9320
2.45	68.768	13.988	2.2065
0.614	73.556	10.373	1.0304
0.153	54.497	7.0508	0.86005
0.0383	49.862	3.9419	0.34969
0.00959	19.337	2.9866	
0.002397	11.680	1.4040	
0.000599	7.3145		
0.000150	2.6652		

The experimental data of Chapter 5.2

c/deg	bright	dim	noise	bright	dim	noise
1.0000	289.34	75.426	6.4262	317.93	63.808	9.0849
2.0000	340.24	82.174	11.209	274.04	54.815	9.6888
3.0000	355.25	93.731	8.0950	344.49	67.249	8.2406
4.0000	312.80	70.562	10.597	312.85	80.409	8.8968
6.0000	259.35	61.148	9.7114	286.81	61.456	8.4570
8.0000	197.52	52.416	7.5378	174.27	54.543	9.0679
11.000	128.94	36.187	9.4300	121.87	47.249	10.321
16.000	74.370	20.345	7.3978	86.780	23.689	8.3170
23.000	37.585	8.0044	6.5294	42.821	7.7753	9.5686

The experimental data of Chapter 5.3

c/deg	ø 8	ø 8 lens	ø 8	ø 6	ø 6	ø 4	ø 4	ø2	ø2	ø 1.5	ø 1.5
1	136.07	130.86	142.50	151.50	84.973	110.59	67.437	82.748	50.472	57.628	34.422
2	125.70	126.39	152.99	156.42	95.307	112.48	85.069	69.299	56.320	48.646	45.249
3	114.79	114.74	178.06	146.55	117.99	109.64	85.950	42.928	51.059	47.246	38.298
4	114.80	128.39	132.97	91.343	160.51	115.69	86.425	53.440	53.641	41.808	63.177
6	96.589	85.673	129.99	66.713	104.50	86.858	90.076	48.076	59.128	29.854	46.057
8	61.298	78.050	77.126	60.994	68.014	83.506	51.421	42.424	48.342	31.205	43.278
11	67.417	43.517	63.521	31.506	70.499	23.910	63.306	26.154	31.005	22.794	18.905
16	26.197	22.595	40.270	23.510	59.083	21.377	35.295	20.147	15.064	15.521	10.075
23	6.6500	6.4615	14.233	10.911	19.263	8.6710	21.906	16.266	5.8902	4.3690	4.3020
32	4.3370	5.6866	6.7812	8.1740	6.3442	5.2110	11.407	2.3110			

The experimental data of Chapter 5.4

Data of Fig. 5.9

Subject KT

deg^2	1 c/deg	0.5 c/deg	0.25 c/deg	0.125 c/deg
1	10.157			
4	19.493	16.728		
16	36.210	29.578	16.348	
64	50.814	43.095	28.188	22.873
256	68.921	59.489	40.128	29.383
1024	65.723	63.352	44.179	37.416

Subject SU

deg^2	1 c/deg	0.5 c/deg	0.25 c/deg	0.125 c/deg
1	20.435			
4	32.863	28.454		
16	58.914	48.179	30.327	
64	73.663	66.023	43.361	28.064
256	90.979	89.089	53.459	39.801
1024	108.54	115.10	75.279	66.823

Data for the relative method

Subject KT

c/deg	fovea	5 deg	10 deg	20 deg	40 deg
16	11.309				
8.0	29.666	5.4772			
4.0	54.345	35.119	19.150		
2.0	76.655	67.410	49.314	7.0598	
1.0	58.039	61.663	78.582	26.451	5.8365
0.5	41.753	69.254	67.950	28.443	23.265
0.25		54.415	55.552	43.900	34.375
0.125			59.999	41.377	33.487
0.0625				34.931	25.033

Subject SU

c/deg	fovea	5 deg	10 deg	20 deg	40 deg
32	4.3595				
16	14.658				
8.0	43.476	4.6132			
4.0	81.548	33.272	7.5494		
2.0	91.437	65.518	46.751	6.3574	
1.0	91.179	108.50	87.257	38.387	4.2476
0.5	71.907	100.61	98.021	54.639	23.690
0.25		86.271	99.593	74.168	31.040
0.125			71.911	73.321	32.809
0.0625				49.679	32.594

Data for the noise method

Eccentricity 0 deg
Subjects OL and JM

c/deg	bright	noise	bright	noise
0.50000	75.801	21.496	92.625	15.982
1.0000	148.49	46.527	141.73	35.479
2.0000	200.82	52.467	255.11	83.185
4.0000	356.38	103.10	470.65	102.37
8.0000	291.33	93.337	288.12	73.517
16.000	71.417	34.648	92.124	45.124

Eccentricity 5 deg
Subjects OL and JM

c/deg	bright	noise	bright	noise
0.25	77.640	23.193	77.878	18.190
0.5	129.12	36.062	153.33	43.440
1.0	248.90	84.711	227.66	73.406
2.0	199.40	75.801	240.13	61.940
4.0	53.598	30.122	83.679	36.351

Eccentricity 10 deg
Subjects OL and JM

c/deg	bright	noise	bright	noise
0.25	53.881	20.647	60.619	23.390
0.50	169.70	57.699	119.89	48.769
1.0	306.88	65.760	215.48	70.781
2.0	219.20	69.154	197.70	49.602
4.0	112.43	42.567	115.58	41.033

Eccentricity 20 deg
Subjects OL and JM

c/deg	bright	noise	bright	noise
0.125	29.557	8.0890	43.757	8.7291
0.25	76.225	20.506	82.045	16.718
0.5	154.15	43.699	112.97	34.274
1.0	292.74	81.741	199.40	59.767
2.0	206.47	51.901	118.68	40.281
4.0	54.588	23.193		